$$\sigma_{x'x'} = \sigma_{xx}\cos^2\theta + \sigma_{yy}\sin^2\theta + \sigma_{xy}\cdot 2\sin\theta\cos\theta = \frac{\sigma_{xx}+\sigma_{yy}}{2} + \frac{\sigma_{xx}-\sigma_{yy}}{2}\cos 2\theta + \sigma_{xy}\sin 2\theta$$

$$\sigma_{y'x'}\cdot dn = \sigma_{yy}\,dx\cos\theta + \sigma_{xy}\,dy\cos\theta - \sigma_{xx}\,dy\sin\theta - \sigma_{yx}\,dx\sin\theta = \left[-\tfrac{1}{2}(\sigma_{xx}-\sigma_{yy})\sin 2\theta + \sigma_{xy}\cos 2\theta\right]$$

$$\sigma_{y'y'} = \frac{1}{2}(\sigma_{xx}+\sigma_{yy}) - \frac{1}{2}(\sigma_{xx}-\sigma_{yy})\cos 2\theta - \sigma_{xy}\sin 2\theta$$

what we find is that principal stresses

$$\sigma_{1,2} = \frac{\sigma_{xx}+\sigma_{yy}}{2} \pm \sqrt{\left(\frac{\sigma_{xx}-\sigma_{yy}}{2}\right)^2 + \sigma_{xy}^2} \qquad \tau_{max} = 0$$

$\sigma_1 + \sigma_2 = \sigma_{xx} + \sigma_{yy}$ = first invariant

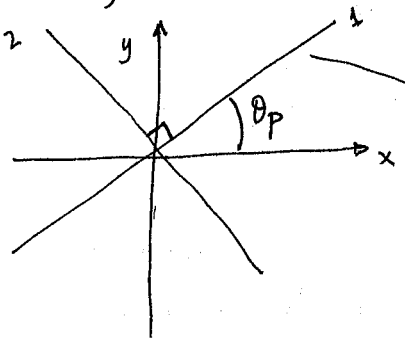

$$\tan 2\theta_p = \frac{2\sigma_{xy}}{\sigma_{xx}-\sigma_{yy}}$$

direction of normal to principal planes

σ_1 is larger principal stress σ_2 smaller

max shear stress $\tau_{max} = \dfrac{\sigma_1 - \sigma_2}{2}$ occurs on planes 45° from principal plane

Mohrs' Circle

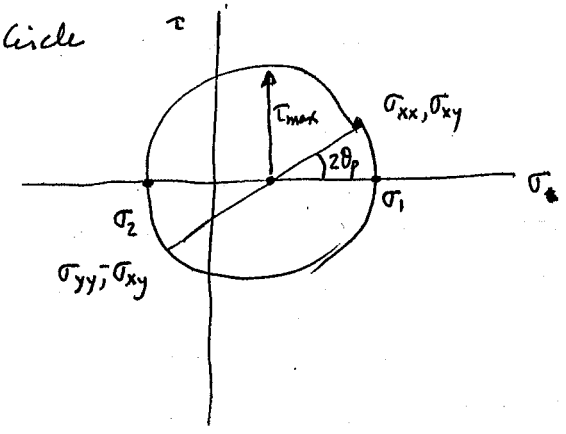

A circle on σ-τ plane

the principal stresses in 3-D for the general state of stress are found from

$$\sigma^3 - I_1\sigma^2 + I_2\sigma - I_3 = 0$$

$$I_1 = \sum \sigma_{ii}$$

$$I_2 = \sum \sigma_{ii}\sigma_{jj} - \sum \sigma_{ij}^2$$

$$I_3 = \det \begin{bmatrix} \sigma_{11} & \sigma_{12} & \sigma_{13} \\ \sigma_{21} & \sigma_{22} & \sigma_{23} \\ \sigma_{31} & \sigma_{32} & \sigma_{33} \end{bmatrix}$$

Given

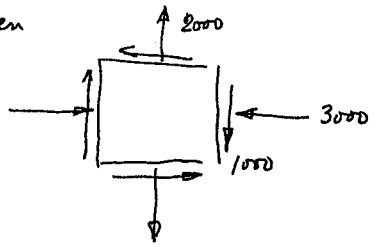

$\sigma_{xx} = -3000$

$\sigma_{yy} = 2000$

$\sigma_{xy} = -1000$

$$\sigma_{1,2} = \frac{(-3000+2000)}{2} \pm \sqrt{\left(\frac{-3000+2000}{2}\right)^2 + (-1000)^2}$$

$$= -500 \pm \sqrt{(-500)^2 + (1000)^2}$$

$$= -500 \pm 500\sqrt{5}$$

$$= 500\left[-1 \pm 2.236\right] = 500\left[-3.236,\ 1.236\right] = 1618,\ 618\ psi$$

$$\tau_{max} = \frac{\sigma_1 - \sigma_2}{2} = 500\left[\frac{1.236 - (-3.236)}{2}\right]$$

$$= 500\left[\frac{4.472}{2}\right] = 500\,(2.236) = 1118\ psi$$

$$\tan 2\theta_p = \frac{2(-1000)}{-3000 - [2000]} = 0.4$$

$$\theta_p = 10.9°$$

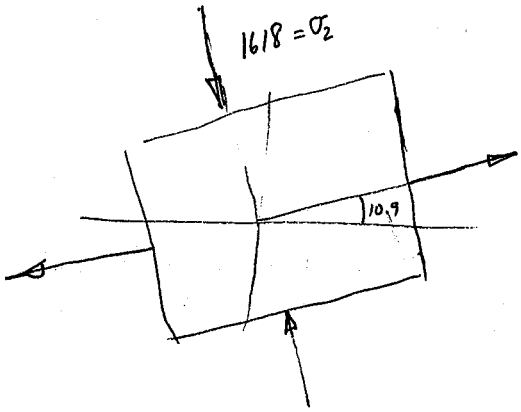

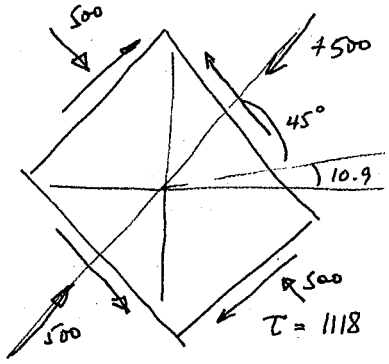

$$\sigma_{x'x'} = -3000\cos(55.9°)\cdot\frac{-1000}{2} + \frac{-5000}{2}\cos 2(55.9°) - 1000\sin 2(55.9°)$$

$$= -500\ psi$$

$$\sigma_{y'y'} = \frac{1}{2}(-1000) - \frac{1}{2}(-5000)\cos 2(55.9°) - (-1000)\sin 2(55.9°)$$

$$= -500\ psi$$

Strain varies from point to point like stress

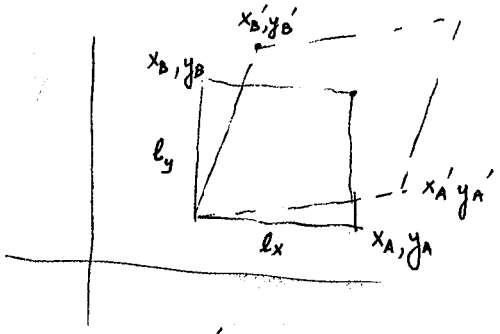

$$\frac{y_B' - y_B}{l_y} = \epsilon_{yy} \qquad \frac{x_A' - x_A}{l_x} = \epsilon_{xx}$$

$$\frac{x_B' - x_B}{l_y + \Delta l_y} + \frac{y_A' - y_A}{l_x + \Delta l_x} \approx \frac{x_B' - x_B}{l_y} + \frac{y_A' - y_A}{l_x} = 2 \text{ average shear angle} =$$

$$\therefore \quad \epsilon_{yy} = \frac{\partial v}{\partial y} \qquad \epsilon_{xx} = \frac{\partial u}{\partial x} \qquad \gamma_{xy} = \frac{\partial u}{\partial y} + \frac{\partial v}{\partial x} = 2\epsilon_{xy}$$

strain units in/in , m/m , μS = microstrain 10^{-6} in/in

when we define the displ strains in this way, where we relate changes to the undeformed body - Lagrangian . These changes occur due to loading on body

in 3-D. $\epsilon_{ij} = \frac{1}{2}\left[\frac{\partial u_i}{\partial x_j} + \frac{\partial u_j}{\partial x_i}\right] \qquad i = j$

These are strain displacement relationships

$$\left[\frac{\partial u_i}{\partial x_j} + \frac{\partial u_j}{\partial x_i}\right] \qquad i \neq j$$

actually $e_{ij} = \epsilon_{ij} + \omega_{ij}$ where $\omega_{ij} = \frac{1}{2}\left(\frac{\partial u_i}{\partial x_j} - \frac{\partial u_j}{\partial x_i}\right)$.

for small deformations $e_{ij} = \epsilon_{ij}$

we can write $\underline{\epsilon} = L\,\underline{u}$

$\underline{\epsilon} = (\epsilon_{xx}, \epsilon_{yy}, \epsilon_{xy})^T$ —— $L = \begin{bmatrix} \frac{\partial}{\partial x} & 0 \\ 0 & \frac{\partial}{\partial y} \\ \frac{\partial}{\partial x} & \frac{\partial}{\partial y} \end{bmatrix}$

$\underline{u} = (u, v)$

strains are not independent but note that

$$\frac{\partial^2}{\partial y^2}\epsilon_{xx} + \frac{\partial^2}{\partial x^2}\epsilon_{yy} = \frac{\partial^2 \gamma_{xy}}{\partial x \partial y} \qquad \text{Compatability}$$

$$\frac{\partial^3 u}{\partial y^2 \partial x} + \frac{\partial^3 v}{\partial x^2 \partial y} = \frac{\partial^2}{\partial x \partial y}\left[\frac{\partial u}{\partial y} + \frac{\partial v}{\partial x}\right]$$

This is because we have 2 displ & 3 strains

in 3-D 3 displ & 6 strains $\Rightarrow$ we get 3 such eqns.

- For linear elastic materials having small deformations, we assume that material remains with its proportional limit. For simple one-D case $\sigma = E\epsilon$ (Constitutive law)

we need constitutive law to have a well posed problem that can be solved

in 3-D analysis 15 unknowns
- 3 Disp
- 6 stresses
- 6 strains

15 eqs.
- 3 equilib.
- 6 strain-disp eqns. (compatibility derived from this)
- 6 stress-strain relationships

in general form $\underline{\sigma} = D(\underline{\epsilon} - \underline{\epsilon}_0) + \underline{\sigma}_0$

D material property matrix

ϵ strain

ϵ_0, σ_0 initial stress & strain conditions. (σ_0 due to temp effects, prestress & prestrain)

for 3-D $D = 6\times 6 = \frac{E}{(1+\nu)(1-2\nu)}\begin{bmatrix} 1-\nu & \nu & \nu & 0 & 0 & 0 \\ \nu & 1-\nu & \nu & 0 & 0 & 0 \\ \nu & \nu & 1-\nu & 0 & 0 & 0 \\ 0 & 0 & 0 & \frac{1-2\nu}{2} & 0 & 0 \\ 0 & 0 & 0 & 0 & \frac{1-2\nu}{2} & 0 \\ 0 & 0 & 0 & 0 & 0 & \frac{1-2\nu}{2} \end{bmatrix}$ in

surface tractions

if you dot a vector w/ a vector you get component of vector A along line of action of vector B or vice versa

since stress is a tensor. $\sigma = n_i \sigma_{ij} n_j$ $\quad i = 1,2,3$ $\quad j = 1,2,3$

$$\sigma \cdot n_j = n_i \sigma_{ij} \Rightarrow \text{vector with 3 components}$$

let $\underline{n}_x = \underline{n}_1 \quad \underline{n}_y = \underline{n}_2 \quad \underline{n}_z = n_3$

$$n_i \sigma_{ij} \underbrace{n_j}_{\substack{\| \\ 1 \text{ if } j=3}} \cdot n_3$$

$$n_i \sigma_{i3} = \underbrace{n_1 \sigma_{13} + n_2 \sigma_{23} + n_3 \sigma_{33}}_{\text{vector which is a traction}}$$

8.1 INTRODUCTION

The failure of engineering materials is almost always an undesirable event for several reasons; these include human lives that are put in jeopardy, economic losses, and the interference with the availability of products and services. Even though the causes of failure and the behavior of materials may be known, prevention of failures is difficult to guarantee. The usual causes are improper materials selection and processing and inadequate design of the component or its misuse. It is the responsibility of the engineer to anticipate and plan for possible failure and, in the event that failure does occur, to assess its cause and then take appropriate preventative measures against future incidents.

Topics to be addressed in this chapter are the following: simple fracture (both ductile and brittle modes), fundamentals of fracture mechanics, impact fracture testing, the ductile-to-brittle transition, fatigue, and creep. These discussions include failure mechanisms, testing techniques, and methods by which failure may be prevented or controlled.

FRACTURE

8.2 FUNDAMENTALS OF FRACTURE

Simple fracture is the separation of a body into two or more pieces in response to an imposed stress that is static (i.e., constant or slowly changing with time) and at temperatures that are low relative to the melting temperature of the material. The applied stress may be tensile, compressive, shear, or torsional; the present discussion will be confined to fractures that result from uniaxial tensile loads. For engineering materials, two fracture modes are possible: **ductile** and **brittle.** Classification is based on the ability of a material to experience plastic deformation. Ductile materials typically exhibit substantial plastic deformation with high energy absorption before fracture. On the other hand, there is normally little or no plastic deformation with low energy absorption accompanying a brittle fracture. The tensile stress–strain behaviors of both fracture types may be reviewed in Figure 6.12.

"Ductile" and "brittle" are relative terms; whether a particular fracture is one mode or the other depends on the situation. Ductility may be quantified in terms of percent elongation (Equation 6.10) and percent area reduction (Equation 6.11). Furthermore, ductility is a function of temperature of the material, the strain rate, and the stress state. The disposition of normally ductile materials to fail in a brittle manner is discussed in Section 8.6.

Any fracture process involves two steps—crack formation and propagation— in response to an imposed stress. The mode of fracture is highly dependent on the mechanism of crack propagation. Ductile fracture is characterized by extensive plastic deformation in the vicinity of an advancing crack. Furthermore, the process proceeds relatively slowly as the crack length is extended. Such a crack is often said to be *stable*. That is, it resists any further extension unless there is an increase in the applied stress. In addition, there will ordinarily be evidence of appreciable gross deformation at the fracture surfaces (e.g., twisting and tearing). On the other hand, for brittle fracture, cracks may spread extremely rapidly, with very little accompanying plastic

deformation. Such cracks may be said to be *unstable*, and crack propagation, once started, will continue spontaneously without an increase in magnitude of the applied stress.

Ductile fracture is almost always preferred for two reasons. First, brittle fracture occurs suddenly and catastrophically without any warning; this is a consequence of the spontaneous and rapid crack propagation. On the other hand, for ductile fracture, the presence of plastic deformation gives warning that fracture is imminent, allowing preventive measures to be taken. Second, more strain energy is required to induce ductile fracture inasmuch as ductile materials are generally tougher. Under the action of an applied tensile stress, most metal alloys are ductile, whereas ceramics are notably brittle, and polymers may exhibit both types of fracture.

8.3 DUCTILE FRACTURE

Ductile fracture surfaces will have their own distinctive features on both macroscopic and microscopic levels. Figure 8.1 shows schematic representations for two characteristic macroscopic fracture profiles. The configuration shown in Figure 8.1*a* is found for extremely soft metals, such as pure gold and lead at room temperature, and other metals, polymers, and inorganic glasses at elevated temperatures. These highly ductile materials neck down to a point fracture, showing virtually 100% area reduction.

The most common type of tensile fracture profile for ductile metals is that represented in Figure 8.1*b*, which fracture is preceded by only a moderate amount of necking. The fracture process normally occurs in several stages (Figure 8.2). First, after necking begins, small cavities, or microvoids, form in the interior of the cross section, as indicated in Figure 8.2*b*. Next, as deformation continues, these microvoids enlarge, come together, and coalesce to form an elliptical crack, which has its long axis perpendicular to the stress direction. The crack continues to grow in a direction parallel to its major axis by this microvoid coalescence process (Figure 8.2*c*). Finally, fracture ensues by the rapid propagation of a crack around the outer perimeter of the neck (Figure 8.2*d*), by shear deformation at an angle of about 45° with the tensile axis—this is the angle at which the shear stress is a maximum. Sometimes a fracture having this characteristic surface contour is termed a *cup-and-cone fracture* because one of the mating surfaces is in the form of a cup, the other like a cone. In this type of fractured specimen (Figure 8.3*a*), the central interior region of the surface has an irregular and fibrous appearance, which is indicative of plastic deformation.

Much more detailed information regarding the mechanism of fracture is available from microscopic examination, normally using electron microscopy. Studies of this

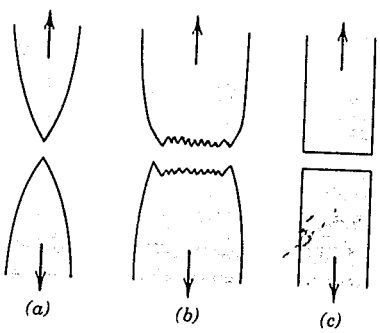

Figure 8.1 (*a*) Highly ductile fracture in which the specimen necks down to a point. (*b*) Moderately ductile fracture after some necking. (*c*) Brittle fracture without any plastic deformation.

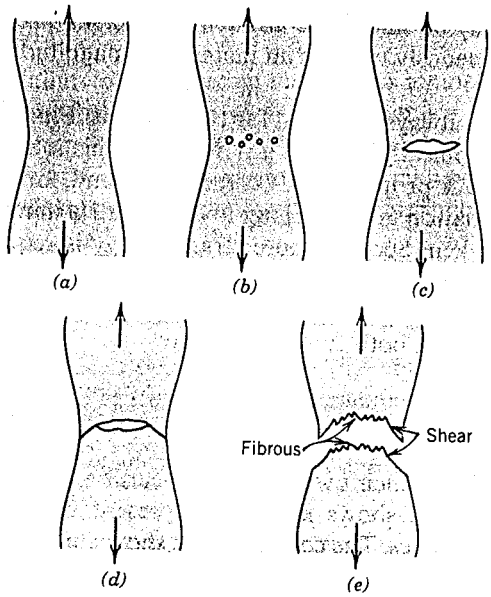

Figure 8.2 Stages in the cup-and-cone fracture. (*a*) Initial necking. (*b*) Small cavity formation. (*c*) Coalescence of cavities to form a crack. (*d*) Crack propagation. (*e*) Final shear fracture at a 45° angle relative to the tensile direction. (From K. M. Ralls, T. H. Courtney, and J. Wulff, *Introduction to Materials Science and Engineering*, p. 468. Copyright © 1976 by John Wiley & Sons, New York. Reprinted by permission of John Wiley & Sons, Inc.)

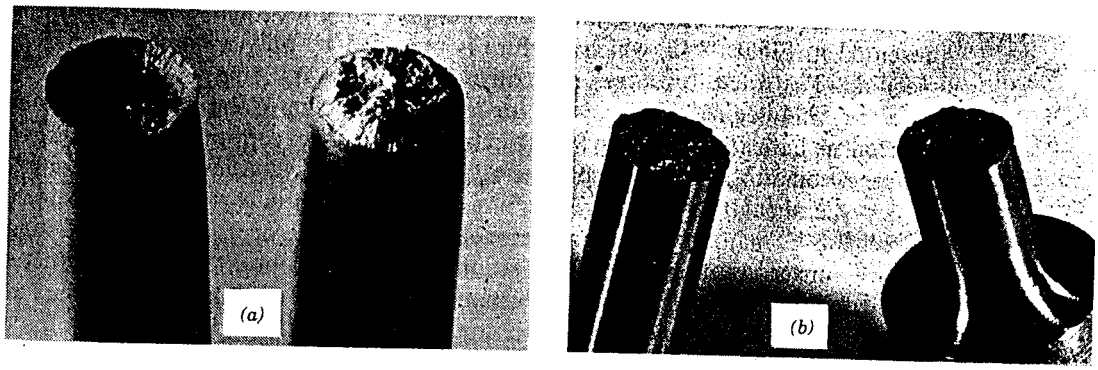

Figure 8.3 (*a*) Cup-and-cone fracture in aluminum. (*b*) Brittle fracture in a mild steel. From H. W. Hayden, W. G. Moffatt, and J. Wulff, *The Structure and Properties of Materials*, Vol. III, *Mechanical Behavior*, p. 144. Copyright © 1965 by John Wiley & Sons, New York. Reprinted by permission of John Wiley & Sons, Inc.)

type are termed *fractographic*. The electron microscope is preferred for fractographic examinations since it has a much better resolution and depth of field than does the optical microscope; these characteristics are necessary to reveal the topographical features of fracture surfaces. Ordinarily, the scanning electron microscope (SEM) is used, wherein the specimen is viewed directly.

When the fibrous central region of a cup-and-cone fracture surface is examined with the electron microscope at a high magnification, it will be found to consist of numerous spherical "dimples" (Figure 8.4*a*); this structure is characteristic of fracture resulting from uniaxial tensile failure. Each dimple is one half of a microvoid that formed and then separated during the fracture process. Dimples also form on the 45° shear lip of the cup-and-cone fracture. However, these will be elongated or C-shaped,

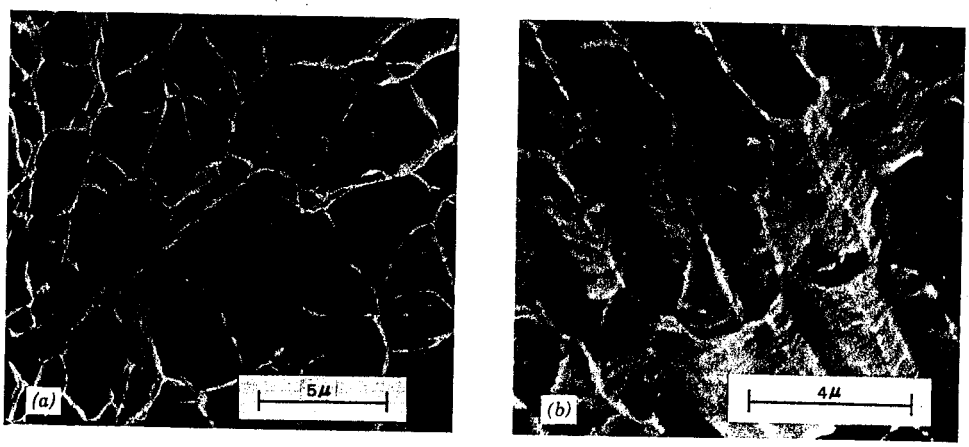

Figure 8.4 (*a*) Scanning electron fractograph showing spherical dimples characteristic of ductile fracture resulting from uniaxial tensile loads. (*b*) Scanning electron fractograph showing parabolic-shaped dimples characteristic of ductile fracture resulting from shear loading. (From R. W. Hertzberg, *Deformation and Fracture Mechanics of Engineering Materials*, 3rd edition. Copyright © 1989 by John Wiley & Sons, New York. Reprinted by permission of John Wiley & Sons, Inc.)

as shown in Figure 8.4*b*. This parabolic shape may be indicative of shear failure. Furthermore, other microscopic fracture surface features are also possible. Fractographs such as those shown in Figures 8.4*a* and 8.4*b* provide valuable information in the analyses of fracture, such as the fracture mode, the stress state, as well as the site of crack initiation.

8.4 BRITTLE FRACTURE

Brittle fracture takes place without any appreciable deformation, and by rapid crack propagation. The direction of crack motion is very nearly perpendicular to the direction of the applied tensile stress and yields a relatively flat fracture surface, as indicated in Figure 8.1*c*.

Fracture surfaces of materials that failed in a brittle manner will have their own distinctive patterns; any signs of gross plastic deformation will be absent. For example, in some steel pieces, a series of V-shaped "chevron" markings may form near the center of the fracture cross section that point back toward the crack initiation site (Figure 8.5*a*). Other brittle fracture surfaces contain lines or ridges that radiate from the origin of the crack in a fanlike pattern (Figure 8.5*b*). Often, both of these marking patterns will be sufficiently coarse to be discerned with the naked eye. For very hard and fine-grained metals, there will be no discernible fracture pattern. Brittle fracture in amorphous materials, such as ceramic glasses, yields a relatively shiny and smooth surface.

For most brittle crystalline materials, crack propagation corresponds to the successive and repeated breaking of atomic bonds along specific crystallographic planes; such a process is termed *cleavage*. This type of fracture is said to be **transgranular** (or *transcrystalline*), because the fracture cracks pass through the grains. Macroscopically, the fracture surface may have a grainy or faceted texture (Figure 8.3*b*), as a result of

8.5 PRINCIPLES OF FRACTURE MECHANICS

Brittle fracture of normally ductile materials, such as that shown on page 189, has demonstrated the need for a better understanding of the mechanisms of fracture. Extensive research endeavors over the past several decades have led to the evolution of the field of **fracture mechanics.** Knowledge gleaned therefrom allows quantification of the relationships between material properties, stress level, the presence of crack-producing flaws, and crack propagation mechanisms. Design engineers are now better equipped to anticipate, and thus prevent, structural failures. The present discussion centers on some of the fundamental principles of the mechanics of fracture.

Stress Concentration

The fracture strength of a solid material is a function of the cohesive forces that exist between atoms. On this basis, the theoretical cohesive strength of a brittle elastic solid has been estimated to be approximately $E/10$, where E is the modulus of elasticity. The experimental fracture strengths of most engineering materials normally lie between 10 and 1000 times below this theoretical value. In the 1920s, A. A. Griffith proposed that this discrepancy between theoretical cohesive strength and observed fracture strength could be explained by the presence of very small, microscopic flaws or cracks that always exist under normal conditions at the surface and within the interior of a body of material. These flaws are a detriment to the fracture strength because an applied stress may be amplified or concentrated at the tip, the magnitude of this amplification depending on crack orientation and geometry. This phenomenon is demonstrated in Figure 8.7, a stress profile across a cross section containing an internal crack. As indicated by this profile, the magnitude of this localized stress diminishes

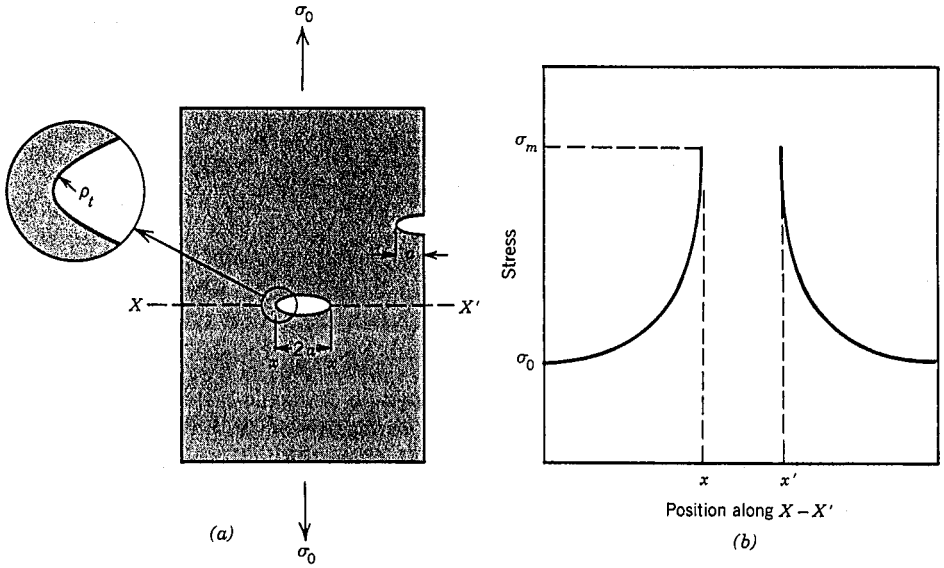

Figure 8.7 (*a*) The geometry of surface and internal cracks. (*b*) Schematic stress profile along the line X–X' in (*a*), demonstrating stress amplification at crack tip positions.

with distance away from the crack tip. At positions far removed, the stress is just the nominal stress σ_0, or the load divided by the specimen cross-sectional area. Due to their ability to amplify an applied stress in their locale, these flaws are sometimes called **stress raisers.**

If it is assumed that a crack has an elliptical shape and is oriented with its long axis perpendicular to the applied stress, the maximum stress at the crack tip, σ_m, may be approximated by

$$\sigma_m = 2\sigma_0\left(\frac{a}{\rho_t}\right)^{1/2} \tag{8.1}$$

where σ_0 is the magnitude of the nominal applied tensile stress, ρ_t is the radius of curvature of the crack tip (Figure 8.7*a*), and a represents the length of a surface crack, or half of the length of an internal one. Thus for a relatively long microcrack that has a small tip radius of curvature, the factor $(a/\rho_t)^{1/2}$ may be very large. This will yield a value of σ_m that is many times that of σ_0.

Sometimes the ratio σ_m/σ_0 is denoted as the *stress concentration factor* K_t:

$$K_t = \frac{\sigma_m}{\sigma_0} = 2\left(\frac{a}{\rho_t}\right)^{1/2} \tag{8.2}$$

which is simply a measure of the degree to which an external stress is amplified at the tip of a small crack.

By way of comment, it should be said that stress amplification is not restricted to these microscopic defects; it may occur at macroscopic internal discontinuities (e.g., holes), at sharp corners, and notches in large structures. Figure 8.8 shows theoretical stress concentration factor curves for several simple and common components.

Furthermore, the effect of a stress raiser is more significant in brittle than in ductile materials. For a ductile material, plastic deformation ensues when the maximum stress exceeds the yield strength. This leads to a more uniform distribution of stress in the vicinity of the stress raiser and to the development of a maximum stress concentration factor less than the theoretical value. Such yielding and stress redistribution do not occur to any appreciable extent around flaws and discontinuities in brittle materials; therefore, essentially the theoretical stress concentration will result.

Griffith then went on to propose that all brittle materials contain a population of small cracks and flaws that have a variety of sizes, geometries, and orientations. Fracture will result when, upon application of a tensile stress, the theoretical cohesive strength of the material is exceeded at the tip of one of these flaws. This leads to the formation of a crack that then rapidly propagates. If no flaws were present, the fracture strength would be equal to the cohesive strength of the material. Very small and virtually defect-free metallic and ceramic whiskers have been grown with fracture strengths that approach their theoretical values.

Griffith Theory of Brittle Fracture

During the propagation of a crack, there is a release of what is termed the *elastic strain energy,* some of the energy that is stored in the material as it is elastically deformed. Furthermore, during the crack extension process, new free surfaces are created at the faces of a crack, which give rise to an increase in surface energy of the system. Griffith developed a criterion for crack propagation of an elliptical crack

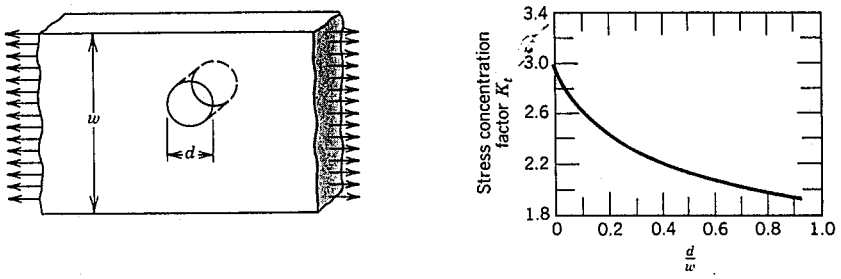

(a)

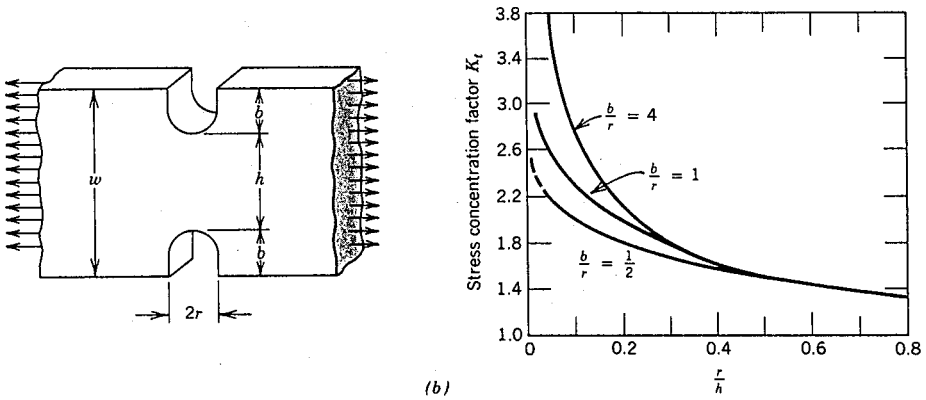

(b)

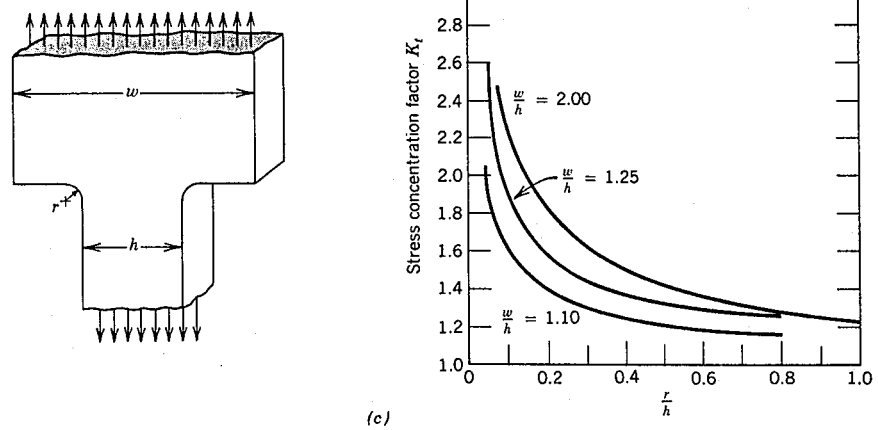

(c)

Figure 8.8 Theoretical stress concentration factor curves for three simple geometrical shapes. (From G. H. Neugebauer, *Prod. Eng.* (NY), Vol. 14, pp. 82–87, 1943.)

(Figure 8.7*a*) by performing an energy balance using these two energies. He demonstrated that the critical stress σ_c required for crack propagation in a brittle material is described by

$$\sigma_c = \left(\frac{2E\gamma_s}{\pi a}\right)^{1/2} \tag{8.3}$$

where

E = modulus of elasticity
γ_s = specific surface energy
a = one half the length of an internal crack

Worth noting is that this expression does not involve the crack tip radius ρ_t, as does the stress concentration equation (Equation 8.1); however, it is assumed that the radius is sufficiently sharp (on the order of the interatomic spacing) so as to raise the local stress at the tip above the cohesive strength of the material.

The previous development applies only to completely brittle materials for which there is no plastic deformation. Most metals and many polymers do experience some plastic deformation during fracture; this leads to a blunting of the tip of a crack, a decrease in the crack tip radius, and subsequently an increase in the fracture strength. Mathematically, this may be accommodated by replacing γ_s in Equation 8.3 by $\gamma_s + \gamma_p$, where γ_p represents a plastic deformation energy associated with crack extension. For highly ductile materials, it may be the case that $\gamma_p \gg \gamma_s$.

In the 1950s, G. R. Irwin chose to incorporate both γ_s and γ_p into a single term, $\mathcal{G}$, as

$$\mathcal{G} = 2(\gamma_s + \gamma_p) \tag{8.4}$$

$\mathcal{G}$ is known as the *strain energy release rate,* and crack extension occurs when it exceeds a critical value, $\mathcal{G}_c$.

Stress Analysis of Cracks

As we continue to explore the development of fracture mechanics, it is worthwhile to examine the stress distributions in the vicinity of the tip of an advancing crack. There are three fundamental ways, or modes, by which a load can operate on a crack, and each will affect a different crack surface displacement; these are illustrated in Figure 8.9. Mode I is an opening (or tensile) load, whereas modes II and III are sliding

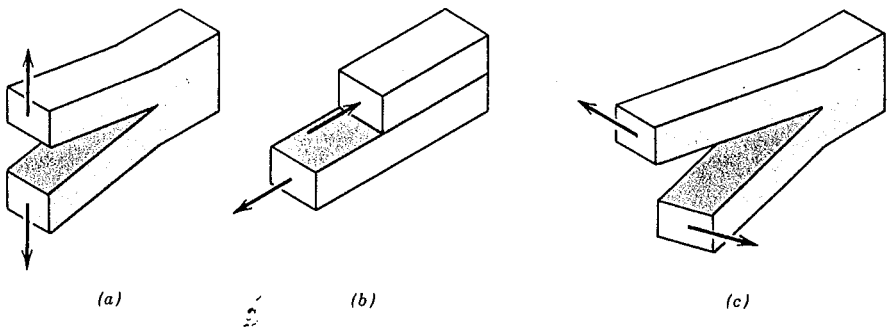

Figure 8.9 The three modes of crack surface displacement. (*a*) Mode I, opening or tensile mode; (*b*) mode II, sliding mode; and (*c*) mode III, tearing mode.

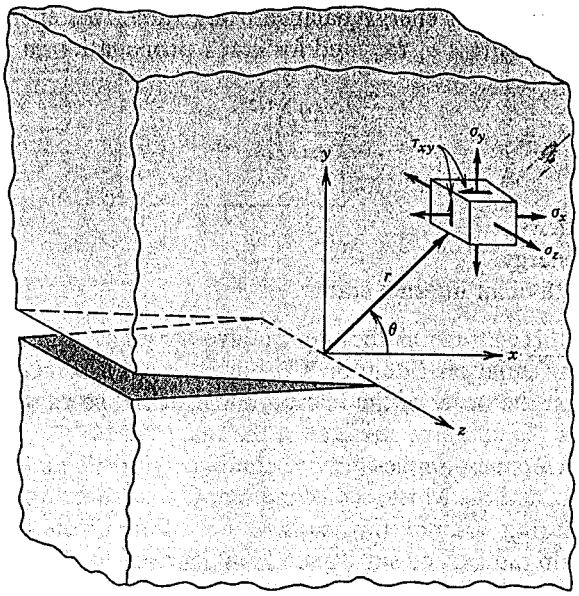

Figure 8.10 The stresses acting in front of a crack that is loaded in a tensile mode I configuration.

and tearing modes, respectively. Mode I is encountered most frequently, and only it will be treated in the ensuing discussion on fracture mechanics.

For this mode I configuration, the stresses acting on an element of material are shown in Figure 8.10. Using elastic theory principles and the notation indicated, tensile (σ_x and σ_y) and shear (τ_{xy}) stresses are functions of both radial distance r and the angle θ as follows:[1]

$$\sigma_x = \frac{K}{\sqrt{2\pi r}} f_x(\theta) \tag{8.5a}$$

$$\sigma_y = \frac{K}{\sqrt{2\pi r}} f_y(\theta) \tag{8.5b}$$

$$\tau_{xy} = \frac{K}{\sqrt{2\pi r}} f_{xy}(\theta) \tag{8.5c}$$

If the plate is thin relative to the dimensions of the crack, then $\sigma_z = 0$, or a condition of *plane stress* is said to exist. At the other extreme (a relatively thick plate)

[1] The $f(\theta)$ functions are as follows:

$$f_x(\theta) = \cos\frac{\theta}{2}\left(1 - \sin\frac{\theta}{2}\sin\frac{3\theta}{2}\right)$$

$$f_y(\theta) = \cos\frac{\theta}{2}\left(1 + \sin\frac{\theta}{2}\sin\frac{3\theta}{2}\right)$$

$$f_{xy}(\theta) = \sin\frac{\theta}{2}\cos\frac{\theta}{2}\cos\frac{3\theta}{2}$$

$\sigma_z = \nu(\sigma_x + \sigma_y)$, and the state is referred to as **plane strain** (since $\epsilon_z = 0$); ν in this expression is Poisson's ratio.

In Equations 8.5, the parameter K is termed the **stress intensity factor;** its use provides for a convenient specification of the stress distribution around a flaw. It should be noted that this stress intensity factor and the stress concentration factor K_t in Equation 8.2, although similar, are not equivalent.

The value of the stress intensity factor is a function of the applied stress, the size and position of the crack, as well as the geometry of the solid piece in which the crack is located.

Fracture Toughness

In the above discussion, a criterion was developed for the crack propagation in a brittle material containing a flaw; fracture occurs when the applied stress level exceeds some critical value σ_c (Equation 8.3). Similarly, since the stresses in the vicinity of a crack tip can be defined in terms of the stress intensity factor, a critical value of this parameter exists, which may be used to specify the conditions for brittle fracture; this critical value is termed the **fracture toughness** K_c. In general, it may be expressed in the form

$$K_c = Y\sigma\sqrt{\pi a} \tag{8.6}$$

where Y is a dimensionless parameter that depends on both the specimen and crack geometries. For example, for the plate of infinite width in Figure 8.11*a*, $Y = 1.0$; or for a plate of semi-infinite width containing an edge crack of length a (Figure 8.11*b*), $Y = 1.1$.

By definition, fracture toughness is a property that is the measure of a material's resistance to brittle fracture when a crack is present. It should also be noted that fracture toughness has the unusual units of psi$\sqrt{\text{in.}}$ (MPa$\sqrt{\text{m}}$).

For relatively thin specimens, the value of K_c will depend on and decrease with increasing specimen thickness B, as indicated in Figure 8.12. Eventually, K_c becomes independent of B, at which time the condition of plane strain is said to exist.[2] The constant K_c value for thicker specimens is known as the **plane strain fracture toughness** K_{Ic}, which is also defined by

$$K_{Ic} = Y\sigma\sqrt{\pi a} \tag{8.7}$$

It is the fracture toughness normally cited since its value is always less than K_c. The I subscript for K_{Ic} denotes that this critical value of K is for mode I crack displacement, as illustrated in Figure 8.9*a*. Brittle materials, for which appreciable plastic deformation is not possible in front of an advancing crack, have low K_{Ic} values and are vulnerable to catastrophic failure. On the other hand, K_{Ic} values are relatively large for ductile materials. Fracture mechanics is especially useful in predicting catastrophic failure in

[2] Experimentally, it has been verified that for plane strain conditions

$$B \geq 2.5\left(\frac{K_{Ic}}{\sigma_y}\right)^2 \tag{8.8}$$

where σ_y is the 0.002 strain offset yield strength of the material.

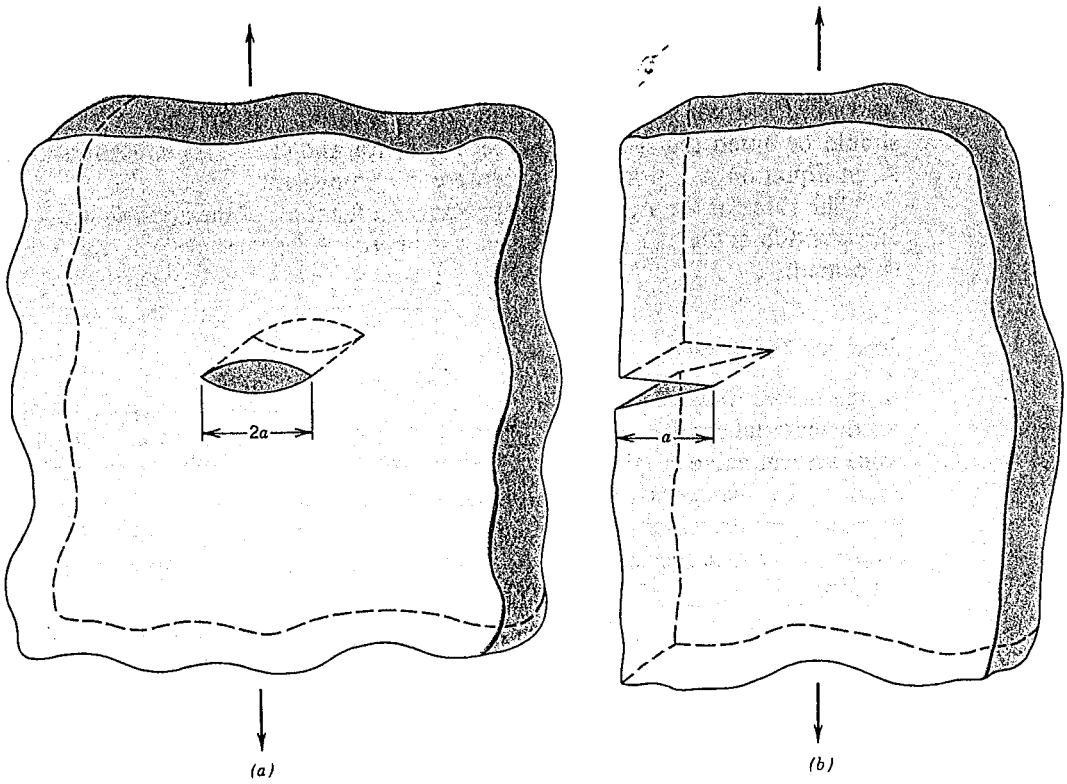

Figure 8.11 Schematic representations of (*a*) an interior crack in a plate of infinite width, and (*b*) an edge crack in a plate of semi-infinite width.

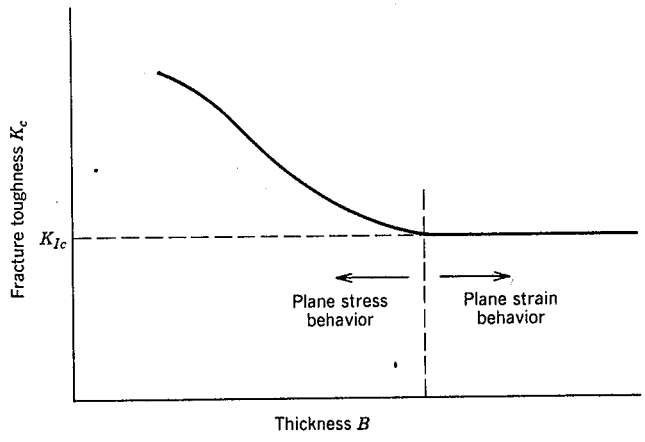

Figure 8.12 Schematic representation showing the effect of plate thickness on fracture toughness.

TABLE 8.1 Room-Temperature Yield Strength and Plane Strain Fracture Toughness Data for Selected Engineering Materials

Material	Yield Strength		K_{Ic}	
	psi × 10^3	MPa	psi$\sqrt{\text{in.}}$ × 10^3	MPa$\sqrt{\text{m}}$
Metals				
Aluminum alloy[a] (2024-T351)	47	325	33	36
Aluminum alloy[a] (7075-T651)	73	505	26	29
Alloy steel[a] (4340 tempered @ 260°C)	238	1640	45.8	50.0
Alloy steel[a] (4340 tempered @ 425°C)	206	1420	80.0	87.4
Titanium alloy[a] (Ti-6Al-4V)	130	910	40–60	44–66
Ceramics				
Aluminum oxide	—	—	2.7–4.8	3.0–5.3
Soda-lime glass	—	—	0.64–0.73	0.7–0.8
Concrete	—	—	0.18–1.27	0.2–1.4
Polymers				
Polymethyl methacrylate (PMMA)	—	—	0.9	1.0
Polystyrene (PS)	—	—	0.73–1.0	0.8–1.1

[a] **Source:** Adapted with permission from *1989 Guide to Selecting Engineered Materials*, ASM INTERNATIONAL, Materials Park, OH, 1989.

materials having intermediate ductilities. Plane strain fracture toughness values for a number of different materials are presented in Table 8.1.

The stress intensity factor K in Equations 8.5 and the plane strain fracture toughness K_{Ic} are related to one another in the same sense as are stress and yield strength. A material may be subjected to many values of stress; however, there is a specific stress level at which the material plastically deforms—that is, the yield strength. Likewise, a variety of K's are possible, whereas K_{Ic} is unique for a particular material.

Several different testing techniques are used to measure K_{Ic}. Virtually any specimen size and shape consistent with mode I crack displacement may be utilized, and accurate values will be realized provided that the Y scale parameter in Equation 8.7 has been properly determined.

The plane strain fracture toughness K_{Ic} is a fundamental material property that depends on many factors, the most influential of which are temperature, strain rate, and microstructure. The magnitude of K_{Ic} diminishes with increasing strain rate and decreasing temperature. Furthermore, an enhancement in yield strength wrought by solid solution or dispersion additions or by strain hardening generally produces a corresponding decrease in K_{Ic}. Furthermore, K_{Ic} normally increases with reduction in grain size as composition and other microstructural variables are maintained constant. Yield strengths are included for some of the materials listed in Table 8.1.

Design Using Fracture Mechanics

According to Equations 8.6 and 8.7, three variables must be considered relative to the possibility for fracture of some structural component—viz the fracture toughness (K_c) or plane strain fracture toughness (K_{Ic}), the imposed stress (σ), and the flaw size (a), assuming, of course, that Y has been determined. When designing a component, it is first important to decide which of these variables are constrained by the application and which are subject to design control. For example, material selection (and hence K_c or K_{Ic}) is often dictated by factors such as density (for lightweight applications) or the corrosion characteristics of the environment. Or, the allowable flaw size is either measured or specified by the limitations of available flaw detection techniques. It is important to realize, however, that once any combination of two of the above parameters is prescribed, the third becomes fixed (Equations 8.6 and 8.7). For example, assume that K_{Ic} and the magnitude of a are specified by application constraints; therefore, the design (or critical) stress σ_c must be

$$\sigma_c \leq \frac{K_{Ic}}{Y\sqrt{\pi a}} \tag{8.9}$$

On the other hand, if stress level and plane strain fracture toughness are fixed by the design situation, then the maximum allowable flaw size a_c is

$$a_c = \frac{1}{\pi}\left(\frac{K_{Ic}}{\sigma Y}\right)^2 \tag{8.10}$$

A number of nondestructive test (NDT) techniques have been developed that permit detection and measurement of both internal and surface flaws. Such NDT methods are used to avoid the occurrence of catastrophic failure by examining structural components for defects and flaws that have dimensions approaching the critical size.

8.6 IM

EXAMPLE PROBLEM 8.1

A structural component in the form of a very wide plate, as shown in Figure 8.11*a*, is to be fabricated from a 4340 steel. Two sheets of this alloy, each having a different heat treatment and thus different mechanical properties are available. One, denoted material A, has a yield strength of 860 MPa (125,000 psi) and a plane strain fracture toughness of 98.9 MPa$\sqrt{\text{m}}$ (90,000 psi$\sqrt{\text{in.}}$). For the other, material Z, σ_y and K_{Ic} values are 1515 MPa (220,000 psi) and 60.4 MPa$\sqrt{\text{m}}$ (55,000 psi$\sqrt{\text{in.}}$), respectively.

(a) For each alloy, determine whether or not plane strain conditions prevail if the plate is 10 mm (0.39 in.) thick.

(b) It is not possible to detect flaw sizes less than 3 mm, which is the resolution limit of the flaw detection apparatus. If the plate thickness is sufficient such that the K_{Ic} value may be used, determine whether or not a critical flaw is subject to detection. Assume that the design stress level is one half of the yield strength; also, for this configuration, the value of Y is 1.0.

SOLUTION

(a) Plane strain is established by Equation 8.8. For material A,

$$B = 2.5\left(\frac{K_{Ic}}{\sigma_y}\right)^2 = 2.5\left(\frac{98.9\ \text{MPa}\sqrt{\text{m}}}{860\ \text{MPa}}\right)^2$$

$$= 0.033\ \text{m} = 33\ \text{mm}\ (1.30\ \text{in.})$$

Thus plane strain conditions *do not* hold for material A because this value of B is greater than 10 mm, the actual plate thickness; the situation is one of plane stress and must be treated as such.

And for material Z,

$$B = 2.5\left(\frac{60.4\ \text{MPa}\sqrt{\text{m}}}{1515\ \text{MPa}}\right)^2 = 0.004\ \text{m} = 4.0\ \text{mm}\ (0.16\ \text{in.})$$

which is less than the actual plate thickness, and therefore the situation is one of plane strain.

(b) We need only determine the critical flaw size for material Z because the situation for material A is not plane strain, and K_{Ic} may not be used. Employing Equation 8.10 and taking σ to be $\sigma_y/2$,

$$a_c = \frac{1}{\pi}\left(\frac{60.4\ \text{MPa}\sqrt{\text{m}}}{(1)(1515/2)\ \text{MPa}}\right)^2$$

$$= 0.002\ \text{m} = 2.0\ \text{mm}\ (0.079\ \text{in.})$$

Therefore, the critical flaw size for material Z is not subject to detection since it is less than 3 mm.

8.6 IMPACT FRACTURE TESTING

Prior to the advent of fracture mechanics as a scientific discipline, impact testing techniques were established so as to ascertain the fracture characteristics of materials. It was realized that the results of laboratory tensile tests could not be extrapolated to predict fracture behavior; for example, under some circumstances normally ductile metals fracture abruptly and with very little plastic deformation. Impact test conditions were chosen to represent those most severe relative to the potential for fracture, namely, (1) deformation at a relatively low temperature, (2) a high strain rate (i.e., rate of deformation), and (3) a triaxial stress state (which may be introduced by the presence of a notch).

Impact Testing Techniques

Two standardized tests, the **Charpy** and **Izod,** were designed and are still used to measure the **impact energy,** sometimes also termed *notch toughness.* The Charpy V-notch (CVN) technique is most commonly used in the United States. For both Charpy and Izod, the specimen is in the shape of a bar of square cross section, into which a V-notch is machined (Figure 8.13*a*). The apparatus for making V-notch impact tests is illustrated schematically in Figure 8.13*b*. The load is applied as an impact blow from a weighted pendulum hammer that is released from a cocked position at a fixed height h. The specimen is positioned at the base as shown. Upon release, a knife edge

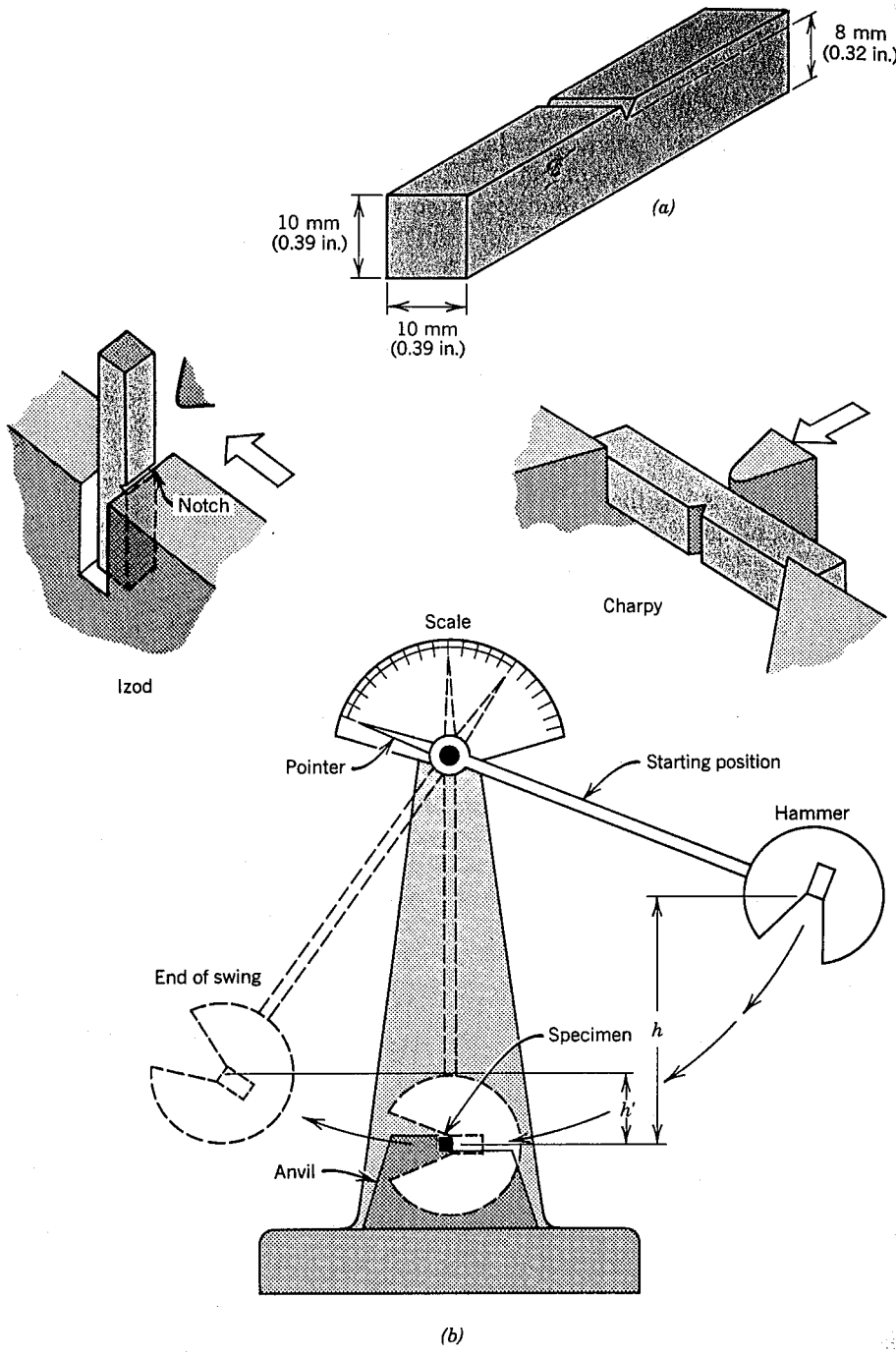

Figure 8.13 (*a*) Specimen used for Charpy and Izod impact tests. (*b*) A schematic drawing of an impact testing apparatus. The hammer is released from fixed height h and strikes the specimen; the energy expended in fracture is reflected in the difference between h and the swing height h'. Specimen placements for both Charpy and Izod tests are also shown. (Figure (*b*) adapted from H. W. Hayden, W. G. Moffatt, and J. Wulff, *The Structure and Properties of Materials*, Vol. III, *Mechanical Behavior*, p. 13. Copyright © 1965 by John Wiley & Sons, New York. Reprinted by permission of John Wiley & Sons, Inc.)

mounted on the pendulum strikes and fractures the specimen at the notch, which acts as a point of stress concentration for this high velocity impact blow. The pendulum continues its swing, rising to a maximum height h', which is lower than h. The energy absorption, computed from the difference between h and h', is a measure of the impact energy. The primary difference between the Charpy and Izod techniques lies in the manner of specimen support, as illustrated in Figure 8.13*b*. Furthermore, these are termed impact tests in light of the manner of load application. Variables including specimen size and shape as well as notch configuration and depth influence the test results.

Both plane strain fracture toughness and these impact tests determine the fracture properties of materials. The former are quantitative in nature, in that a specific property of the material is determined (i.e., K_{Ic}). The results of the impact tests, on the other hand, are more qualitative and are of little use for design purposes. Impact energies are of interest mainly in a relative sense and for making comparisons—absolute values are of little significance. Attempts have been made to correlate plane strain fracture toughnesses and CVN energies, with only limited success. Plane strain toughness tests are not as simple to perform as impact tests; furthermore, equipment and specimens are more expensive.

Ductile-to-Brittle Transition

One of the primary functions of Charpy and Izod tests is to determine whether or not a material experiences a ductile-to-brittle transition with decreasing temperature and, if so, the range of temperatures over which it occurs. The ductile-to-brittle transition is related to the temperature dependence of the measured impact energy absorption. This transition is represented for a steel by curve *A* in Figure 8.14. At

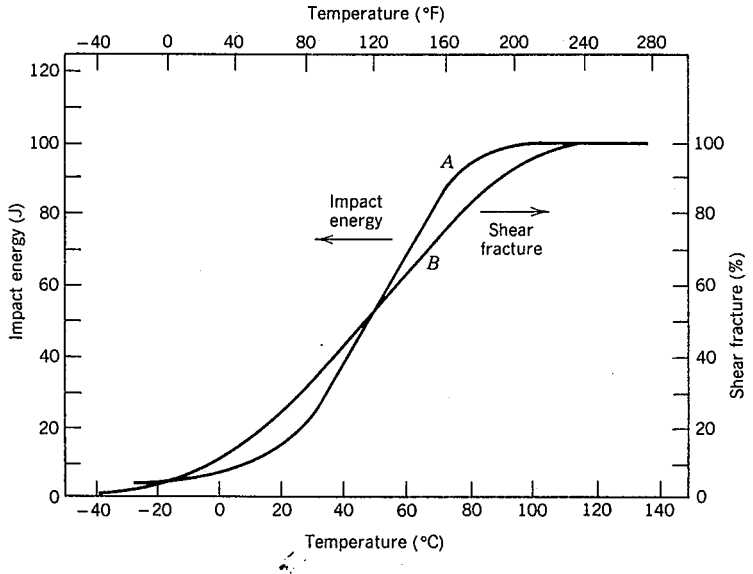

Figure 8.14 Temperature dependence of the Charpy V-notch impact energy (curve *A*) and percent shear fracture (curve *B*) for an A283 steel. (Reprinted from *Welding Journal*. Used by permission of the American Welding Society.)

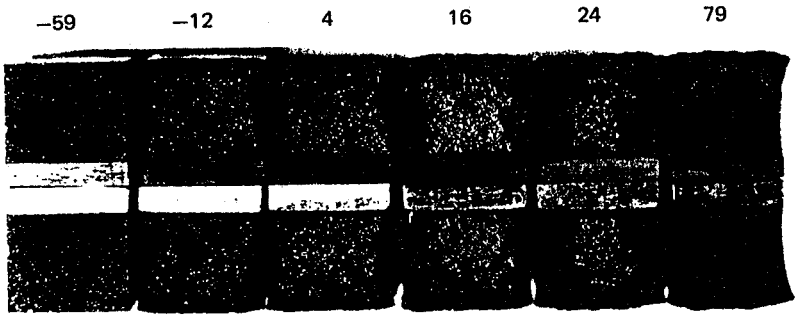

Figure 8.15 Photograph of fracture surfaces of A36 steel Charpy V-notch specimens tested at indicated temperatures (in °C). (From R. W. Hertzberg, *Deformation and Fracture Mechanics of Engineering Materials*, 3rd edition, Fig. 9.6, p. 329. Copyright © 1989 by John Wiley & Sons, Inc., New York. Reprinted by permission of John Wiley & Sons, Inc.)

higher temperatures the CVN energy is relatively large, in correlation with a ductile mode of fracture. As the temperature is lowered, the impact energy drops suddenly over a relatively narrow temperature range, below which the energy has a constant but small value; that is, the mode of fracture is brittle.

Alternatively, appearance of the failure surface is indicative of the nature of fracture, and may be used in transition temperature determinations. For ductile fracture this surface appears fibrous (or of shear character); conversely, totally brittle surfaces have a granular texture (or cleavage character). Over the ductile-to-brittle transition, features of both types will exist (Figure 8.15). Frequently, the percent shear fracture is plotted as a function of temperature—curve *B* in Figure 8.14.

For many alloys there is a range of temperatures over which the ductile-to-brittle transition occurs (Figure 8.14); this presents some difficulty in specifying a single ductile-to-brittle transition temperature. No explicit criterion has been established, and so this temperature is often defined as that temperature at which the CVN energy assumes some value (e.g., 20 J or 15 ft-lb_f), or corresponding to some given fracture appearance (e.g., 50% fibrous fracture). Matters are further complicated inasmuch as a different transition temperature may be realized for each of these criteria. Perhaps the most conservative transition temperature is that at which the fracture surface becomes 100% fibrous; on this basis, the transition temperature is approximately 110°C (230°F) for the steel alloy that is the subject of Figure 8.14.

Structures constructed from alloys that exhibit this ductile-to-brittle behavior should be used only at temperatures above the transition temperature, to avoid brittle and catastrophic failure. Classic examples of this type of failure occurred, with disastrous consequences, during World War II when a number of welded transport ships, away from combat, suddenly and precipitously split in half. The vessels were constructed of a steel alloy that possessed adequate ductility from room-temperature tensile tests. The brittle fractures occurred at relatively low ambient temperatures, at about 4°C (40°F), in the vicinity of the transition temperature of the alloy. Each fracture crack originated at some point of stress concentration, probably a sharp corner or fabrication defect, which crack then propagated around the entire girth of the ships that split.

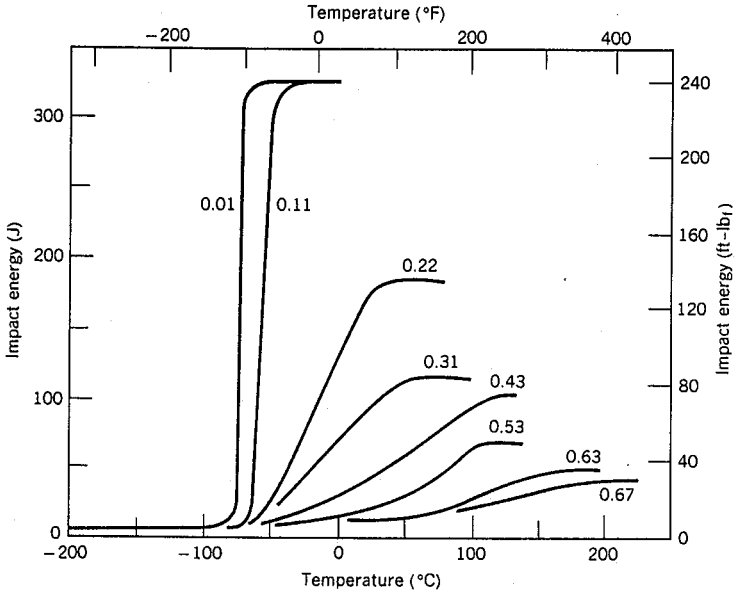

Figure 8.16 Influence of carbon content on the Charpy V-notch energy-versus-temperature behavior for steel. (Reprinted with permission from ASM International, Metals Park, OH 44073-9989, USA; Rinebolt, J. A. and Harris, W. J., Jr., "Affect of Alloying Elements on Notch Toughness of Pearlitic Steels," *Transactions of ASM*, Vol. 43, 1951.)

Not all metal alloys display a ductile-to-brittle transition. Those having FCC crystal structures (including aluminum- and copper-based alloys) remain ductile even at extremely low temperatures. However, BCC and HCP alloys experience this transition. For these materials the transition temperature is sensitive to both alloy composition and microstructure. For example, decreasing the average grain size of steels results in a lowering of the transition temperature. Also, carbon content has a decided influence on the CVN energy–temperature behavior of a steel, as indicated in Figure 8.16.

Most ceramics and polymers also experience a ductile-to-brittle transition. For ceramic materials, the transition occurs only at elevated temperatures, ordinarily in excess of 1000°C (1850°F). This behavior, as related to polymers, is discussed in Section 16.9.

FATIGUE

Fatigue is a form of failure that occurs in structures subjected to dynamic and fluctuating stresses (e.g., bridges, aircraft, and machine components). Under these circumstances it is possible for failure to occur at a stress level considerably lower than the tensile or yield strength for a static load. The term "fatigue" is used because this

type of failure normally occurs after a lengthy period of repeated stress or strain cycling. Fatigue is important inasmuch as it is the single largest cause of failure in metals, estimated to comprise approximately 90% of all metallic failures; polymers and ceramics (except for glasses) are also susceptible to this type of failure. Furthermore, it is catastrophic and insidious, occurring very suddenly and without warning.

Fatigue failure is brittlelike in nature even in normally ductile metals, in that there is very little, if any, gross plastic deformation associated with failure. The process occurs by the initiation and propagation of cracks, and ordinarily the fracture surface is perpendicular to the direction of an applied tensile stress.

8.7 CYCLIC STRESSES

The applied stress may be axial (tension-compression), flexural (bending), or torsional (twisting) in nature. In general, three different fluctuating stress–time modes are possible. One is represented schematically by a regular and sinusoidal time dependence in Figure 8.17*a*, wherein the amplitude is symmetrical about a mean zero stress level, for example, alternating from a maximum tensile stress (σ_{max}) to a minimum compressive stress (σ_{min}) of equal magnitude; this is referred to as a *reversed stress cycle.* Another type, termed *repeated stress cycle,* is illustrated in Figure 8.17*b*; the maxima and minima are asymmetrical relative to the zero stress level. Finally, the stress level may vary randomly in amplitude and frequency, as exemplified in Figure 8.17*c*.

Also indicated in Figure 8.17*b* are several parameters used to characterize the fluctuating stress cycle. The stress amplitude alternates about a *mean stress* σ_m, defined as the average of the maximum and minimum stresses in the cycle, or

$$\sigma_m = \frac{\sigma_{max} + \sigma_{min}}{2} \tag{8.11}$$

Furthermore, the *range of stress* σ_r is just the difference between σ_{max} and σ_{min}, namely,

$$\sigma_r = \sigma_{max} - \sigma_{min} \tag{8.12}$$

Stress amplitude σ_a is just one half of this range of stress, or

$$\sigma_a = \frac{\sigma_r}{2} = \frac{\sigma_{max} - \sigma_{min}}{2} \tag{8.13}$$

Finally, the *stress ratio* R is just the ratio of minimum and maximum stress amplitudes:

$$R = \frac{\sigma_{min}}{\sigma_{max}} \tag{8.14}$$

By convention, tensile stresses are positive and compressive stresses are negative. For example, for the reversed stress cycle, the value of R is -1.

8.8 THE *S–N* CURVE

As with other mechanical characteristics, the fatigue properties of materials can be determined from laboratory simulation tests. A test apparatus should be designed to duplicate as nearly as possible the service stress conditions (stress level, time frequency, stress pattern, etc.). A schematic diagram of a rotating-bending test apparatus, commonly used for fatigue testing, is shown in Figure 8.18; the compression and tensile

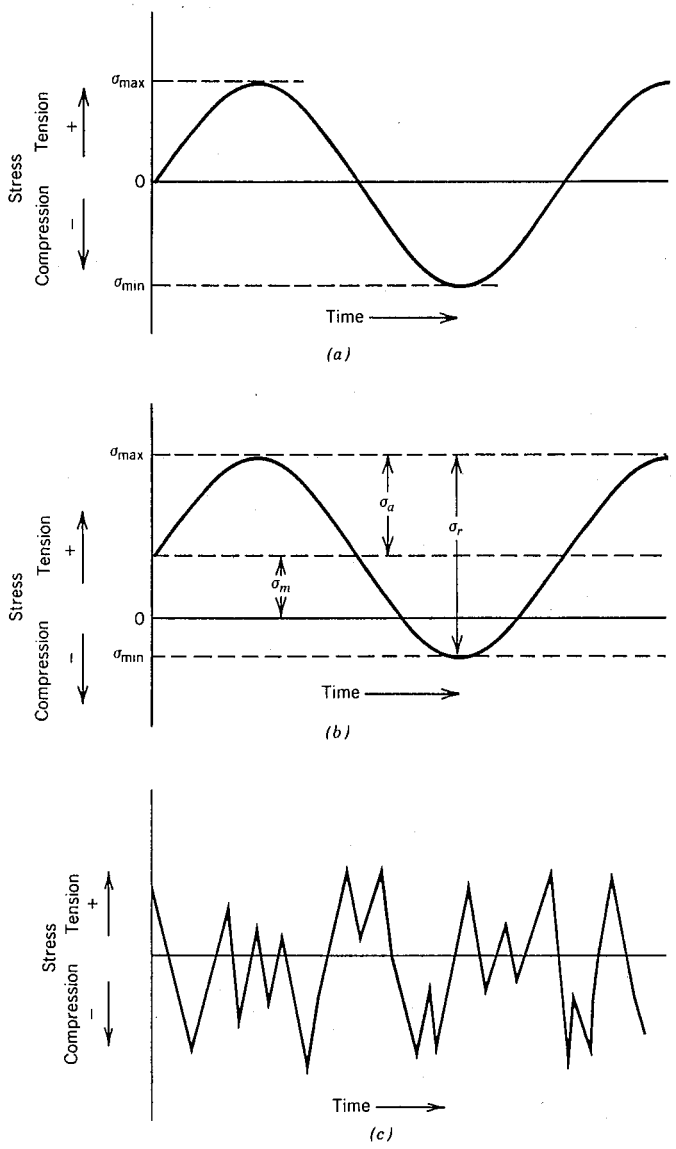

Figure 8.17 Variation of stress with time that accounts for fatigue failures. (*a*) Reversed stress cycle, in which the stress alternates from a maximum tensile stress (+) to a maximum compressive stress (−) of equal magnitude. (*b*) Repeated stress cycle, in which maximum and minimum stresses are asymmetrical relative to the zero stress level; mean stress σ_m, range of stress σ_r, and stress amplitude σ_a are indicated. (*c*) Random stress cycle.

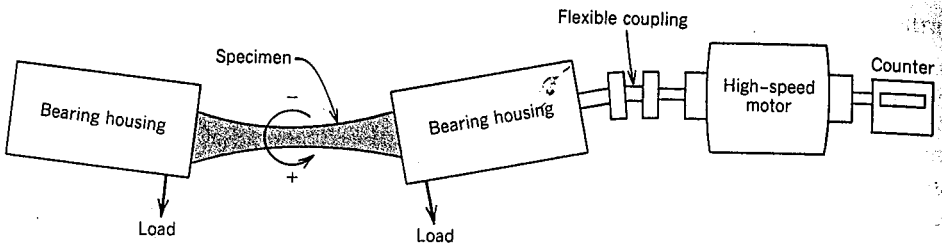

Figure 8.18 Schematic diagram of fatigue testing apparatus for making rotating-bending tests. (Adapted from C. A. Keyser, *Materials Science in Engineering*, 4th edition, Merrill Publishing Company, Columbus, OH, 1986. Reprinted by permission of the publisher.)

stresses are imposed on the specimen as it is simultaneously bent and rotated. Tests are also frequently conducted using an alternating uniaxial tension-compression stress cycle.

A series of tests are commenced by subjecting a specimen to the stress cycling at a relatively large maximum stress amplitude (σ_{max}), usually on the order of two thirds of the static tensile strength; the number of cycles to failure is counted. This procedure is repeated on other specimens at progressively decreasing maximum stress amplitudes. Data are plotted as stress S versus the logarithm of the number N of cycles to failure for each of the specimens. The values of S are normally taken as stress amplitudes (σ_a, Equation 8.13); on occasion, σ_{max} or σ_{min} values may be used.

Two distinct types of S–N behavior are observed, which are represented schematically in Figures 8.19. As these plots indicate, the higher the magnitude of the stress, the smaller the number of cycles the material is capable of sustaining before failure. For some ferrous (iron base) and titanium alloys, the S–N curve (Figure 8.19*a*) becomes horizontal at higher N values; or, there is a limiting stress level, called the **fatigue limit** (also sometimes the *endurance limit*), below which fatigue failure will not occur. This fatigue limit represents the largest value of fluctuating stress that will *not* cause failure for essentially an infinite number of cycles. For many steels, fatigue limits range between 35 and 60% of the tensile strength.

Most nonferrous alloys (e.g., aluminum, copper, magnesium) do not have a fatigue limit, in that the S–N curve continues its downward trend at increasingly greater N values (Figure 8.19*b*). Thus fatigue will ultimately occur regardless of the magnitude of the stress. For these materials, the fatigue response is specified as **fatigue strength**, which is defined as the stress level at which failure will occur for some specified number of cycles (e.g., 10^7 cycles). The determination of fatigue strength is also demonstrated in Figure 8.19*b*.

Another important parameter that characterizes a material's fatigue behavior is **fatigue life** N_f. It is the number of cycles to cause failure at a specified stress level, as taken from the S–N plot (Figure 8.19*b*).

Unfortunately, there always exists considerable scatter in fatigue data, that is, a variation in the measured N value for a number of specimens tested at the same stress level. This may lead to significant design uncertainties when fatigue life and/or fatigue limit (or strength) are being considered. The scatter in results is a consequence of the fatigue sensitivity to a number of test and material parameters that are impossible to control precisely. These parameters include specimen fabrication and surface prep-

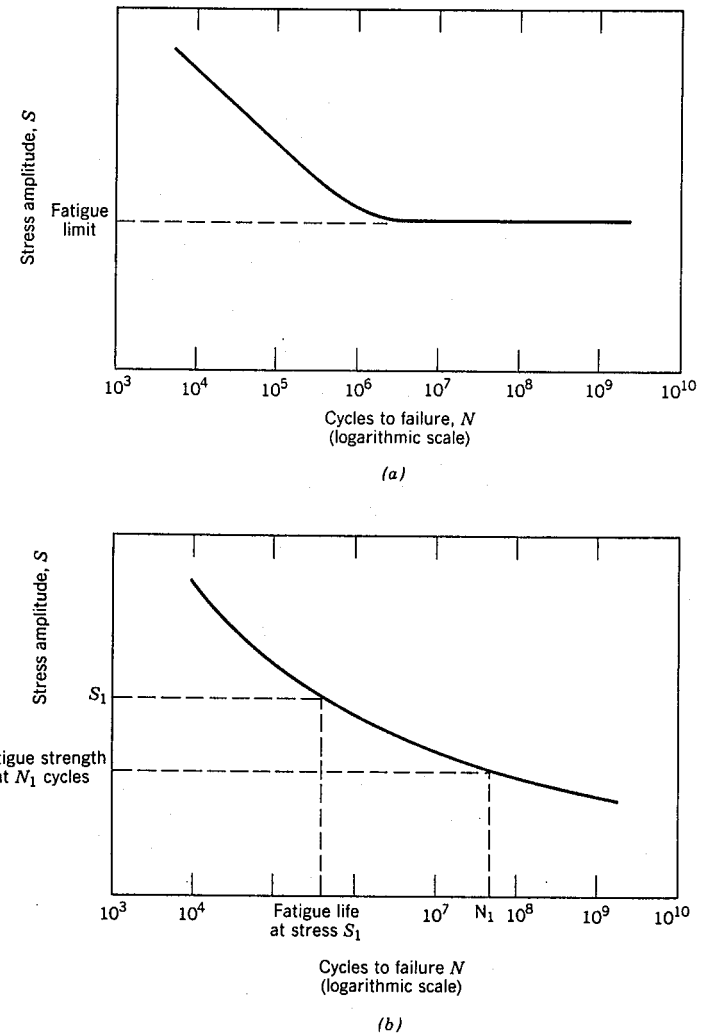

Figure 8.19 Stress amplitude (S) versus logarithm of the number of cycles to fatigue failure (N) for (*a*) a material that displays a fatigue limit, and (*b*) a material that does not display a fatigue limit.

aration, metallurgical variables, specimen alignment in the apparatus, mean stress, and test frequency.

Fatigue S–N curves similar to those shown in Figure 8.19 represent "best fit" curves which have been drawn through average-value data points. It is a little unsettling to realize that approximately one half of the specimens tested actually failed at stress levels lying nearly 25% below the curve (as determined on the basis of statistical treatments).

Several statistical techniques have been developed which are used to specify fatigue life and fatigue limit in terms of probabilities. One convenient way of representing data treated in this manner is with a series of constant probability curves, several of which are plotted in Figure 8.20. The P value associated with each curve represents

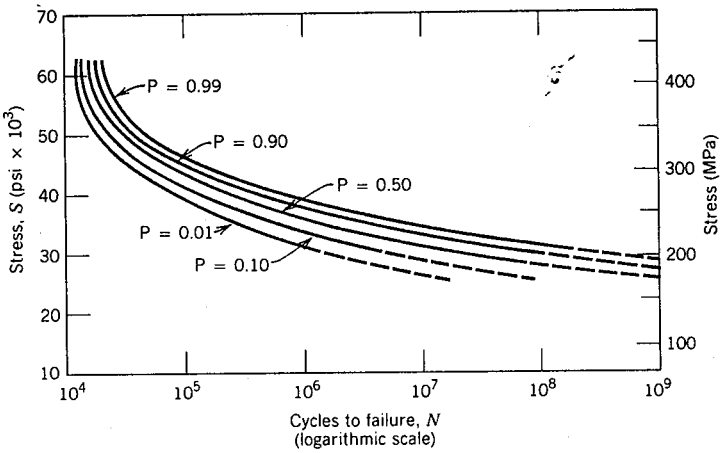

Figure 8.20 Fatigue S–N probability of failure curves for a 7075-T6 aluminum alloy; P denotes the probability of failure. (G. M. Sinclair and T. J. Dolan, *Trans., ASME,* **75,** 1953. Reprinted with permission of the American Society of Mechanical Engineers.)

the probability of failure. For example, at a stress of 30,000 psi, we would expect 1% of the specimens to fail at about 10^6 cycles and 50% to fail at about 2×10^7 cycles, and so on. It should be remembered that S–N curves represented in the literature are normally average values, unless noted otherwise.

The fatigue behaviors represented in Figures 8.19*a* and 8.19*b* may be classified into two domains. One is associated with relatively high loads that produce not only elastic strain but also some plastic strain during each cycle. Consequently, fatigue lives are relatively short; this domain is termed *low-cycle fatigue* and occurs at less than about 10^4 to 10^5 cycles. For lower stress levels wherein deformations are totally elastic, longer lives result. This is called *high-cycle fatigue* inasmuch as relatively large numbers of cycles are required to produce fatigue failure. High-cycle fatigue is associated with fatigue lives greater than about 10^4 to 10^5 cycles.

8.9 CRACK INITIATION AND PROPAGATION

The process of fatigue failure is characterized by three distinct stages: (1) crack initiation, wherein a small crack forms at some point of high stress concentration; (2) crack propagation, during which this crack advances incrementally with each stress cycle; and (3) final failure, which occurs very rapidly once the advancing crack has reached a critical size. The fatigue life N_f, the total number of cycles to failure, therefore can be taken as the sum of the number of cycles for crack initiation N_i and crack propagation N_p:

$$N_f = N_i + N_p \tag{8.15}$$

The contribution of the final failure stage to the total fatigue life is insignificant since it occurs so rapidly. Relative proportions to the total life of N_i and N_p depend on the particular material and test conditions. At low stress levels (i.e., for high-cycle fatigue), a large fraction of the fatigue life is utilized in crack initiation. With increasing

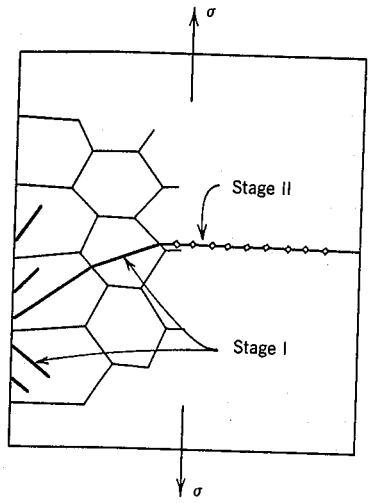

Figure 8.21 Schematic representation showing stages I and II of fatigue crack propagation in polycrystalline metals. (Copyright ASTM. Reprinted with permission.)

stress level, N_i decreases and the cracks form more rapidly. Thus for low-cycle fatigue (high stress levels), the propagation stage predominates (i.e., $N_p > N_i$).

Cracks associated with fatigue failure almost always initiate (or nucleate) on the surface of a component at some point of stress concentration. Crack nucleation sites include surface scratches, sharp fillets, keyways, threads, dents, and the like. In addition, cyclic loading can produce microscopic surface discontinuties resulting from dislocation slip steps which may also act as stress raisers, and therefore as crack initiation sites.

Once a stable crack has nucleated, it then initially propagates very slowly and, in polycrystalline metals, along crystallographic planes of high shear stress; this is sometimes termed *stage I propagation* (Figure 8.21). This stage may constitute a large or small fraction of the total fatigue life depending on stress level and the nature of the test specimen; high stresses and the presence of notches favor a short-lived stage I. In polycrystalline metals, cracks normally extend through only several grains during this propagation stage. The fatigue surface that is formed during stage I propagation has a flat and featureless appearance.

Eventually, a second propagation stage (*stage II*) takes over, wherein the crack extension rate increases dramatically. Furthermore, at this point there is also a change in propagation direction to one that is roughly perpendicular to the applied tensile stress (see Figure 8.21). During this stage of propagation, crack growth proceeds by a repetitive plastic blunting and sharpening process at the crack tip, a mechanism illustrated in Figure 8.22. At the beginning of the stress cycle (zero load), the crack tip has the shape of a sharp double-notch (Figure 8.22*a*). As the tensile stress is applied (Figure 8.22*b*), localized deformation occurs at each of these tip notches along slip planes that are oriented at 45° angles relative to the plane of the crack. With increased crack widening, the tip advances by continued shear deformation and the assumption of a blunted configuration (Figure 8.22*c*). During compression, the directions of shear deformation at the crack tip are reversed (Figure 8.22*d*) until, at the culmination of the cycle, a new sharp double-notch tip has formed (Figure 8.22*e*). Thus the crack tip has advanced a one-notch distance during the course of a complete cycle. This process

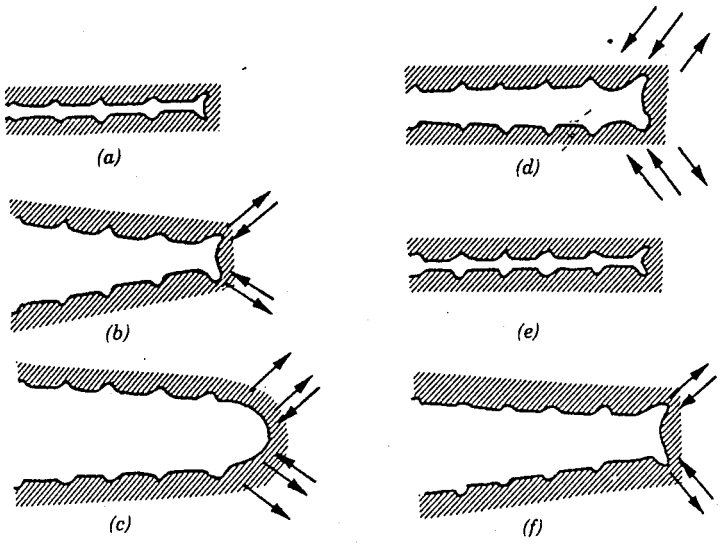

Figure 8.22 Fatigue crack propagation mechanism (stage II) by repetitive crack tip plastic blunting and sharpening: (*a*) zero load, (*b*) small tensile load, (*c*) maximum tensile load, (*d*) small compressive load, (*e*) maximum compressive load, (*f*) small tensile load. The loading axis is vertical. (Copyright ASTM. Reprinted with permission.)

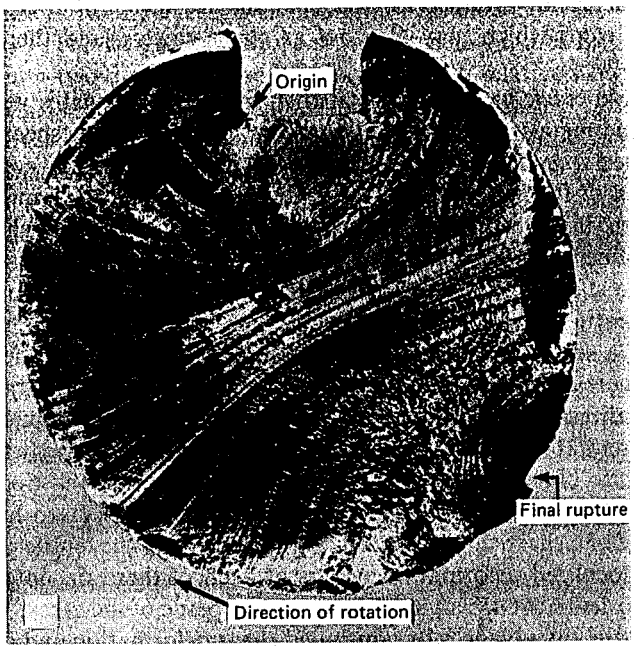

Figure 8.23 Fracture surface of a rotating steel shaft that experienced fatigue failure. Beachmark ridges are visible in the photograph. (Reproduced with permission from D. J. Wulpi, *Understanding How Components Fail,* American Society for Metals, Materials Park, OH, 1985.)

is repeated with each subsequent cycle until eventually some critical crack dimension is achieved which precipitates the final failure stage and catastrophic failure ensues.

The region of a fracture surface that formed during stage II propagation may be characterized by two types of markings termed *beachmarks* and *striations*. Both of these features indicate the position of the crack tip at some point in time and appear as concentric ridges that expand away from the crack initiation site(s), frequently in a circular or semicircular pattern. Beachmarks (sometimes also called "clamshell marks") are of macroscopic dimensions (Figure 8.23), and may be observed with the unaided eye. These markings are found for components that experienced interruptions during stage II propagation—for example, a machine that operated only during normal work-shift hours. Each beachmark band represents a period of time over which crack growth occurred.

On the other hand, fatigue striations are microscopic in size and subject to observation with the electron microscope (either TEM or SEM). Figure 8.24 is an electron fractograph which shows this feature. Each striation is thought to represent the advance distance of the crack front during a single load cycle. Striation width depends on, and increases with, increasing stress range.

At this point it should be emphasized that although both beachmarks and striations are fatigue fracture surface features having similar appearances, they are nevertheless different, both in origin and size. There may be literally thousands of striations within a single beachmark.

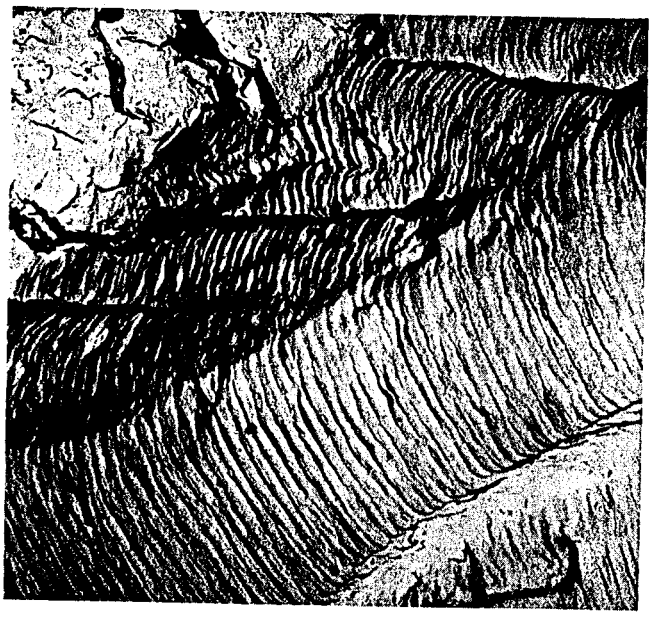

Figure 8.24 Transmission electron fractograph showing fatigue striations in aluminum. (From V. J. Colangelo and F. A. Heiser, *Analysis of Metallurgical Failures*, 2nd edition. Copyright © 1987 by John Wiley & Sons, New York. Reprinted by permission of John Wiley & Sons, Inc.)

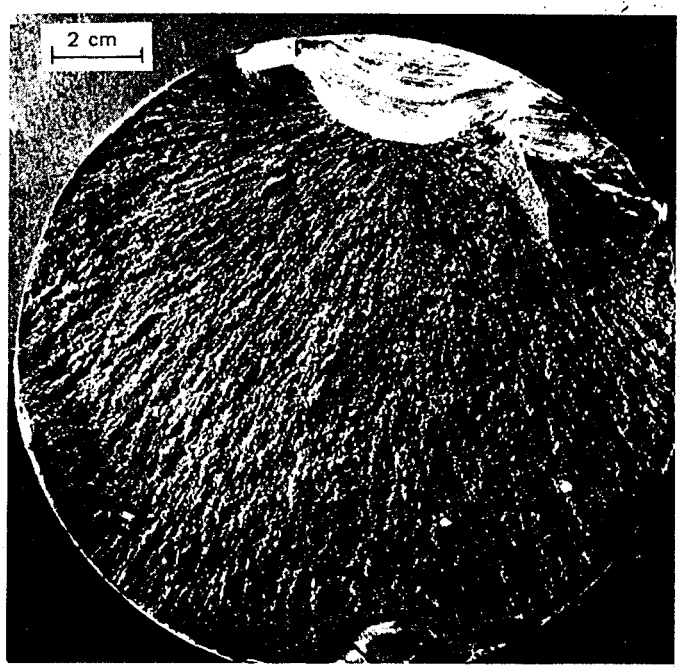

Figure 8.25 Fatigue failure surface. A crack formed at the top edge. The smooth region also near the top corresponds to the area over which the crack propagated slowly. Rapid failure occurred over the area having a dull and fibrous texture (the largest area). Approximately 0.5 ×. (Reproduced by permission from *Metals Handbook: Fractography and Atlas of Fractographs,* Vol. 9, 8th edition, H. E. Boyer (Editor), American Society for Metals, 1974.)

Often, the cause of failure may be deduced after examination of the failure surfaces. The presence of beachmarks and/or striations on a fracture surface confirms that the cause of failure was fatigue. Nevertheless, the absence of either or both does not exclude fatigue as the cause of failure.

One final comment regarding fatigue failure surfaces: Beachmarks and striations will not appear on that region over which the rapid failure occurs. Rather, the rapid failure may be either ductile or brittle; evidence of plastic deformation will be present for ductile, and absent for brittle, failure. This region of failure may be noted in Figure 8.25.

8.10 CRACK PROPAGATION RATE

Even though measures may be taken to minimize the possibility of fatigue failure, cracks and crack nucleation sites will always exist in structural components. Under the influence of cyclic stresses, cracks will inevitably form and grow; this process, if unabated, can ultimately lead to failure. The intent of the present discussion is to develop a criterion whereby fatigue life may be predicted on the basis of material and stress state parameters. Principles of fracture mechanics (Section 8.5) will be employed

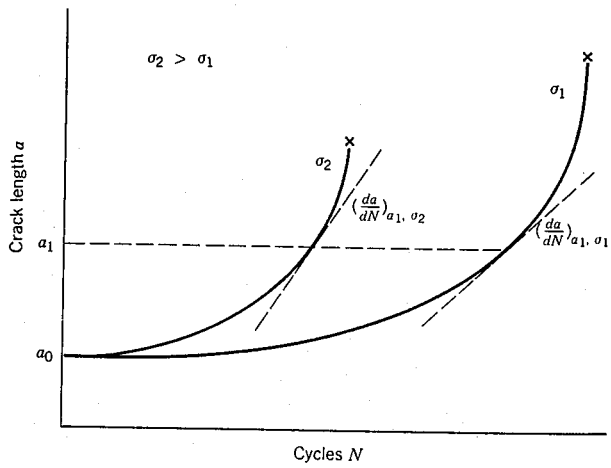

Figure 8.26 Crack length versus the number of cycles at stress levels σ_1 and σ_2 for fatigue studies. Crack growth rate da/dN is indicated at crack length a_1 for both stress levels.

inasmuch as the treatment involves determination of a maximum crack length that may be tolerated without inducing failure. It should be noted that this discussion relates to the domain of high-cycle fatigue, that is, for fatigue lives greater than about 10^4 to 10^5 cycles.

Results of fatigue studies have shown that the life of a structural component may be related to the rate of crack growth. During stage II propagation, cracks may grow from a barely perceivable size to some critical length. Experimental techniques are available which are employed to monitor crack length during the cyclic stressing. Data are recorded and then plotted as crack length a versus the number of cycles N.[3] A typical plot is shown in Figure 8.26, where curves are included from data generated at two different stress levels; the initial crack length a_0 for both sets of tests is the same. Crack growth rate da/dN is taken as the slope at some point of the curve. Two important results are worth noting: (1) initially, growth rate is small, but increases with increasing crack length; and (2) growth rate is enhanced with increasing applied stress level and for a specific crack length (a_1 in Figure 8.26).

Fatigue crack propagation rate is a function of not only stress level and crack size but also material variables. Mathematically, this rate may be expressed in terms of the stress intensity factor K (developed using fracture mechanics in Section 8.5) and takes the form

$$\frac{da}{dN} = A(\Delta K)^m \tag{8.16}$$

[3] The symbol N in the context of Section 8.8 represents the number of cycles to fatigue failure; in the present discussion it denotes the number of cycles associated with some crack length prior to failure.

The parameters A and m are constants for the particular material, which will also depend on environment, frequency, and the stress ratio (R in Equation 8.14). The value of m normally ranges between 1 and 6.

Furthermore, ΔK is the stress intensity factor range at the crack tip, that is,

$$\Delta K = K_{max} - K_{min} \tag{8.17a}$$

or, from Equation 8.6,

$$\Delta K = Y\Delta\sigma\sqrt{\pi a} = Y(\sigma_{max} - \sigma_{min})\sqrt{\pi a} \tag{8.17b}$$

Since crack growth stops or is negligible for a compression portion of the stress cycle, if σ_{min} is compressive, then K_{min} and σ_{min} are taken to be zero: that is, $\Delta K = K_{max}$ and $\Delta\sigma = \sigma_{max}$. Also note that K_{max} and K_{min} in Equation 8.17a represent stress

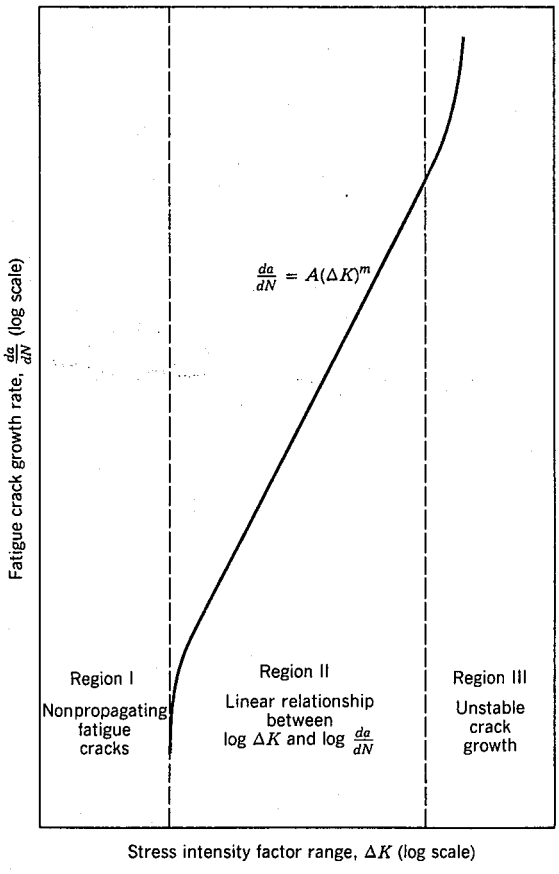

Figure 8.27 Schematic representation of logarithm fatigue crack propagation rate da/dN versus logarithm stress intensity factor range ΔK. The three regions of different crack growth response (I, II, and III) are indicated. (Reprinted with permission from ASM International, Metals Park, OH 44073-9989, Clark, W. G., Jr., "How Fatigue Crack Initiation and Growth Properties Affect Material Selection and Design Criteria," *Metals Engineering Quarterly*, Vol. 14, No. 3, 1974.)

intensity factors, not the fracture toughness K_c nor the plane strain fracture toughness K_{Ic}.

The typical fatigue crack growth rate behavior of materials is represented schematically in Figure 8.27 as the logarithm of crack growth rate da/dN versus the logarithm of the stress intensity factor range ΔK. The resulting curve has a sigmoidal shape which may be divided into three distinct regions, labeled I, II, and III. In region I (at low stress levels and/or small crack sizes), preexisting cracks will not grow with cyclic loading. Furthermore, associated with region III is accelerated crack growth, which occurs just prior to the rapid fracture.

The curve is essentially linear in region II, which is consistent with Equation 8.16. This may be confirmed by taking the logarithm of both sides of this expression, which leads to

$$\log\left(\frac{da}{dN}\right) = \log[A(\Delta K)^m] \tag{8.18a}$$

$$\log\left(\frac{da}{dN}\right) = m \log \Delta K + \log A \tag{8.18b}$$

Indeed, according to Equation 8.18b, a straight line segment will result when $\log(da/dN)$-versus-$\log \Delta K$ data are plotted; the slope and intercept correspond to the values of m and $\log A$, respectively, which may be determined from test data that have been represented in the manner of Figure 8.27. Figure 8.28 is one such plot for a Ni–Mo–V steel alloy. The linearity of the data may be noted, which verifies the power law relationship of Equation 8.16. Furthermore, the slope yields a value of 3 for m; A is approximately 1.8×10^{-14}, as taken from the extrapolated intercept for da/dN in in./cycle and ΔK in psi$\sqrt{\text{in.}}$.

One of the goals of failure analysis is to be able to predict fatigue life for some component, given its service constraints and laboratory test data. We are now able to develop an analytical expression for N_f by integration of Equation 8.16. Rearrangement is first necessary as follows:

$$dN = \frac{da}{A(\Delta K)^m} \tag{8.19}$$

which may be integrated as

$$N_f = \int_0^{N_f} dN = \int_{a_0}^{a_c} \frac{da}{A(\Delta K)^m} \tag{8.20}$$

The limits on the second integral are between the initial flaw length a_0, which may be measured using nondestructive examination techniques, and the critical crack length a_c determined from fracture toughness tests.

Substitution of the expression for ΔK (Equation 8.17b) leads to

$$\begin{aligned} N_f &= \int_{a_0}^{a_c} \frac{da}{A(Y \Delta\sigma \sqrt{\pi a})^m} \\ &= \frac{1}{A\pi^{m/2}(\Delta\sigma)^m} \int_{a_0}^{a_c} \frac{da}{Y^m a^{m/2}} \end{aligned} \tag{8.21}$$

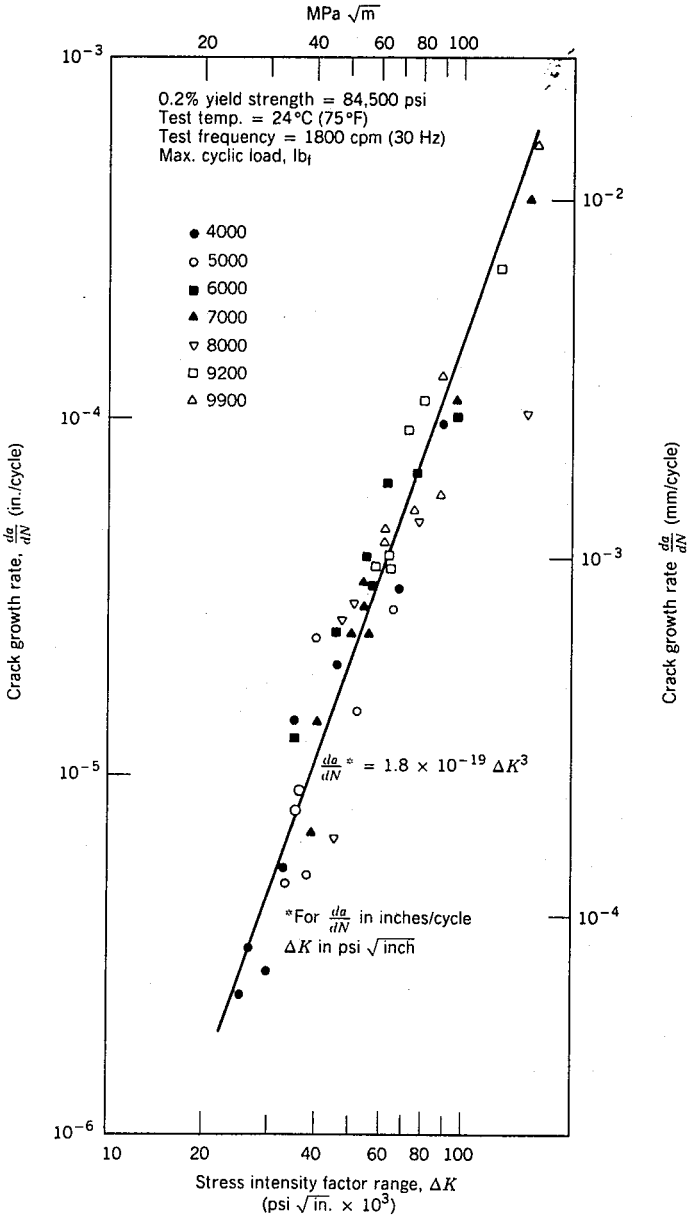

Figure 8.28 Logarithm crack growth rate versus logarithm stress intensity factor range for a Ni–Mo–V steel. (Reprinted by permission of the Society for Experimental Mechanics, Inc.)

Here it is assumed that $\Delta\sigma$ (or $\sigma_{max} - \sigma_{min}$) is constant; furthermore, in general Y will depend on crack length a and therefore cannot be removed from within the integral.

A word of caution: Equation 8.21 presumes the validity of Equation 8.16 over the entire life of the component, which may or may not hold true. Therefore, this expression should only be taken as an estimate of N_f.

PROBLEM 8.2

A relatively large sheet of steel is to be exposed to cyclic tensile and compressive stresses of magnitudes 100 MPa and 50 MPa, respectively. Prior to testing, it has been determined that the length of the largest surface crack is 2.0 mm (2×10^{-3} m). Estimate the fatigue life of this sheet if its plane strain fracture toughness is 25 MPa$\sqrt{\text{m}}$ and the values of m and A in Equation 8.16 are 3.0 and 1.0×10^{-12}, respectively, for $\Delta\sigma$ in MPa and a in m. Assume that the parameter Y is independent of crack length and has a value of 1.0.

SOLUTION

It first becomes necessary to compute the critical crack length a_c, the integration upper limit in Equation 8.21. Equation 8.10 is employed for this computation, assuming a stress level of 100 MPa, since this is the maximum tensile stress. Therefore,

$$a_c = \frac{1}{\pi}\left(\frac{K_{Ic}}{\sigma Y}\right)^2$$

$$= \frac{1}{\pi}\left(\frac{25\ \text{MPa}\sqrt{\text{m}}}{(100\ \text{MPa})(1)}\right)^2 = 0.02\ \text{m}$$

We now want to solve Equation 8.21 using 0.002 m as the lower integration limit a_0, as stipulated in the problem. The value of $\Delta\sigma$ is just 100 MPa, the magnitude of the tensile stress, since σ_{min} is compressive. Therefore, integration yields

$$N_f = \frac{1}{A\pi^{m/2}(\Delta\sigma)^m}\int_{a_0}^{a_c}\frac{da}{Y^m a^{m/2}}$$

$$= \frac{1}{A\pi^{3/2}(\Delta\sigma)^3 Y^3}\int_{a_0}^{a_c} a^{-3/2}\,da$$

$$= \frac{1}{A\pi^{3/2}(\Delta\sigma)^3 Y^3}(-2)a^{-1/2}\Big|_{a_0}^{a_c}$$

$$= \frac{2}{A\pi^{3/2}(\Delta\sigma)^3 Y^3}\left(\frac{1}{\sqrt{a_0}} - \frac{1}{\sqrt{a_c}}\right)$$

$$= \frac{2}{(1.0 \times 10^{-12})(\pi)^{3/2}(100)^3(1)^3}\left(\frac{1}{\sqrt{0.002}} - \frac{1}{\sqrt{0.02}}\right)$$

$$= 5.49 \times 10^6\ \text{cycles}$$

8.11 FACTORS THAT AFFECT FATIGUE LIFE

As was mentioned in Section 8.8, the fatigue behavior of engineering materials is highly sensitive to a number of variables. Some of these factors include mean stress level, geometrical design, surface effects, metallurgical variables, as well as the environment. This section is devoted to a discussion of these factors and, in addition, to measures that may be taken to improve the fatigue resistance of structural components.

Mean Stress

The dependence of fatigue life on stress amplitude is represented on the S–N plot. Such data are taken for a constant mean stress σ_m, often for the reversed cycle situation ($\sigma_m = 0$). Mean stress, however, will also affect fatigue life, which influence may be represented by a series of S–N curves, each measured at a different σ_m; this is depicted schematically in Figure 8.29. As may be noted, increasing the mean stress level leads to a decrease in fatigue life.

Surface Effects

For many common loading situations, the maximum stress within a component or structure occurs as its surface. Consequently, most cracks leading to fatigue failure originate at surface positions, specifically at stress amplification sites. Therefore, it has been observed that fatigue life is especially sensitive to the condition and configuration of the component surface. Numerous factors influence fatigue resistance, the proper management of which will lead to an improvement in fatigue life. These include design criteria as well as various surface treatments.

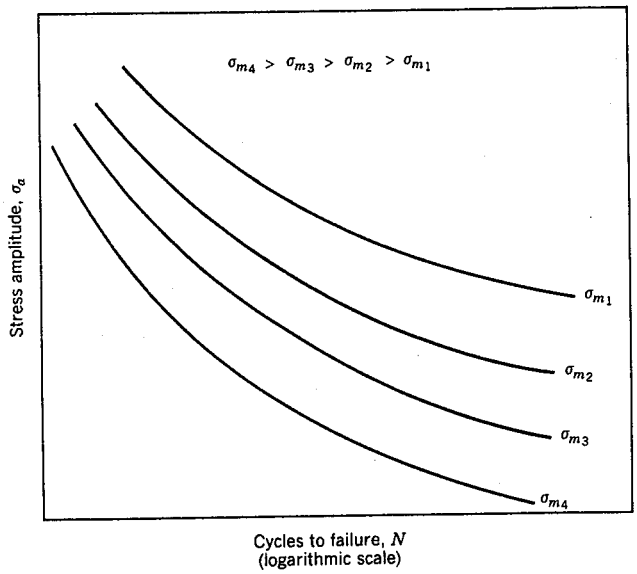

Figure 8.29 Demonstration of influence of mean stress σ_m on S–N fatigue behavior.

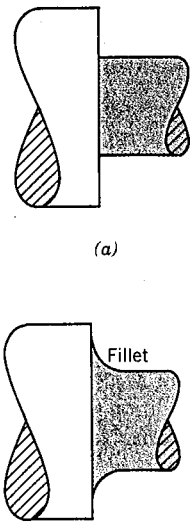

Figure 8.30 Demonstration of how design can reduce stress amplification. (*a*) Poor design: sharp corner. (*b*) Good design: fatigue lifetime improved by incorporating rounded fillet into a rotating shaft at the point where there is a change in diameter.

Design Factors. The design of a component can have a significant influence on its fatigue characteristics. Any notch or geometrical discontinuity can act as a stress raiser and fatigue crack initiation site; these design features include grooves, holes, keyways, threads, and so on. The sharper the discontinuity (i.e., the smaller the radius of curvature), the more severe the stress concentration. The probability of fatigue failure may be reduced by avoiding (when possible) these structural irregularities, or by making design modifications whereby sudden contour changes leading to sharp corners are eliminated—for example, calling for rounded fillets with large radii of curvature at the point where there is a change in diameter for a rotating shaft (Figure 8.30).

Surface Treatments. During machining operations, small scratches and grooves are invariably introduced into the workpiece surface by cutting tool action. These surface markings can limit the fatigue life. It has been observed that improving the surface finish by polishing will enhance fatigue life significantly.

One of the most effective methods of increasing fatigue performance is by imposing residual compressive stresses within a thin outer surface layer. Thus a surface tensile stress of external origin will be partially nullified and reduced in magnitude by the residual compressive stress. The net effect is that the likelihood of crack formation and therefore of fatigue failure is reduced.

Residual compressive stresses are commonly introduced into ductile metals mechanically by localized plastic deformation within the outer surface region. Commercially, this is often accomplished by a process termed *shot peening*. Small, hard particles (shot) having diameters within the range of 0.1 to 1.0 mm are projected at high velocities onto the surface to be treated. The resulting deformation induces compressive stresses to a depth of between one quarter and one half of the shot diameter.

Case hardening is a technique whereby both surface hardness and fatigue life are enhanced for steel alloys. This is accomplished by a carburizing or nitriding process

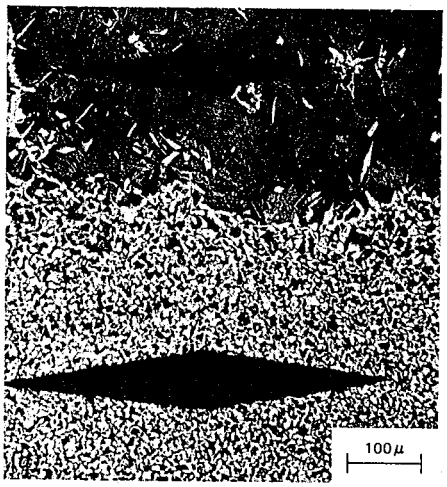

Figure 8.31 Photomicrograph showing both core (bottom) and carburized outer case (top) regions of a case-hardened steel. The case is harder as attested by the smaller microhardness indentation. (From R. W. Hertzberg, *Deformation and Fracture Mechanics of Engineering Materials*, 3rd edition. Copyright © 1989 by John Wiley & Sons, New York. Reprinted by permission of John Wiley & Sons, Inc.)

whereby a component is exposed to a carbonaceous or nitrogenous atmosphere at an elevated temperature. A carbon- or nitrogen-rich outer surface layer (or "case") is introduced by atomic diffusion from the gaseous phase. The case is normally on the order of 1 mm deep and is harder than the inner core of material. (The influence of carbon content on hardness for Fe–C alloys is demonstrated in Figure 10.21*a*.) The improvement of fatigue properties results from increased hardness within the case, as well as the desired residual compressive stresses the formation of which attends the carburizing or nitriding process. A carbon-rich outer case may be observed for the gear shown in the photograph on page 94; it appears as a dark outer rim within the sectioned segment. The increase in case hardness is demonstrated in the photomicrograph appearing in Figure 8.31. The dark and elongated diamond shapes are Knoop microhardness indentations. The upper indentation, lying within the carburized layer, is smaller than the core indentation.

8.12 ENVIRONMENTAL EFFECTS

Environmental factors may also affect the fatigue behavior of materials. A few brief comments will be given relative to two types of environment-assisted fatigue failure: thermal fatigue and corrosion fatigue.

Thermal fatigue is normally induced at elevated temperatures by fluctuating thermal stresses; mechanical stresses from an external source need not be present. The origin of these thermal stresses is the restraint to the dimensional expansion and/or contraction that would normally occur in a structural member with variations in temperature. The magnitude of a thermal stress developed by a temperature change ΔT is dependent on the coefficient of thermal expansion α_l and the modulus of elasticity E according to

$$\sigma = \alpha_l E \Delta T \tag{8.22}$$

(The topics of thermal expansion and thermal stresses are discussed in Sections 20.4 and 20.5.) Of course, thermal stresses will not arise if this mechanical restraint is absent. Therefore, one obvious way to prevent this type of fatigue is to eliminate

at least reduce, the restraint source, thus allowing unhindered dimensional changes with temperature variations, or to choose materials with appropriate physical properties.

Failure which occurs by the simultaneous action of a cyclic stress and chemical attack is termed **corrosion fatigue.** Corrosive environments have a deleterious influence and produce shorter fatigue lives. Even the normal ambient atmosphere will affect the fatigue behavior of some materials. Small pits may form as a result of chemical reactions between the environment and material, which serve as points of stress concentration, and therefore as crack nucleation sites. In addition, crack propagation rate is enhanced as a result of the corrosive environment. The nature of the stress cycles will influence the fatigue behavior; for example, lowering the load application frequency leads to longer periods during which the opened crack is in contact with the environment and to a reduction in the fatigue life.

Several approaches to corrosion fatigue prevention exist. On one hand, we can take measures to reduce the rate of corrosion by some of the techniques discussed in Chapter 18, for example, apply protective surface coatings, select a more corrosion-resistant material, and reduce the corrosiveness of the environment. And/or it might be advisable to take actions to minimize the probability of normal fatigue failure, as outlined above, for example, reduce the applied tensile stress level and impose residual compressive stresses on the surface of the member.

Materials are often placed in service at elevated temperatures and exposed to static mechanical stresses (e.g., turbine rotors in jet engines and steam generators that experience centrifugal stresses, and high-pressure steam lines). Deformation under such circumstances is termed **creep.** Defined as the time-dependent and permanent deformation of materials when subjected to a constant load or stress, creep is normally an undesirable phenomenon and is often the limiting factor in the lifetime of a part. It is observed in all materials types; for metals it only becomes important for temperatures greater than about $0.4T_m$ (T_m = absolute melting temperature). Amorphous polymers, which include plastics and rubbers, are especially sensitive to creep deformation as discussed in Section 16.6.

8.13 GENERALIZED CREEP BEHAVIOR

A typical creep test consists of subjecting a specimen to a constant load or stress while maintaining the temperature constant; deformation or strain is measured and plotted as a function of elapsed time. Most tests are the constant load type, which yield information of an engineering nature; constant stress tests are employed to provide a better understanding of the mechanisms of creep.

Figure 8.32 is a schematic representation of the typical constant load creep behavior of metals. Upon application of the load there is an instantaneous deformation, as indicated in the figure, which is mostly elastic. The resulting creep curve consists of three regions, each of which has its own distinctive strain–time feature. *Primary* or *transient creep* occurs first, typified by a continuously decreasing creep rate; that

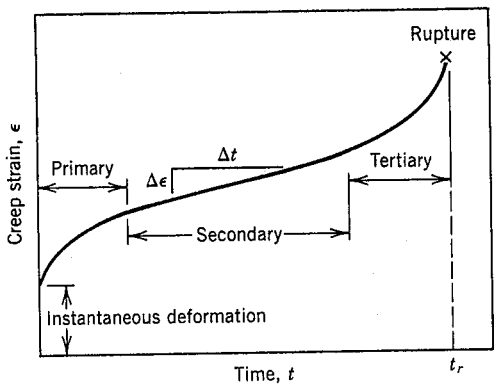

Figure 8.32 Typical creep curve of strain versus time at constant stress and elevated temperature. The minimum creep rate $\Delta\epsilon/\Delta t$ is the slope of the linear segment in the secondary region. Rupture lifetime t_r is the total time to rupture.

is, the slope of the curve diminishes with time. This suggests that the material is experiencing an increase in creep resistance or strain hardening (Section 7.10)—deformation becomes more difficult as the material is strained. For *secondary creep*, sometimes termed *steady-state creep*, the rate is constant; that is, the plot becomes linear. This is often the stage of creep that is of the longest duration. The constancy of creep rate is explained on the basis of a balance between the competing processes of strain hardening and recovery, recovery (Section 7.11) being the process whereby a material becomes softer and retains its ability to experience deformation. Finally, for *tertiary creep*, there is an acceleration of the rate and ultimate failure. This failure is frequently termed *rupture* and results from microstructural and/or metallurgical changes; for example, grain boundary separation, and the formation of internal cracks, cavities, and voids. Also, for tensile loads, a neck may form at some point within the deformation region. These all lead to a decrease in the effective cross-sectional area and an increase in strain rate.

For metallic materials most creep tests are conducted in uniaxial tension using a specimen having the same geometry as for tensile tests (Figure 6.2). On the other hand, uniaxial compression tests are more appropriate for brittle materials; these provide a better measure of the intrinsic creep properties inasmuch as there is no stress amplification and crack propagation, as with tensile loads. Compressive test specimens are usually right cylinders or parallelepipeds having length-to-diameter ratios ranging from about 2 to 4. For most materials creep properties are virtually independent of loading direction.

Possibly the most important parameter from a creep test is the slope of the secondary portion of the creep curve ($\Delta\epsilon/\Delta t$ in Figure 8.32); this is often called the minimum or *steady-state creep rate* $\dot{\epsilon}_s$. It is the engineering design parameter that is considered for long-life applications, such as a nuclear power plant component that is scheduled to operate for several decades, and when failure or too much strain is not an option. On the other hand, for many relatively short-life creep situations (e.g., turbine blades in military aircraft and rocket motor nozzles), *time to rupture*, or the *rupture lifetime* t_r is the dominant design consideration; it is also indicated in Figure 8.32. Of course, for its determination, creep tests must be conducted to the point of failure; these are termed *creep rupture* tests. Thus a knowledge of these creep characteristics of a material allows the design engineer to ascertain its suitability for a specific application.

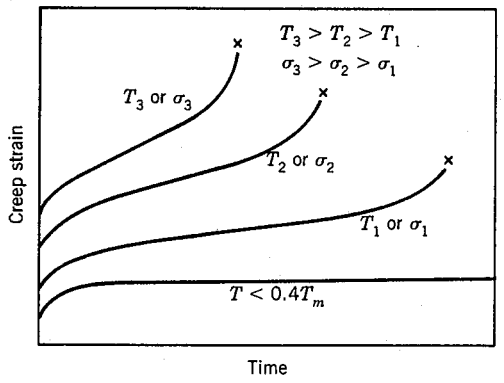

Figure 8.33 Influence of stress σ and temperature T on creep behavior.

8.14 STRESS AND TEMPERATURE EFFECTS

Both temperature and the level of the applied stress influence the creep characteristics (Figure 8.33). At a temperature substantially below $0.4T_m$, and after the initial deformation, the strain is virtually independent of time. With either increasing stress or temperature, the following will be noted: (1) the instantaneous strain at the time of stress application increases; (2) the steady-state creep rate is increased; and (3) the rupture lifetime is diminished.

The results of creep rupture tests are most commonly presented as the logarithm of stress versus the logarithm of rupture lifetime. Figure 8.34 is one such plot for a nickel alloy in which a linear relationship can be seen to exist at each temperature. For some alloys and over relatively large stress ranges, nonlinearity in these curves is observed.

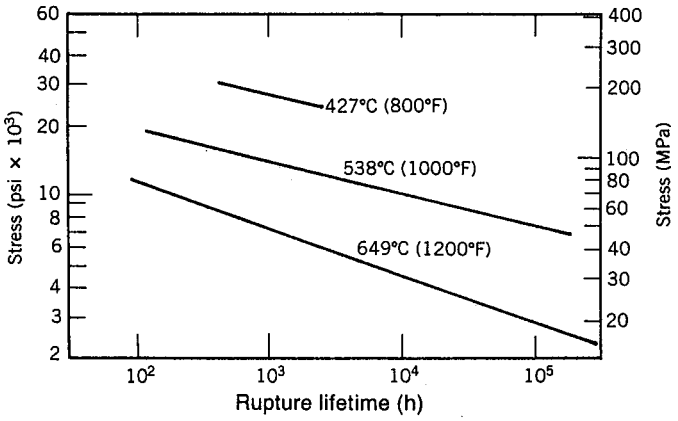

Figure 8.34 Logarithm of stress versus logarithm of rupture lifetime for a low carbon–nickel alloy at three temperatures. (From *Metals Handbook: Properties and Selection: Stainless Steels, Tool Materials and Special-Purpose Metals*, Vol. 3, 9th edition, D. Benjamin, Senior Editor, American Society for Metals, 1980, p. 130.)

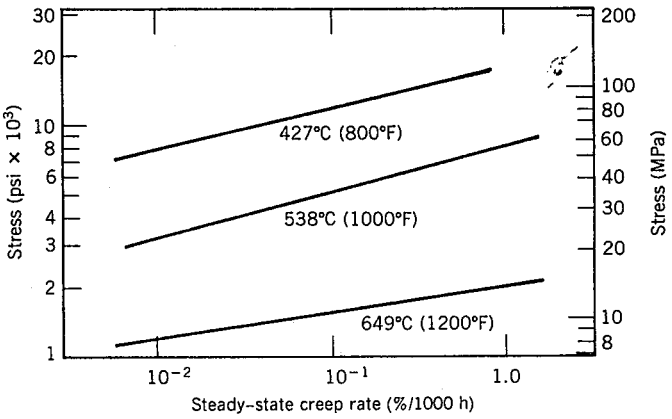

Figure 8.35 Logarithm of stress versus logarithm of steady-state creep rate for a low carbon–nickel alloy at three temperatures. (From *Metals Handbook: Properties and Selection: Stainless Steels, Tool Materials and Special-Purpose Metals,* Vol. 3, 9th edition, D. Benjamin, Senior Editor, American Society for Metals, 1980, p. 131.)

Empirical relationships have been developed in which the steady-state creep rate as a function of stress and temperature is expressed. Its dependence on stress can be written

$$\dot{\epsilon}_s = K_1 \sigma^n \tag{8.23}$$

where K_1 and n are material constants. A plot of the logarithm of $\dot{\epsilon}_s$ versus the logarithm of σ yields a straight line with slope of n; this is shown in Figure 8.35 for a nickel alloy at three temperatures. Clearly, a straight line segment is drawn at each temperature.

Now, when the influence of temperature is included,

$$\dot{\epsilon}_s = K_2 \sigma^n \exp\left(-\frac{Q_c}{RT}\right) \tag{8.24}$$

where K_2 and Q_c are constants; Q_c is termed the activation energy for creep.

Several theoretical mechanisms have been proposed to explain the creep behavior for various materials; these mechanisms involve stress-induced vacancy diffusion, grain boundary diffusion, dislocation motion, and grain boundary sliding. Each leads to a different value of the stress exponent n in Equation 8.23. It has been possible to elucidate the creep mechanism for a particular material by comparing its experimental n value with values predicted for the various mechanisms. In addition, correlations have been made between the activation energy for creep (Q_c) and the activation energy for diffusion (Q_d, Equation 5.8).

Creep data of this nature are represented pictorially for some well-studied systems in the form of stress–temperature diagrams, which are termed *deformation mechanism maps*. These maps indicate stress–temperature regimes (or areas) over which various mechanisms operate. Constant strain rate contours are often also included. Thus for

some creep situation, given the appropriate deformation mechanism map and any two of the three parameters—temperature, stress level, and creep strain rate—the third parameter may be determined.

8.15 DATA EXTRAPOLATION METHODS

The need often arises for engineering creep data that are impractical to collect from normal laboratory tests. This is especially true for prolonged exposures (on the order of years). One solution to this problem involves performing creep and/or creep rupture tests at temperatures in excess of those required, for shorter time periods, and at a comparable stress level, and then by making a suitable extrapolation to the in-service condition. A commonly used extrapolation procedure employs the Larson–Miller parameter, defined as

$$T(C + \log t_r) \tag{8.25}$$

where C is a constant (usually on the order of 20), for T in Kelvin and the rupture lifetime t_r in hours. The rupture lifetime of a given material measured at some specific stress level will vary with temperature such that this parameter remains constant. Or, the data may be plotted as the logarithm of stress versus the Larson–Miller parameter, as shown in Figure 8.36. Utilization of this technique is demonstrated in the following example problem.

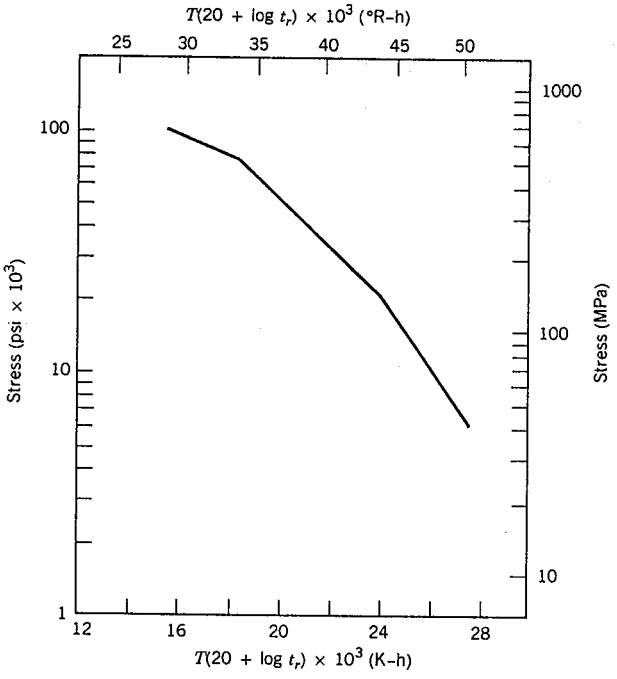

Figure 8.36 Logarithm stress versus the Larson–Miller parameter for an S-590 iron. (From F. R. Larson and J. Miller, *Trans. ASME*, **74**, 765 (1952). Reprinted by permission of ASME.)

EXAMPLE PROBLEM 8.3

Using the Larson–Miller data for S-590 iron shown in Figure 8.36, predict the time to rupture for a component that is subjected to a stress of 20,000 psi (140 MPa) at 800°C (1073 K).

SOLUTION

From Figure 8.36, at 20,000 psi (140 MPa) the value of the Larson–Miller parameter is 24.0×10^3, for T in K and t_r in h; therefore,

$$24.0 \times 10^3 = T(20 + \log t_r)$$
$$= 1073(20 + \log t_r)$$

and, solving for the time,

$$22.37 = 20 + \log t_r$$
$$t_r = 233 \text{ h (9.7 days)}$$

8.16 ALLOYS FOR HIGH-TEMPERATURE USE

There are several factors that affect the creep characteristics of metals. These include melting temperature, elastic modulus, and grain size. In general, the higher the melting temperature, the greater the elastic modulus, and the larger the grain size, the better is a material's resistance to creep. Stainless steels (Section 12.5), the refractory metals (Section 12.11), and the superalloys (Section 12.12) are especially resilient to creep

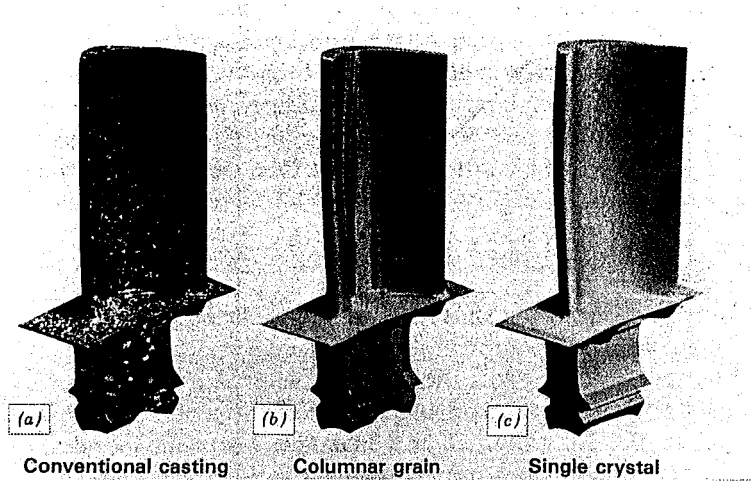

Figure 8.37 (*a*) Polycrystalline turbine blade that was produced by a conventional casting technique. High-temperature creep resistance is improved as a result of an oriented columnar grain structure (*b*) produced by a sophisticated directional solidification technique. Creep resistance is further enhanced when single-crystal blades (*c*) are used. (Courtesy of Pratt & Whitney.)

and are commonly employed in high-temperature service applications. The creep resistance of the cobalt and nickel superalloys is enhanced by solid-solution alloying, and also by the addition of a dispersed phase which is virtually insoluble in the matrix. In addition, advanced processing techniques have been utilized; one such technique is directional solidification, which produces either highly elongated grains or single-crystal components (Figure 8.37). Another is the controlled unidirectional solidification of alloys having specially designed compositions wherein two-phase composites result.

SUMMARY

Fracture is one form of failure that occurs for static applied loads and at relatively low temperatures. Ductile and brittle modes are possible, both of which involve the formation and propagation of cracks. For ductile fracture, evidence will exist of gross plastic deformation at the fracture surface. In tension, highly ductile metals will neck down to essentially a point fracture; cup-and-cone mating fracture surfaces result for moderate ductility. Microscopically, dimples (spherical and parabolic) are produced. Cracks in ductile materials are said to be stable (i.e., resist extension without an increase in applied stress); and inasmuch as fracture is noncatastrophic, this fracture mode is almost always preferred.

For brittle fracture, cracks are unstable, and the fracture surface is relatively flat and perpendicular to the direction of the applied tensile load. Chevron and ridgelike patterns are possible, which indicate the direction of crack propagation. Transgranular (through-grain) and intergranular (between-grain) fractures are found in brittle polycrystalline materials.

The discipline of fracture mechanics allows for a better understanding of the fracture process and provides for structural design wherein the probability of failure is minimized. The significant discrepancy between actual and theoretical fracture strengths of brittle materials is explained by the existence of small flaws that are capable of amplifying an applied tensile stress in their vicinity, leading ultimately to crack formation. Stress amplification is greatest for long flaws that have small tip radii of curvature. Fracture ensues when the theoretical cohesive strength is exceeded at the tip of one of these flaws. Consideration of elastic strain and crack surface energies led Griffith to develop an expression for a crack propagation critical stress in brittle materials; this parameter is a function of elastic modulus, specific surface energy, and crack length.

The stress distributions in front of an advancing crack may be expressed in terms of position (as radial and angular coordinates) as well as stress intensity factor. The critical value of the stress intensity factor (i.e., that at which fracture occurs) is termed the fracture toughness, which is related to stress level, crack length, and a geometrical factor. The fracture toughness of a material is indicative of its resistance to brittle fracture when a crack is present. It depends on specimen thickness, and, for relatively thick specimens (i.e., conditions of plane strain), is termed the plane strain fracture toughness. This parameter is the one normally cited for design purposes; its value is relatively large for ductile materials (and small for brittle ones), and is a function of microstructure, strain rate, and temperature. With regard to designing against the

possibility of fracture, consideration must be given to material (its fracture toughness), the stress level, and the flaw size detection limit.

Qualitatively, the fracture behavior of materials may be determined using Charpy and Izod impact testing techniques; impact energy (or notch toughness) is measured for specimens into which a V-shaped notch has been machined. On the basis of the temperature dependence of this impact energy (or appearance of the fracture surface), it is possible to ascertain whether or not a material experiences a ductile-to-brittle transition and the temperature range over which such a transition occurs. Metal alloys having BCC and HCP crystal structures experience this transition, and, for structural applications, should be used at temperatures in excess of this transition range.

Fatigue is a common type of catastrophic failure wherein the applied stress level fluctuates with time. Test data are plotted as stress versus the logarithm of the number of cycles to failure. For many materials, the number of cycles to failure increases continuously with diminishing stress. Fatigue strength represents the failure stress for a specified number of cycles. For some steels and titanium alloys, stress ceases to decrease with, and becomes independent of, the number of cycles; fatigue limit is the magnitude of this constant stress level, below which fatigue will not occur even for virtually an infinite number of cycles. Another fatigue property is fatigue life, which, for a specific stress, is the number of cycles to failure.

As a result of significant scatter in measured fatigue data, statistical analyses are performed that lead to specification of fatigue life and limit in terms of probabilities.

The processes of fatigue crack initiation and propagation were discussed. Cracks normally nucleate on the surface of a component at some point of stress concentration. Propagation proceeds in two stages, which are characterized by propagation direction and rate. The mechanism for the more rapid stage II corresponds to a repetitive plastic blunting and sharpening process at the advancing crack tip.

Two characteristic fatigue surface features are beachmarks and striations. Beachmarks form on components that experience applied stress interruptions; they normally may be observed with the naked eye. Fatigue striations are of microscopic dimensions, and each is thought to represent the crack tip advance distance over a single load cycle.

An analytical expression was proposed for fatigue crack propagation rate in terms of the stress intensity range at the crack tip. Integration of the expression yields an equation whereby fatigue life may be estimated.

Measures that may be taken to extend fatigue life include (1) reducing the mean stress level, (2) eliminating sharp surface discontinuities, (3) improving the surface finish by polishing, (4) imposing surface residual compressive stresses by shot peening, and (5) case hardening by using a carburizing or nitriding process.

The fatigue behavior of materials may also be affected by the environment. Thermal stresses may be induced in components that are exposed to elevated temperature fluctuations and when thermal expansion and/or contraction is restrained; fatigue for these conditions is termed thermal fatigue. The presence of a chemically active environment may lead to a reduction in fatigue life for corrosion fatigue; small pit crack nucleation sites form on the component surface as a result of chemical reactions.

The time-dependent plastic deformation of materials subjected to a constant load (or stress) and temperatures greater than about $0.4T_m$ is termed creep. A typical creep

curve (strain versus time) will normally exhibit three distinct regions. For transient (or primary) creep, the rate (or slope) diminishes with time. The plot becomes linear (i.e., creep rate is constant) in the steady-state (or secondary) region. And finally, deformation accelerates for tertiary creep, just prior to failure (or rupture). Important design parameters available from such a plot include the steady-state creep rate (slope of the linear region) and rupture lifetime.

Both temperature and applied stress level influence creep behavior. Increasing either of these parameters produces the following effects: (1) an increase in the instantaneous initial deformation, (2) an increase in the steady-state creep rate, and (3) a diminishment of the rupture lifetime. Analytical expressions were presented which relate $\dot{\epsilon}_s$ to both temperature and stress. Creep mechanisms may be discerned on the basis of steady-state rate stress exponent and creep activation energy values.

Extrapolation of creep test data to lower temperature-longer time regimes is possible using the Larson–Miller parameter.

Metal alloys that are especially resistant to creep have high elastic moduli and melting temperatures; these include the superalloys, the stainless steels, and the refractory metals. Various processing techniques are employed to improve the creep properties of these materials.

IMPORTANT TERMS AND CONCEPTS

Brittle fracture
Case hardening
Charpy test
Corrosion fatigue
Creep
Ductile fracture
Ductile-to-brittle transition
Fatigue
Fatigue life
Fatigue limit
Fatigue strength
Fracture mechanics
Fracture toughness
Impact energy
Intergranular fracture
Izod test
Plane strain
Plane strain fracture toughness
Stress intensity factor
Stress raiser
Thermal fatigue
Transgranular fracture

REFERENCES

COLANGELO, V. J. and F. A. HEISER, *Analysis of Metallurgical Failures*, 2nd edition, John Wiley & Sons, New York, 1987.

COLLINS, J. A., *Failure of Materials in Mechanical Design*, John Wiley & Sons, New York, 1981.

DIETER, G. E., *Mechanical Metallurgy*, 3rd edition, McGraw-Hill Book Co., New York, 1986.

HERTZBERG, R. W., *Deformation and Fracture Mechanics of Engineering Materials*, 3rd edition, John Wiley & Sons, New York, 1989.

Metals Handbook, 9th edition, Vol. 11, *Failure Analysis and Prevention*, American Society for Metals, Metals Park, OH, 1986.

Metals Handbook, 9th edition, Vol. 12, *Fractography*, ASM International, Metals Park, OH, 1987.

TETELMAN, A. S. and A. J. MCEVILY, *Fracture of Structural Materials*, John Wiley & Sons, New York, 1967.

WULPI, D. J., *Understanding How Components Fail*, American Society for Metals, Metals Park, OH, 1985.

QUESTIONS AND PROBLEMS

8.1 Cite the three principal causes for mechanical failure.

8.2 Estimate the theoretical cohesive strengths of the ceramic materials listed in Table 13.4.

8.3 What is the magnitude of the maximum stress that exists at the tip of an internal crack having a radius of curvature of 10^{-5} in. (2.5×10^{-4} mm) and a crack length of 10^{-3} in. (2.5×10^{-2} mm) when a tensile stress of 25,000 psi (170 MPa) is applied?

8.4 Estimate the theoretical fracture strength of a brittle material if it is known that fracture occurs by the propagation of an elliptically shaped surface crack of length 0.02 in. (0.5 mm) and having a tip radius of curvature of 2×10^{-4} in. (5×10^{-3} mm) when a stress of 150,000 psi (1035 MPa) is applied.

8.5 A specimen of a ceramic material having a modulus of elasticity of 25×10^4 MPa (36.3×10^6 psi) is pulled in tension with a stress of 750 MPa (109,000 psi). Will the specimen fail if its "most severe flaw" is an internal crack that has a length of 0.20 mm (7.87×10^{-3} in.) and a tip radius of curvature of 0.001 mm (3.94×10^{-5} in.)? Why or why not?

8.6 If the specific surface energy for aluminum oxide is 0.90 J/m^2, using data contained in Table 13.4, compute the critical stress required for the propagation of an internal crack of length 0.40 mm.

8.7 An MgO component must not fail when a tensile stress of 13.5 MPa (1960 psi) is applied. Determine the maximum allowable surface crack length if the surface energy of MgO is 1.0 J/m^2. Data found in Table 13.4 may prove helpful.

8.8 The parameter K in Equations 8.5a, 8.5b, and 8.5c is a function of the applied nominal stress σ and crack length a as

$$K = \sigma\sqrt{\pi a}$$

Compute the magnitudes of the normal stresses σ_x and σ_y in front of a surface crack of length 2.0 mm (0.079 in.) (as depicted in Figure 8.10) in response to a nominal tensile stress of 100 MPa (14,500 psi) at the following positions:

(a) $r = 0.1$ mm (3.9×10^{-3} in.), $\theta = 0°$

(b) $r = 0.1$ mm (3.9×10^{-3} in.), $\theta = 45°$

(c) $r = 0.5$ mm (0.02 in.), $\theta = 0°$

(d) $r = 0.5$ mm (0.02 in.), $\theta = 45°$

8.9 The parameter K in Equations 8.5a, 8.5b, and 8.5c is defined in the previous problem.

(a) For a surface crack of length 2.0 mm (7.87×10^{-2} in.), determine the radial position at an angle θ of 30° at which the normal stress σ_x is 100 MPa (14,500 psi) when the magnitude of the nominal applied stress is 150 MPa

(21,750 psi).

(b) Compute the normal stress σ_y at this same position.

8.10 Below is shown a portion of a tensile specimen.

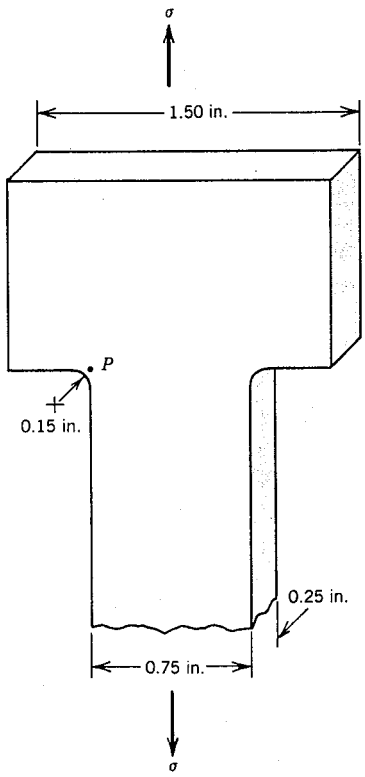

(a) Compute the magnitude of the stress at point P when the externally applied stress is 20,000 psi (140 MPa).

(b) How much will the radius of curvature at point P have to be increased to reduce this stress by 25%?

8.11 A cylindrical hole 0.75 in. (19.0 mm) in diameter passes entirely through the thickness of a steel plate 0.5 in. (12.7 mm) thick, 5 in. (127 mm) wide, and 10 in. (254 mm) long.

(a) Compute the magnitude of the stress at the edge of this hole when a tensile stress of 5000 psi (34.5 MPa) is applied in a lengthwise direction.

(b) Calculate the stress at the hole edge when this same stress is applied in a widthwise direction.

8.12 Cite the significant differences between the stress intensity factor, the plane stress fracture toughness, and the plane strain fracture toughness.

8.13 For each of the metal alloys listed in Table 8.1, compute the minimum component thickness for which the condition of plane strain is valid.

8.14 A specimen of a 4340 steel alloy having a plane strain fracture toughness of 50,000 psi$\sqrt{\text{in.}}$ (54.8 MPa$\sqrt{\text{m}}$) is exposed to a stress of 150,000 psi (1030 MPa).

Will this specimen experience fracture if it is known that the largest surface crack is 0.02 in. (0.5 mm) long? Why or why not? Assume that the parameter Y has a value of 1.0.

8.15 Some aircraft component is fabricated from an aluminum alloy that has a plane strain fracture toughness of 40 MPa$\sqrt{\text{m}}$ (3.64×10^4 psi$\sqrt{\text{in.}}$). It has been determined that fracture results at a stress of 300 MPa (43,500 psi) when the maximum (or critical) internal crack length is 4.0 mm (0.16 in.). For this same component and alloy, will fracture occur at a stress level of 260 MPa (38,000 psi) when the maximum internal crack length is 6.0 mm (0.24 in.)? Why or why not?

8.16 Suppose that a wing component on an aircraft is fabricated from an aluminum alloy that has a plane strain fracture toughness of 26 MPa$\sqrt{\text{m}}$ (23,700 psi$\sqrt{\text{in.}}$). It has been determined that fracture results at a stress of 112 MPa (16,240 psi) when the maximum internal crack length is 8.6 mm (0.34 in.). For this same component and alloy, compute the stress level at which fracture will occur for a critical internal crack length of 6.0 mm (0.24 in.).

8.17 A large plate is fabricated from a steel alloy that has a plane strain fracture toughness of 75,000 psi$\sqrt{\text{in.}}$ (82.4 MPa$\sqrt{\text{m}}$). If, during service use, the plate is exposed to a tensile stress of 50,000 psi (345 MPa), determine the minimum length of a surface crack that will lead to fracture. Assume a value of 1.0 for Y.

8.18 Calculate the maximum internal crack length allowable for a Ti–6Al–4V titanium alloy (Table 8.1) component that is loaded to a stress one half of its yield strength. Assume that the value of Y is 1.50.

8.19 A structural component in the form of a wide plate is to be fabricated from a steel alloy that has a plane strain fracture toughness of 98.9 MPa$\sqrt{\text{m}}$ (90,000 psi$\sqrt{\text{in.}}$) and a yield strength of 860 MPa (125,000 psi). The flaw size resolution limit of the flaw detection apparatus is 3.0 mm (0.12 in.). If the design stress is one half of the yield strength and the value of Y is 1.0, determine whether or not a critical flaw for this plate is subject to detection.

8.20 A structural component in the shape of a flat plate 25.4 mm (1.0 in.) thick is to be fabricated from a metal alloy for which the yield strength and plane strain fracture toughness values are 700 MPa (101,500 psi) and 49.5 MPa$\sqrt{\text{m}}$ (45,000 psi$\sqrt{\text{in.}}$), respectively; for this particular geometry, the value of Y is 1.65. Assuming a design stress of one half of the yield strength, is it possible to compute the critical length of a surface flaw? If so, determine its length; if this computation is not possible from the given data, then explain why.

8.21 For a flat plate of width w containing an internal crack of length $2a$ which is centrally positioned as illustrated in the figure below, the parameter Y for tensile loading may be determined as

$$Y = \left(\frac{w}{\pi a} \tan \frac{\pi a}{w} \right)^{1/2} \tag{8.26}$$

Assuming an internal crack length (i.e., $2a$) of 1.0 in. (25.4 mm) within a plate of width 4.0 in. (101.6 mm), determine the minimum plane strain fracture toughness necessary to ensure that fracture will not occur for a design stress of 60,000 psi (415 MPa).

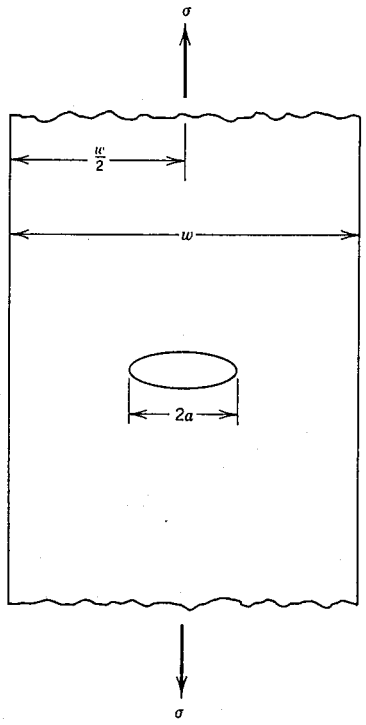

8.22 After consultation of other references, write a brief report on one or two nondestructive test techniques that are used to detect and measure internal and/or surface flaws in metal alloys.

8.23 Tabulated below are data that were gathered from a series of Charpy impact tests on a tempered 4340 steel alloy:

Temperature (°C)	Impact Energy (J)
0	105
−25	104
−50	103
−75	97
−100	63
−113	40
−125	34
−150	28
−175	25
−200	24

(a) Plot the data as impact energy versus temperature.
(b) Determine a ductile-to-brittle transition temperature as that temperature corresponding to the average of the maximum and minimum impact energies.
(c) Determine a ductile-to-brittle transition temperature as that temperature at which the impact energy is 50 J.

8.24 Tabulated below are data that were gathered from a series of Charpy impact tests on a commercial low-carbon steel alloy:

Temperature (°C)	Impact Energy (J)
50	76
40	76
30	71
20	58
10	38
0	23
−10	14
−20	9
−30	5
−40	1.5

(a) Plot the data as impact energy versus temperature.
(b) Determine a ductile-to-brittle transition temperature as that temperature corresponding to the average of the maximum and minimum impact energies.
(c) Determine a ductile-to-brittle transition temperature as that temperature at which the impact energy is 20 J.

8.25 Briefly explain why BCC and HCP metal alloys may experience a ductile-to-brittle transition with decreasing temperature, whereas FCC alloys do not experience such a transition.

8.26 A fatigue test was conducted in which the mean stress was 10,000 psi (70 MPa) and the stress amplitude was 30,000 psi (210 MPa).
(a) Compute the maximum and minimum stress levels.
(b) Compute the stress ratio.
(c) Compute the magnitude of the stress range.

8.27 A cylindrical 1045 steel bar (Figure 8.38) is subjected to repeated compression-tension stress cycling along its axis. If the load amplitude is 15,000 lb_f (66,700 N), compute the minimum allowable bar diameter to ensure that fatigue failure will not occur.

8.28 A 0.25 in. (6.4 mm) diameter cylindrical rod fabricated from a 2014-T6 aluminum alloy (Figure 8.38) is subjected to a reversed tension-compression load cycling along its axis. If the maximum tensile and compressive loads are $+1200\ lb_f$ ($+5340$ N) and $-1200\ lb_f$ (-5340 N), respectively, determine its fatigue life. Assume the stress plotted in Figure 8.38 is stress amplitude.

8.29 A 0.60 in. (15.2 mm) diameter cylindrical rod fabricated from a 2014-T6 alloy (Figure 8.38) is subjected to a repeated tension-compression load cycling along its axis. Compute the maximum and minimum loads that will be applied to yield a fatigue life of 1.0×10^8 cycles. Assume that the stress plotted on the vertical axis is stress amplitude, and data were taken for a mean stress of 5000 psi (35 MPa).

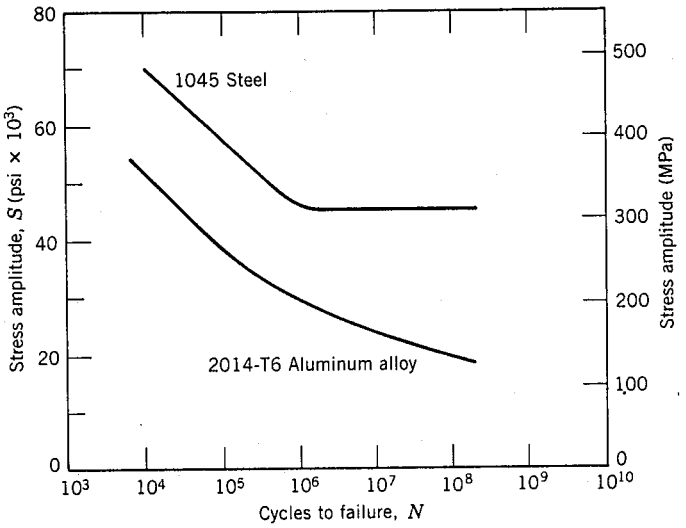

Figure 8.38 Stress magnitude S versus the logarithm of the number of cycles to fatigue failure N for an aluminum alloy and a plain carbon steel. (Adapted from H. W. Hayden, W. G. Moffatt, and J. Wulff, *The Structure and Properties of Materials*, Vol. III, *Mechanical Behavior*, p. 15. Copyright © 1965 by John Wiley & Sons, New York. Reprinted by permission of John Wiley & Sons, Inc.)

8.30 The fatigue data for a brass alloy are given below:

Stress Amplitude (MPa)	Cycles to Failure
170	3.7×10^4
148	1.0×10^5
130	3.0×10^5
114	1.0×10^6
92	1.0×10^7
80	1.0×10^8
74	1.0×10^9

(a) Make an S–N plot (stress amplitude versus logarithm cycles to failure) using these data.
(b) Determine the fatigue strength at 4×10^6 cycles.
(c) Determine the fatigue life for 120 MPa.

8.31 Suppose that the fatigue data for the brass alloy in Problem 8.30 were taken from torsional tests, and that a shaft of this alloy is to be used for a coupling that is attached to an electric motor operating at 1800 rpm. Give the maximum torsional stress amplitude possible for each of the following lifetimes of the coupling: **(a)** 1 year, **(b)** 1 month, **(c)** 1 day, and **(d)** 1 hour.

8.32 The fatigue data for a steel alloy are given below:

Stress Amplitude [psi (MPa)]	Cycles to Failure
68,000 (470)	10^4
63,400 (440)	3×10^4
56,200 (390)	10^5
51,000 (350)	3×10^5
45,300 (310)	10^6
42,200 (290)	3×10^6
42,200 (290)	10^7
42,200 (290)	10^8

(a) Make an *S–N* plot (stress amplitude versus logarithm cycles to failure) using the data.
(b) What is the fatigue limit for this alloy?
(c) Determine fatigue lifetimes at stress amplitudes of 60,000 psi (415 MPa) and 40,000 psi (275 MPa).
(d) Estimate fatigue strengths at 2×10^4 and 6×10^5 cycles.

8.33 Suppose that the fatigue data for the steel alloy in Problem 8.32 were taken for bending-rotating tests, and that a rod of this alloy is to be used for an automobile axle that rotates at an average rotational velocity of 600 revolutions per minute. Give the maximum lifetimes of continuous driving that are allowable for the following stress levels: **(a)** 65,000 psi (450 MPa); **(b)** 55,000 psi (380 MPa); **(c)** 45,000 psi (310 MPa); and **(d)** 40,000 psi (275 MPa).

8.34 Three identical fatigue specimens (denoted A, B, and C) are fabricated from a nonferrous alloy. Each is subjected to one of the maximum-minimum stress cycles listed below; the frequency is the same for all three tests.

Specimen	σ_{max} (MPa)	σ_{min} (MPa)
A	+450	−150
B	+300	−300
C	+500	−200

(a) Rank the fatigue lifetimes of these three specimens from the longest to the shortest.
(b) Now justify this ranking using a schematic *S–N* plot.

8.35 Cite five factors that may lead to scatter in fatigue life data.

8.36 Make a schematic sketch of the fatigue behavior for some metal for which the stress ratio R has a value of $+1$.

8.37 Using Equations 8.13 and 8.14, demonstrate that increasing the value of the stress ratio R produces a decrease in stress amplitude σ_a.

8.38 Surfaces for some steel specimens that have failed by fatigue have a bright crystalline or grainy appearance. Laymen may explain the failure by saying that the metal crystallized while in service. Offer a criticism for this explanation.

8.39 Briefly explain the difference between fatigue striations and beachmarks both in terms of **(a)** size and **(b)** origin.

8.40 Consider a flat plate of some metal alloy that is to be exposed to repeated tensile-compressive cycling in which the mean stress is 25 MPa. If the initial and critical surface crack lengths are 0.25 and 5.0 mm, respectively, and the values of m and A are 4.0 and 5×10^{-15}, respectively (for $\Delta\sigma$ in MPa and a in m), estimate the maximum tensile stress to yield a fatigue life of 3.2×10^5 cycles. Assume that Y has a value of 2.0, which is independent of crack length.

8.41 Consider a large, flat plate of a metal alloy which is to be exposed to reversed tensile-compressive cycles of stress amplitude 150 MPa. If initially the length of the largest surface crack in this specimen is 0.75 mm and the plane strain fracture toughness is 35 MPa$\sqrt{\text{m}}$, whereas the values of m and A are 2.5 and 2×10^{-12}, respectively (for $\Delta\sigma$ in MPa and a in m), estimate the fatigue life of this plate. Assume that the parameter Y has a value of 1.75 which is independent of crack length.

8.42 Consider a metal component that is exposed to cyclic tensile-compressive stresses. If the fatigue lifetime must be a minimum of 5×10^6 cycles and it is known that the maximum initial surface crack length is 2.0×10^{-2} in. and the maximum tensile stress is 25,000 psi, compute the critical surface crack length. Assume that Y is independent of crack length and has a value of 2.25, and that m and A have values of 3.5 and 1.3×10^{-23}, respectively, for $\Delta\sigma$ and a in units of psi and in., respectively.

8.43 List four measures that may be taken to increase the resistance to fatigue of a metal alloy.

8.44 Give the approximate temperature at which creep deformation becomes an important consideration for each of the following metals: nickel, copper, iron, tungsten, lead, aluminum.

8.45 Superimpose on the same strain-versus-time plot schematic creep curves for both constant tensile stress and constant load, and explain the difference in behavior.

8.46 The following creep data were taken on an aluminum alloy at 400°C (750°F) and a constant stress of 3660 psi (25 MPa). Plot the data as strain versus time, then determine the steady-state or minimum creep rate. *Note:* The initial and instantaneous strain is not included.

Time (min)	Strain	Time (min)	Strain
0	0.000	16	0.135
2	0.025	18	0.153
4	0.043	20	0.172
6	0.065	22	0.193
8	0.078	24	0.218
10	0.092	26	0.255
12	0.109	28	0.307
14	0.120	30	0.368

8.47 A specimen 40 in. (1015 mm) long of a low carbon–nickel alloy (Figure 8.35) is to be exposed to a tensile stress of 10,000 psi (70 MPa) at 427°C (800°F). Determine its elongation after 10,000 h. Assume that the total of both instantaneous and primary creep elongations is 0.05 in. (1.3 mm).

8.48 For a cylindrical low carbon–nickel alloy specimen (Figure 8.35) originally 0.75 in. (19.05 mm) in diameter and 25 in. (635 mm) long, what tensile load is necessary to produce a total elongation of 0.25 in. (6.4 mm) after 5000 h at 538°C (1000°F)? Assume that the sum of instantaneous and primary creep elongations is 0.07 in. (1.8 mm).

8.49 If a component fabricated from a low carbon–nickel alloy (Figure 8.34) is to be exposed to a tensile stress of 31 MPa (4500 psi) at 649°C (1200°F), estimate its rupture lifetime.

8.50 A cylindrical component constructed from a low carbon–nickel alloy (Figure 8.34) has a diameter of 0.75 in. (19.1 mm). Determine the maximum load which may be applied for it to survive 10,000 h at 538°C (1000°F).

8.51 From Equation 8.23, if the logarithm of $\dot{\epsilon}_s$ is plotted versus the logarithm of σ, then a straight line should result, the slope of which is the stress exponent n. Using Figure 8.35, determine the value of n for the low carbon–nickel alloy at each of the three temperatures.

8.52 **(a)** Estimate the activation energy for creep (i.e., Q_c in Equation 8.24) for the low carbon–nickel alloy having the steady-state creep behavior shown in Figure 8.35. Use data taken at a stress level of 8000 psi (55 MPa) and temperatures of 427°C and 538°C. **(b)** Estimate $\dot{\epsilon}_s$ at 649°C (922 K).

8.53 Steady-state creep rate data are given below for some alloy taken at 200°C (473 K):

$\dot{\epsilon}_s$ (h^{-1})	σ [MPa (psi)]
2.5×10^{-3}	55 (8,000)
2.4×10^{-2}	69 (10,000)

If it is known that the activation energy for creep is 140,000 J/mol, compute the steady-state creep rate at a temperature of 250°C (523 K) and a stress level of 48 MPa (7000 psi).

8.54 Steady-state creep data taken for an iron alloy at a stress level of 20,000 psi (140 MPa) are given below:

$\dot{\epsilon}_s$ (h^{-1})	T(K)
6.6×10^{-4}	1090
8.8×10^{-2}	1200

If it is known that the value of the stress exponent n for this alloy is 8.5, compute the steady-state creep rate at 1300 K and a stress level of 12,000 psi (83 MPa).

8.55 An S-590 iron component (Figure 8.36) must have a creep rupture lifetime of at least 20 days at 650°C (923 K). Compute the maximum allowable stress level.

8.56 Consider an S-590 iron component (Figure 8.36) that is subjected to a stress of 8000 psi (55 MPa). At what temperature will the rupture lifetime be 200 h?

8.57 An 18-8 Mo stainless steel (Figure 8.39) must have a creep rupture lifetime of at least 5 years at 500°C (773 K). Compute the maximum allowable stress level.

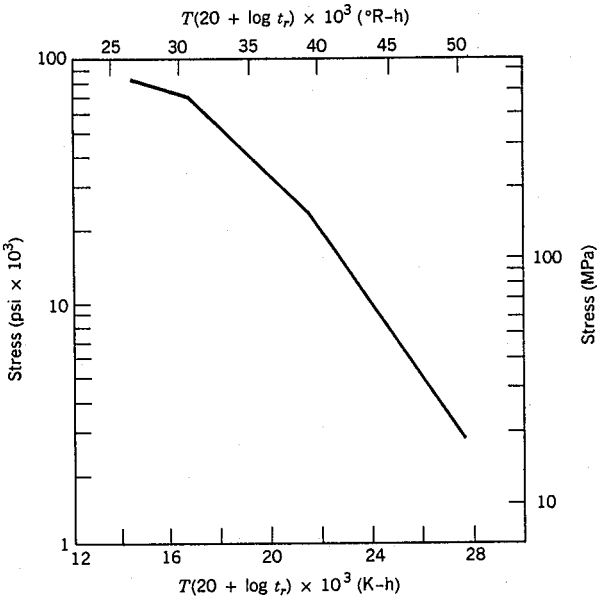

Figure 8.39 Logarithm stress versus the Larson–Miller parameter for an 18-8 Mo stainless steel. (From F. R. Larson and J. Miller, *Trans. ASME*, **74**, 765 (1952). Reprinted by permission of ASME.)

8.58 Consider an 18-8 Mo stainless steel component (Figure 8.39) that is subjected to a stress of 5000 psi (34.5 MPa). At what temperature will the rupture lifetime be 10 years? 20 years?

8.59 Cite three metallurgical/processing techniques that are employed to enhance the creep resistance of metal alloys.

Basic Concepts in Elasticity

In finite elements we want to relate the forces on the system to the displacements of the system nodes. to do this we need to look at some basic concepts

Stress - defined as force/unit area.

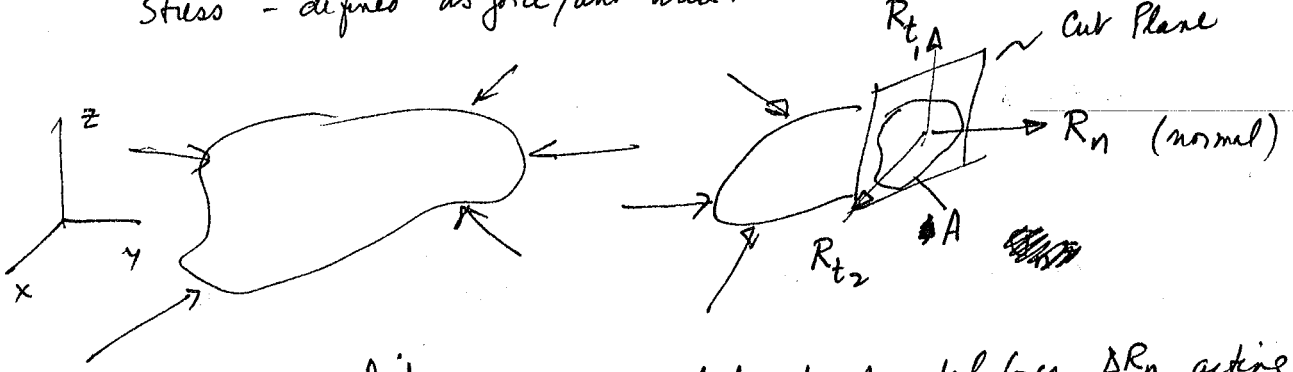

look at body on which forces

look at elemental force ΔR_n acting over

$$\Delta A \Rightarrow \sigma_n = \lim_{\Delta A \to 0} \frac{\Delta R_n}{\Delta A}$$ - normal stress

$$\Delta R_{t_1} \Rightarrow \sigma_{t_1} = \lim_{\Delta A \to 0} \frac{\Delta R_{t_1}}{\Delta A}$$

$$\Delta R_{t_2} \qquad \sigma_{t_2} = \lim_{\Delta A \to 0} \frac{\Delta R_{t_2}}{\Delta A}$$

} shear stresses

units of stress are #/sq in, #/ft², pascals = N/m^2

$$1 psi = 6895 N/m^2$$

Let's look at how we can derive the equations of equilibrium.

Sign Convention

σ_{ab}

a - dir of normal

b - dir of stress

→ in + dir if normal in + dir

→ in - dir if normal in - dir

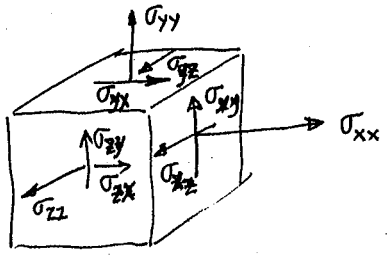

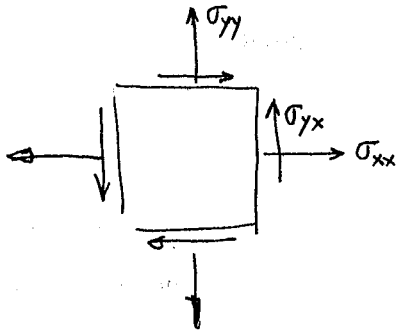

look at equilib in 2-D

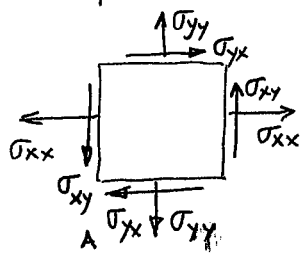

$$\sum M_A \circlearrowleft + = \left[\sigma_{yy}\frac{\Delta x}{2}\cdot\frac{\Delta x}{2} - \sigma_{yy}\frac{\Delta x}{2} + \sigma_{yx}\frac{\Delta y}{2} - \sigma_{yx}\frac{\Delta y}{2} + \sigma_{xy}\cdot\Delta x + \sigma_{xx}\frac{\Delta y}{2} - \sigma_{xx}\frac{\Delta y}{2}\right] W = 0$$

$$\Rightarrow \sigma_{xy} = \sigma_{yx}$$

equil in 2-D

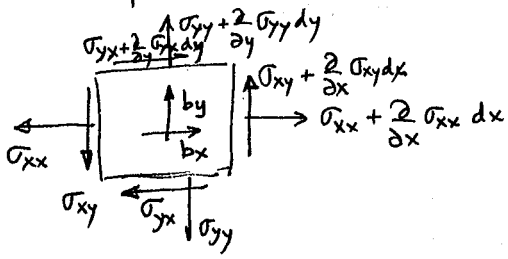

b_x, b_y are body forces per unit vol.

$$\sum F_x = 0 \quad \left[\sigma_{xx} + \frac{\partial}{\partial x}\sigma_{xx}dx\right]dydz - \sigma_{xx}dydz + \left[\sigma_{yx} + \frac{\partial}{\partial y}\sigma_{yx}dy\right]dxdz - \sigma_{yx}dxdz + b_x dxdydz = 0$$

$$= \left[\frac{\partial}{\partial x}\sigma_{xx} + \frac{\partial \sigma_{yx}}{\partial y} + b_x\right] vol = 0$$

$$\sum F_y = \left[\sigma_{yx} + \frac{\partial}{\partial y}\sigma_{yy}dy - \sigma_{yy}\right]dxdz + \left[\sigma_{xy} + \frac{\partial}{\partial x}\sigma_{xy}dx - \sigma_{xy}\right]dydz + b_y \cdot dxdydz = 0$$

$$= \left[\frac{\partial}{\partial y}\sigma_{yy} + \frac{\partial}{\partial x}\sigma_{xy} + b_y\right] Vol = 0$$

in 3-D

$$\frac{\partial}{\partial x}\sigma_{xx} + \frac{\partial}{\partial y}\sigma_{yx} + \frac{\partial}{\partial z}\sigma_{zx} + b_x = 0$$

$$\frac{\partial}{\partial x}\sigma_{xy} + \frac{\partial}{\partial y}\sigma_{yy} + \frac{\partial}{\partial z}\sigma_{zy} + b_y = 0$$

$$\frac{\partial}{\partial x}\sigma_{xz} + \frac{\partial}{\partial x}\sigma_{yz} + \frac{\partial}{\partial z}\sigma_{zz} + b_z = 0$$

$$\sigma_{xy} = \sigma_{yx} \qquad \sigma_{xz} = \sigma_{zx} \qquad \sigma_{yz} = \sigma_{zy}$$

stress & tractions are different $t_j = \sigma \cdot n_j \qquad \sigma = \sigma_{ij} n_i n_j$

stress is a tensor ; stress dotted with the normal vector to a surface yields the traction (a vector)

the principal transformations

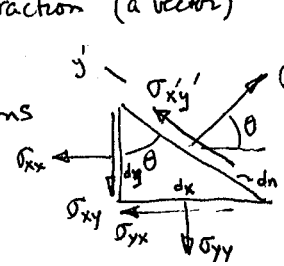

$$\sigma_{x'x'} \cdot dn\cos\theta - \sigma_{x'y'}dn\sin\theta = \sigma_{xx}dy + \sigma_{yx}dx$$

$$\sigma_{x'x'} \cdot dn\sin\theta + \sigma_{x'y'}dn\cos\theta = \sigma_{yy}dx + \sigma_{xy}dy$$

$$\sigma_{x'x'} \cdot dn = \sigma_{xx}\cos\theta\, dy + \sigma_{yx}dx\cos\theta + \sigma_{xy}\sin\theta\, dy + \sigma_{yy}dx\sin\theta$$

$dx = dn\cos\theta \qquad dx = d\cdot\sin\theta$

13. PRACTICE PROBLEMS

This chapter contains practice problems that correspond to material in Chapters 1 to 11. Some of the problems for Chapters 7 to 10 require a computer program or spreadsheet macro. This level of complexity was necessary in order to make the application-oriented problems realistic.

All quantitative data are given in SI units, although the corresponding values in English units are also provided in many cases.

13.1 CHAPTER 1

1.1 Compile a list of five mechanical or structural failures that have occurred within the last 20 years. Describe the factors that led to each failure and identify the failures that resulted from misapplication of existing knowledge (Type 1) and those that involved new technology or a significant design modification (Type 2).

HW 1 **1.2** A flat plate with a through-thickness crack (Fig. 1.8) is subject to a 100 MPa (14.5 ksi) tensile stress and has a fracture toughness (K_{Ic}) of 50.0 MPa $\sqrt{\text{m}}$ (45.5 ksi $\sqrt{\text{in}}$). Determine the critical crack length for this plate, assuming the material is linear elastic. $K_{Ic} = \sigma\sqrt{\pi a}$ $\quad a = .079$ $\quad 2a = .159$ m

HW 1 **1.3** Compute the critical energy release rate (G_c) of the material in the previous problem for E = 207,000 MPa (30,000 ksi). $G_c = K_{Ic}^2/E = .01201$ MPa-m

1.4 Suppose that you plan to drop a bomb out of an airplane and that you are interested in the time of flight before it hits the ground, but you cannot remember the appropriate equation from your undergraduate physics course. Your decide to infer a relationship for time of flight of a falling object by experimentation. You reason that the time of flight, t, must depend on the height above the ground, h, and the weight of the object, mg, where m is the mass and g is the gravitational acceleration. Therefore, neglecting aerodynamic drag, the time of flight is given by the following function:

$$t = f(h,m,g)$$

Apply dimensional analysis to this equation and determine how many experiments would be required to determine f to a reasonable approximation, assuming you know the numerical value of g. Does the time of flight depend on the mass of the object?

13.2 CHAPTER 2

2.1 According to Eq. (2.25), the energy required to increase the crack area a unit amount is equal to *twice* the fracture work per unit surface area, w_f. Why is the factor of 2 in this equation necessary?

2.2 Derive Eq. (2.30) for both load control and displacement control by substituting Eq. (2.29) into Eqs. (2.27) and (2.28), respectively.

HW 1 **2.3** Figure 2.10 illustrates that the driving force is linear for a through-thickness crack in an infinite plate when the stress is fixed. Suppose that a remote displacement (rather than load) were fixed in this configuration. Would the driving force curves be altered? Explain. (Hint: see Section 2.5.3).

HW 1 **2.4** A plate $2W$ wide contains a centrally located crack $2a$ long and is subject to a tensile load, P. Beginning with Eq. (2.24), derive an expression for the elastic compliance, $C\ (= \Delta/P)$ in terms of the plate dimensions and elastic modulus, E. The stress in Eq. (2.24) is the nominal value; i.e., $\sigma = P/2BW$ in this problem. (Note: Eq. (2.24) only applies when $a << W$; the expression you derive is only approximate for a finite width plate.) yes $C_m = \infty$ & $C_m = 0$ in the 2 cases

HW 1 **2.5** A material exhibits the following crack growth resistance behavior:

$$R = 6.95(a - a_o)^{0.5}$$

where a_o is the initial crack size. R has units of kJ/m^2 and crack size is in millimeters. Alternatively,

$$R = 200(a - a_o)^{0.5}$$

$G = R$
$dG/da = dR/da$

where R has units of in-lb/in^2 and crack size is in inches. The elastic modulus of this material = 207,000 MPa (30,000 ksi). Consider a wide plate with a through crack ($a << W$) that is made from this material.

(a) If this plate fractures at 138 MPa (20.0 ksi), compute the following:
  (i) The half crack size at failure (a_c). 28?.4 mm
  (ii) The amount of stable crack growth (at each crack tip) that precedes failure (a_c - a_o). 144.7 mm

(b) If this plate has an initial crack length ($2a_o$) of 50.8 mm (2.0 in) and the plate is loaded to failure, compute the following:
  (i) The stress at failure. 213.2 MPa
  (ii) The half crack size at failure. $a_c = 50.8$ mm
  (iii) The stable crack growth at each crack tip. 25.4 mm

2.14 A semicircular surface crack in a pressure vessel is 10 mm (0.394 in) deep. The crack is on the inner wall of the pressure vessel and is oriented such that the hoop stress is perpendicular to the crack plane. Calculate K_I if the local hoop stress = 200 MPa (29.0 ksi) and the internal pressure = 20 MPa (2900 psi). Assume that the wall thickness >> 10 mm.

2.15 Calculate K_I for a semielliptical surface flaw at $\phi = 0°, 30°, 60°, 90°$.

$\sigma = 150$ MPa (21.8 ksi); $a = 8.00$ mm (0.315 in); $2c = 40$ mm (1.57 in).

2.16 Consider a plate subject to biaxial tension with a through crack of length $2a$, oriented at an angle β from the σ_2 axis (Fig. 13.1). Derive expressions for K_I and K_{II} for this configuration. What happens to each K expression when $\sigma_1 = \sigma_2$?

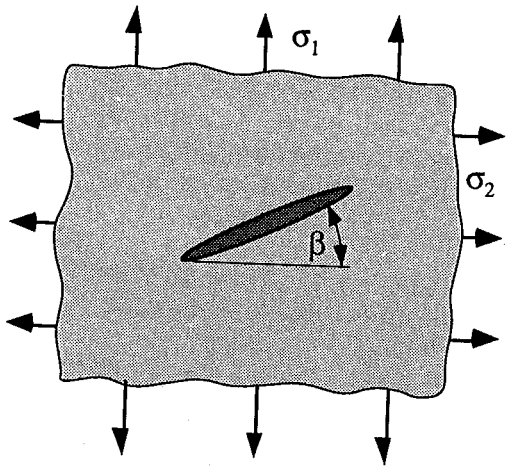

FIGURE 13.1 Through-thickness crack in a biaxially loaded plate (Problem 2.16).

2.17 A wide flat plate with a through-thickness crack experiences a nonuniform normal stress which can be represented by the following crack face traction:

$$p(x) = p_o e^{-x/\beta}$$

where $p_o = 300$ MPa and $\beta = 25$ mm. The origin ($x = 0$) is at the left crack tip, as illustrated in Fig. 2.27. Using the weight function derived in Example 2.6, calulate K_I at each crack tip for $2a = 25$, 50, and 100 mm. You will need to integrate the weight function *numerically*.

2.18 Calculate K_{eff} (Irwin correction) for a through crack in a plate of width $2W$ (Fig. 2.20(b)). Assume plane stress conditions and the following stress intensity relationship:

Describe a set of experiments you could perform to determine $f(a/W)$ for this specimen configuration. Hint: you may want to take advantage of the relationship between K_I and energy release rate for linear elastic materials.

2.22 Derive the Griffith-Inglis result for the potential energy of a through crack in an infinite plate subject to a remote tensile stress (Eq. (2.16)). Hint: solve for the work required to close the crack faces; Eq. (A2.43b) gives the crack opening displacement for this configuration.

2.23 Using the Westergaard stress function approach, derive the stress intensity factor relationship for an infinite array of collinear cracks in a plate subject to biaxial tension (Fig. 2.21).

13.3 CHAPTER 3

3.1 Repeat the derivation of Eqs. (3.1) to (3.3) for the plane strain case.

3.2 A *CTOD* test is performed on a three point bend specimen. Figure 13.3 shows the deformed specimen after it has been unloaded. That is, the displacements shown are the *plastic components*.

(a) Derive an expression for plastic *CTOD* (δ_p) in terms of Δ_p and specimen dimensions.

(b) Suppose that V_p and Δ_p are measured on the same specimen, but that the plastic rotational factor, r_p, is unknown. Derive an expression for r_p in terms of Δ_p, V_p and specimen dimensions, assuming the angle of rotation is small.

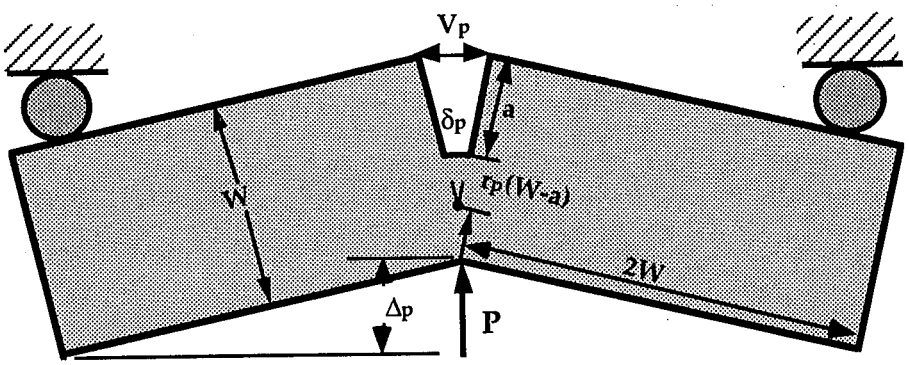

FIGURE 13.2 Three-point bend specimen rotating about a plastic hinge (Problem 3.2).

13.4 CHAPTER 4

4.1 A high rate fracture toughness test is to be performed on a high strength steel with K_{Id} = 110 MPa $\sqrt{m}$ (100 ksi $\sqrt{in}$). A three-point bend specimen will be used, with W = 50.8 mm (2.0 in), a/W = 0.5, B = $W/2$, and span = $4W$. Also, c_1 = 5940 m/sec (19,500 ft/sec) for steel. Estimate the maximum loading rate at which the quasistatic formula for estimating K_{Id} is approximately valid.

4.2 Unstable fracture initiates in a steel specimen and arrests after the crack propagates 8.0 mm (0.32 in). The total propagation time was 7.52 x 10^{-6} sec. The initial ligament length in the specimen was 30.0 mm (1.18 in) and c_1 for steel = 5940 m/sec (19,500 ft/sec). Determine whether or not reflected stress waves influenced the propagating crack.

30
8 14.88

prop time · c_1 = 44.88mm > lig length.
crack 22mm from edge. reflected wave comes back to only 14.88

4.3 Fracture initiates at an edge crack in a 2.0 m (78.7 in) wide steel plate and rapidly propagates through the material. The stress in the plate is fixed at 300 MPa (43.5 ksi). Plot the crack speed versus crack size for crack lengths ranging from 10 to 60 mm (or 0.4 to 2.4 in). The dynamic fracture toughness of the material is given by

$$K_{ID} = \frac{K_{IA}}{1 - \left(\frac{V}{V_l}\right)^2}$$

where K_{IA} = 55 MPa $\sqrt{m}$ (50 ksi $\sqrt{in}$) and V_l = 1500 m/sec (4920 ft/sec) Use the Rose approximation (Eqs. (4.17) and (4.18)) for the driving force. The elastic wave speeds for steel are given below.

c_1	5940 m/sec	19,500 ft/sec
c_2	3220 m/sec	10,600 ft/sec
c_r	2980 m/sec	9780 ft/sec

4.4 Derive an expression for C^* in a double edge notched tension panel in terms of specimen dimensions, creep exponent, load, and displacement rate. See Section 3.2.5 for the corresponding J expression.

intensity factor characterize the crack tip conditions in this case? Explain. What is the relationship between J and K_I for a linear viscoelastic material? Hint: refer to the second equation in the previous problem.

13.5 CHAPTER 5

5.1 A body-centered cubic (BCC) material contains second phase particles. The size of these particles can be controlled through thermal treatment. Discuss the anticipated effect of particle size on the material's resistance to both cleavage fracture and microvoid coalescence, assuming the volume fraction of the second phase remains constant.

5.2 An aluminum alloy fails by microvoid coalescence when the average void size reaches ten times the initial value. If the voids grow according to Eq. (5.11), with σ_{YS} replaced by σ_e, plot the equivalent plastic strain (ε_{eq}) at failure versus σ_m/σ_e for σ_m/σ_e ranging from 0 to 2.5. Assume the triaxiality ratio remains constant during deformation of a given sample; i.e.,

$$\ln\left(\frac{\bar{R}}{R_o}\right) = 0.283\exp\left(\frac{1.5\sigma_m}{\sigma_e}\right)\int_0^{\varepsilon_{eq}} d\varepsilon_{eq}$$

5.3 The critical microstructural feature for cleavage initiation in a steel sample is a 6.67 μm diameter spherical carbide; failure occurs when this particle forms a microcrack that satisfies the Griffith criterion (Eq. (5.18)), where γ_p = 14 J/m^2, E = 207,000 MPa, and ν = 0.30 for the material. Assuming Fig. 5.14 describes the stress distribution ahead of the macroscopic crack, where σ_O = 350 MPa, estimate the critical J value of the sample if the particle is located 0.1 mm ahead of the crack tip, on the crack plane. Repeat this calculation for the case where the critical particle is 0.4 mm ahead of the crack tip.

5.4 Cleavage initiates in a ferritic steel at 3.0 μm diameter spherical particles. The fracture energy on a single grain, γ_p, is 14 J/m^2 and the fracture energy required for propagation across grain boundaries, γ_{gb}, is 50 J/m^2. At what grain size does propagation across grain boundaries become the controlling step for cleavage fracture?

5.5 Compute the relative size of the 90% confidence band of K_{Ic} data (as in Example 5.1), assuming Eq. (5.24) describes the toughness distribution. Compute the confidence band width for K_O/Θ_K = 0, 0.5, 1.0, 2.0, and 5.0. What is the effect of the threshold toughness, K_O, on the relative scatter? What is the physical significance of Θ_K in this case?

quantities: (a) specimen dimensions, (b) precracking loads, and (c) required load capacity of the test machine.

7.3 A titanium alloy is supplied in 15.9 mm (0.625 in) thick plate. If σ_{YS} = 807 MPa (117 ksi), calculate the maximum valid K_{Ic} that can be measured in this material.

7.4 Recall Problem 2.16, where a material with K_{Ic} = 110 MPa $\sqrt{\text{m}}$ (100 ksi $\sqrt{\text{in}}$) required a 254 mm (10.0 in) thick specimen for a valid K_{Ic} test. Suppose that a compact specimen of the appropriate dimensions has been fabricated. Estimate the required load capacity of the test machine for such a test.

7.5 A 25.4 mm (1 in) thick steel plate has material properties which are tabulated below. Determine the highest temperature at which it is possible to perform a valid K_{IC} test.

Temperature, °C	Yield Strength, MPa	K_{Ic}, MPa$\sqrt{\text{m}}$
-10	760	34
-5	725	36
0	690	42
5	655	50
10	620	62
15	586	85
20	550	110
25	515	175

7.6 A fracture toughness test is performed on a compact specimen fabricated from a 5 mm thick sheet aluminum alloy. The specimen width (W) = 50.0 mm and B = 5 mm (the sheet thickness). The initial crack length is 26.0 mm. Young's modulus = 70,000 MPa. Compute the K-R curve from the load-displacement data tabulated below. Assume that all nonlinearity in the P-Δ curve is due to crack growth. (See Chapter 12 for the appropriate compliance and stress intensity relationships.)

(b) Determine J_{Ic} according to ASTM E 813.

B = 25.0 mm; W = 50.0 mm; a_O = 26.1 mm; E = 210,000 MPa, ν = 0.3

σ_{YS} = 345 MPa (50 ksi); σ_{TS} = 483 MPa (70 ksi)

(c) Plot and compare the J-R curves obtained from the simplified expression (Eq. (7.10)) and the incremental approach that takes account of crack growth (Eq. (7.15)). At what point does the crack growth correction become significant?

LOAD , kN	Plastic Displacement, mm	Crack Extension, mm
20.8	0	0.013
31.2	0.0032	0.020
35.4	0.011	0.023
37.4	0.020	0.025
41.6	0.056	0.031
43.7	0.092	0.036
45.7	0.146	0.044
47.6	0.228	0.055
49.9	0.349	0.071
51.6	0.525	0.091
53.5	0.777	0.128
55.3	1.13	0.183
56.6	1.63	0.321
56.7	2.32	0.723
56.5	2.66	0.928
55.8	3.25	1.29
54.7	3.96	1.74
53.7	4.51	2.08
52.5	5.13	2.48
50.1	6.20	3.17
44.4	8.43	4.67
40.0	10.09	5.81
36.6	11.37	6.70
30.9	13.54	8.23
26.8	15.19	9.41

1 kN = 224.8 lb 25.4 mm = 1 in 1 MPa = 0.145 ksi

7.9 A CTOD test was performed on a three point bend specimen with $B = W$ = 25.4 mm (1.0 in). The crack depth, a, was 12.3 mm (0.484 in). Examination of the

where E is in GPa and t is in seconds. Assuming P_Q is determined from a 5% secant construction, estimate the test duration (i.e. the time to reach P_Q) at which 90% of the nonlinearity in the load-displacement curve at P_Q is due to viscoelastic effects. Does the 5% secant load give an appropriate indication of material toughness in this case? Explain.

8.4 Derive a relationship between the conventional J integral and the isochronous J integral, J_t, in a constant displacement rate test on a viscoelastic material for which Eqs. (8.10) and (8.15) describe the load-displacement behavior.

8.5 A 500 mm wide plastic plate contains a through-thickness center crack that is initially 50 mm long. The crack velocity in this material is given by

$$\dot{a} = 10^{-40} K^{10}$$

where K is in kPa $\sqrt{\text{m}}$ and $\dot{a}$ is in mm/sec (1 psi $\sqrt{\text{in}}$ = 1.1 kPa $\sqrt{\text{m}}$, 1 in = 24.5 mm). Calculate the time to failure in this plate assuming remote tensile stresses of 5 MPa and 10 MPa (1 ksi = 6.897 MPa). Comment on the sensitivity of the time to failure on the applied stress. (As a first approximation, neglect the finite width correction on K. For an optional exercise, repeat the calculations with this correction to assess its effect on the computed failure times.)

8.6 A composite double cantilever beam (DCB) specimen is loaded to 445 N (100 lb) at which time crack growth begins. Calculate $\mathcal{G}_{Ic}$ for this material assuming linear beam theory.

E = 124,000 MPa (18,000 ksi); a = 76.2 mm (3.0 in); h = 2.54 mm (0.10 in); B = 25.4 mm (1.0 in).

8.7 One of the problems with testing brittle materials is that crack growth tends to be unstable in conventional test specimens and test machines. Consider, for example, a single edge notched bend (SENB) specimen loaded in three point bending. The influence of the test machine can be represented by a spring in series, as Fig. 13.4 illustrates. Show that the stress intensity factor for this specimen can be expressed as a function of crosshead displacement and compliance as follows:

$$K_I = \frac{\Delta_t f(a/W)}{(C + C_m) B \sqrt{W}}$$

where Δ_t is the crosshead displacement, C is the specimen compliance, C_m is the machine compliance, and $f(a/W)$ is defined in Table 12.2. Construct a

p = 17.2 MPa (2500 psi); R_i = 1.00 m; t/R_i = 0.10; a/t = 0.20; a/c = 0.40.

9.3 A nuclear reactor pressure vessel operates at an internal pressure of 17.2 MPa (2500 psi) and a temperature of 200°C (392°F). The steel in this pressure vessel has an RT_{NDT} of 100°C (212°F), and thus is relatively brittle at room temperature. Consequently, the full design pressure is not applied when the reactor is cold. Upon start-up, the temperature and pressure must be increased in tandem in order to avoid brittle fracture.

(a) Determine the maximum allowable pressure-temperature curve, ranging from ambient to the design temperature. As a worst case, assume the vessel contains an internal axial surface flaw with a/t = 0.25 and a/c = 0.50, and that the fracture toughness is given by the K_{IR} curve (Eq. (9.17b)). Assume linear elastic conditions. The vessel dimensions are given below.

$$R_i = 2.16 \text{ m (85.0 in)}; \quad t = 21.6 \text{ mm (8.50 in)}$$

(b) As the reactor operates over a period of several years, the steel becomes embrittled due to radiation damage, and the RT_{NDT} increases with time. Estimate the RT_{NDT} at which it is no longer safe to start up the reactor.

(c) The pressure vessel is made from A 533 Grade B steel, which has a yield strength of 460 MPa (66.7 ksi). Was the assumption of linear elastic conditions acceptable in this case?

9.4 A structure contains a through-thickness crack 20 mm long. Strain gages indicate an applied normal strain of 0.0042 when the structure is loaded to its design limit. The structure is made of a steel with ε_y = 0.0020 and δ_{crit} = 0.15 mm. Is this structure safe, according to the *CTOD* design curve?

9.5 A welded structure is loaded in combined bending and tension, with P_m = 200 MPa and P_b = 150 MPa. The structure is in the as-welded condition; the precise residual stress distribution in the weldment is unknown. Determine the maximum allowable flaw size, $\tilde{a}$, according to the 1980 version of the PD 6493 approach (Eqs. (9.18) and (9.19)).

σ_{YS} = 400 MPa; E = 207,000 MPa; δ_{crit} = 0.23 mm

9.6 A flat plate 1.0 m (39.4 in) wide and 50 mm (2.0 in) thick which contains a semi-elliptical surface flaw is loaded in uniaxial tension to 0.75 σ_{YS}. Assuming the ratio $a/2c$ = constant = 0.3, plot K_r and S_r values on a strip yield failure assessment diagram for various flaw sizes. Estimate the critical flaw size for failure. (See Tables 12.22 and 12.24 for K_I and limit load solutions.)

a, b fin
a, c init
a, d, b both
b, c, d both
b, d init
c, d fin
a, c, d both

	Initial Crack Radius	Final Crack Radius
a	1 mm	10 mm
b	1 mm	20 mm
c	2 mm	10 mm
d	2 mm	20 mm

1 .1 MPa $\sqrt{\text{in}}$ = 1 ksi $\sqrt{\text{in}}$ 25.4 mm = 1 in 1 MPa = 0.145 ksi use a Δa = 1 mm

Discuss the relative sensitivity of N_{tot} to:
- initial crack size.
- final crack size.

10.2 A structural component made from a high strength steel is subject to cyclic loading, with σ_{max} = 210 MPa and σ_{min} = 70 MPa. This component experiences 100 stress cycles per day. Prior to going into service, the component was inspected by nondestructive evaluation (NDE), and no flaws were found. The material has the following properties: σ_{YS} = 1000 MPa, K_{Ic} = 25 MPa $\sqrt{\text{m}}$. The fatigue crack growth rate in this material is the same as in Problem 10.1.

(a) The NDE technique can find flaws ≥ 2 mm deep. Estimate the maximum safe design life of this component, assuming that subsequent in-service inspections will not be performed. Assume that any flaws that may be present are semicircular surface cracks and that they are small relative to the cross section of the component.

(b) Repeat part (a), assuming an NDE detectability limit of 10 mm.

10.3 Fatigue tests are performed on two samples of an alloy for aerospace applications. In the first experiment, R = 0, while R = 0.8 in the second experiment. Sketch the expected trends in the data for the two experiments on a schematic log(da/dN) *v.* log(ΔK) plot. Assume that the experiments cover a wide range of ΔK values. Briefly explain the trends in the curves.

10.4 Write a program or spreadsheet macro to compute fatigue crack growth behavior in a compact specimen, assuming the fatigue crack growth is governed by the Paris-Erdogan equation.

Consider a 1T compact specimen (see Section 7.1.1) that is loaded cyclically at a constant load amplitude with P_{max} = 18 kN and P_{min} = 5 kN. Using the fatigue crack growth data in Problem 10.1, calculate the number of cycles required to

grow the crack from $a/W = 0.35$ to $a/W = 0.60$. Plot crack size versus cumulative cycles for this range of a/W.

10.5 Write a program or spreadsheet macro to compute the fatigue crack growth behavior in a flat plate that contains a semielliptical surface flaw and is subject to a cyclic membrane (tensile) stress. Assume that the flaw remains semielliptical, but take account of the difference in K at $\phi = 0°$ and $\phi = 90°$. Also, assume that $c << W$, but that a/t is finite. Use the Paris-Erdogan equation to compute the crack growth rate.

Consider a 25.4 mm (1.0 in) thick plate that is loaded cyclically at a constant stress amplitude of 200 MPa (29 ksi). Given an initial flaw with $a/t = 0.1$ and $a/2c = 0.1$, calculate the number of cycles required to grow the crack to $a/t = 0.8$, using the fatigue crack growth data in Problem 10.1. Construct a contour plot that shows the crack size and shape at $a/t = 0.1$, 0.2, 0.4, 0.6, and 0.8. What happens to the $a/2c$ ratio as the crack grows?

10.6 Estimate U and K_{op} as a function of R and ΔK for the data in Fig. 10.8. Does Eq. (10.19) fit the data adequately or does U depend on K_{max}? Does Eq. (10.20) adequately describe the data? If so, determine the parameter K_O.

10.7 Suppose that the 1T compact specimen in Problem 10.4 experiences a single overload of 36 kN when $a/W = 0.45$. During all other cycles the load amplitude is constant, with P_{max} = 18 kN and P_{min} = 5 kN. Using the Wheeler retardation model with $\gamma = 1.5$, estimate the number of cycles required to grow the crack from $a/W = 0.35$ to $a/W = 0.60$. Plot crack size versus cumulative cycles, comparing the present case to the constant load amplitude case of Problem 10.4. Assume plane strain conditions at the crack tip and σ_{YS} = 250 MPa.

10.8 You have been asked to perform K-decreasing tests on a material to determine the near-threshold behavior at $R = 0.1$. Your laboratory has a computer-controlled test machine that can be programmed to vary P_{max} and P_{min} on a cycle-by-cycle basis.

(a) Compute and plot P_{max} and P_{min} versus crack length for the range $0.5 \leq a/W \leq 0.75$ corresponding to a normalized K gradient of - 0.07 mm^{-1} in a 1T compact specimen.

(b) Suppose that the material exhibits the following crack growth behavior near the threshold:

$$\frac{da}{dN} = 4.63x10^{-12}(\Delta K^3 - \Delta K_{th}^3)$$

11.3 Displacements at nodes along the upper crack face (u_2 at $\theta = \pi$) in the previous problem are tabulated below. The elastic constants are as follows: μ = 80,000 MPa and $\kappa = 1.80$. Estimate K_I by means of the displacement matching approach (Eq. 11.15) and compare your estimate to the exact solution for this geometry. Is the mesh refinement sufficient to obtain an accurate solution in this case?

$\frac{r}{a}$ $(\theta = \pi)$	$\frac{u_2}{a}$
0.005	9.99×10^{-5}
0.010	1.41×10^{-4}
0.020	1.99×10^{-4}
0.040	2.80×10^{-4}
0.060	3.41×10^{-4}

$\frac{r}{a}$ $(\theta = \pi)$	$\frac{u_2}{a}$
0.080	3.92×10^{-4}
0.100	4.36×10^{-4}
0.150	5.27×10^{-4}
0.200	6.00×10^{-4}
0.250	6.61×10^{-4}

11.4 Figure 13.6 illustrates a one-dimensional element with three nodes. Consider two cases: (1) Node 2 at $x = 0.50$L and (2) Node 2 at $x = 0.25$L.

(a) Determine the relationship between the global and parametric coordinates, $x(\xi)$, in each case.

(b) Compute the axial strain, $\varepsilon(\xi)$ for each case in terms of the nodal displacements and parametric coordinate.

(c) Show that $x_2 = 0.25$L leads to a $1/\sqrt{x}$ singularity in the axial strain.

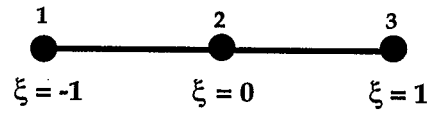

(a) Parametric coordinates.

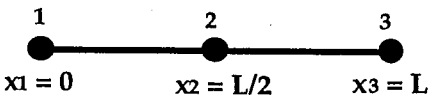

(b) Global coordinates, Case (1).

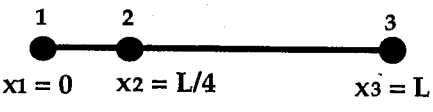

(c) Global coordinates, Case (2).

FIGURE 13.6 One-dimensional element with 3 nodes (Problem 11.4).

MILESTONES IN F.M. OF BRITTLE MATERIALS - 1

Stone Age

Middle Age

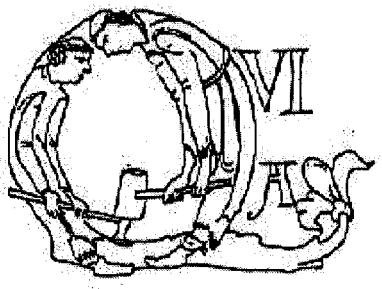

Coulomb Criterion
1776

$$|\tau| = c - \sigma \cdot \mathrm{tg}\,\varphi$$

Griffith Model
1920

Griffith propagation criterion for an elliptical crack in an elastic plate $\sigma^2 \geq 2\gamma E/\pi a$
Surface Energy $2\gamma = G$

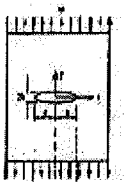

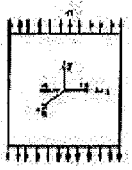

Irwin's Model
1957

Irwin line-crack

Fracture Energy $G = \dfrac{\sigma^2 \pi a}{E}$

Stress Intensity Factor $K_I = \sigma\sqrt{\pi a}$

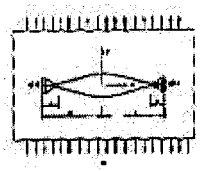

Barenblatt Model
1959

Cohesive crack model with unknown distibution of cohesive forces

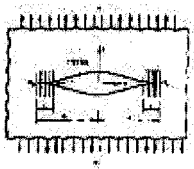

Dugdale Model
1960

Cohesive crack model with constant distribution of closing stresses in the fracture process zone for elastic-perfectly plastic materials

MILESTONES IN F.M. OF BRITTLE MATERIALS - 2

Hillerborg Model 1976

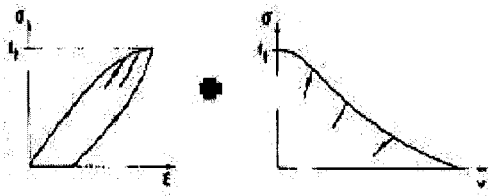

Carpinteri Brittleness Number 1980

$$G_F = \int_0^{w_c} \sigma(w)\,dw$$

$$l_{ch} = G_F E / f_t^2$$

$$s = K_{IC} / \sigma_y h^{1/2}$$

Bazant Size Effect Law 1984

$$\sigma_N = B f_t (1+\beta)^{-1/2}$$

Carpinteri Energy Number 1986

$$s_e = G_F / f_t h$$

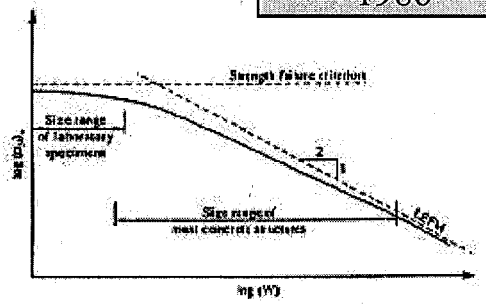

Size Effect Law (by Bazant)

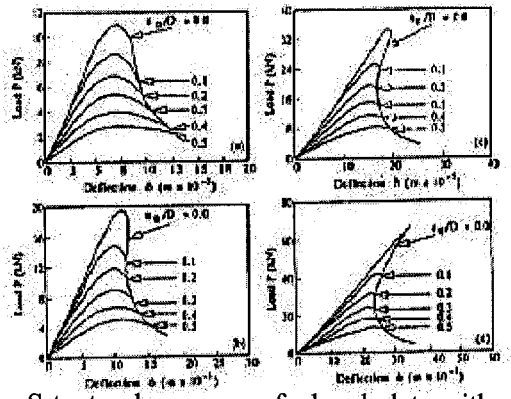

Srtuctural response of a bend plate with four different sizes (by Carpinteri)

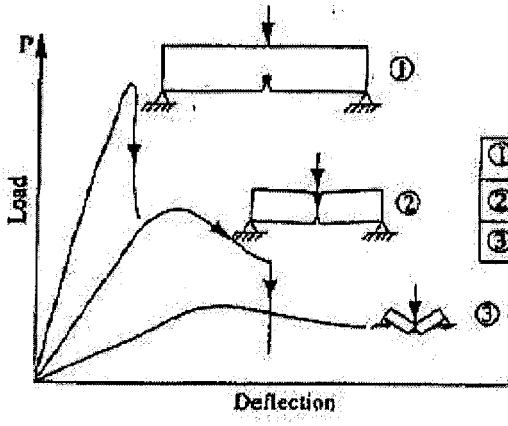

	Structural Behaviour	Crack Growth Process
①	Brittle	Unstable
②	Ductile-Brittle	Stable-Unstable
③	Ductile	Stable

Ductile-Brittle dimensional transition in a three point bend test (by Carpinteri)

EMA 519

Fracture Mechanics

Spring 2000

Assessment and Grading:

Class Participation required

Facilitation of Friday Discussions 20%

Homework Sets 20%

Projects and Case Studies 30%

2 Hour Exams (In-Class) 30%

Date	Week Lect #	Topic	Reading/Assignment Due
M 1/24	Wk 1 1	Introduction	
W 1/26	2	Review of Elasticity Overview of Fracture Mechanics	Anderson: Appendix 2 (p. 101-103) Chou and Pagano, Elasticity, Ch. 1 and 2 Anderson: 1.1 thru 1.2.5 (p. 1-14)
F 1/28	3	Discussion	Petroski, "When Cracks Become Breakthroughs" (e)
M 1/31	Wk 2 4	Linear Elastic Fracture Mechanics	Anderson: 2.1 thru 2.3.1 (p.31-39) A.A. Griffith, 1920, Phil. Trans. Roy. Soc. London A221, p163-198 (e)
W 2/2	5	Microscopic and Macroscopic Fracture Mechanisms	Anderson: 5.1 thru 5.4 (p. 265-302)
Homework #1 Due 2/2: problems 4-5, 4-6, and 4-8 from Chou and Pagano handout			
F 2/4	6	Case Study and Discussion – Material Behavior (April Hammer)	Foecke, "Metallurgy of the RMS Titanic," NIST Report "Did a Metalurgical Failure Cause a Night to Remember?," Felkins et. al. (e) Williams and Keast, "Can Analytical Electron Microscopy Tell Us Why

			Materials Break?"
M 2/7	Wk 3 7	Continuum Mechanics Analysis of Crack Tip Fields	Anderson: p. 51-66, p. 101-109
W 2/9	8	Continuum Mechanics Analysis of Crack Tip Fields	
Homework #2 Due 2/9 For Friday 2/11: Bring in some fracture example from your everyday life			
F 2/11	9	Case Study and Discussion - Ductile-Brittle Transition (Jeremy Severson)	Anderson: p. 407-413 Richards, "Brittle Fracture of Welded Structures" Williams, "Failures in Welded Ships" (e)
M 2/14	Wk 4 10	Plane Linear Elastic Crack Tip Stress Fields	Anderson: p. 109-115
W 2/16	11	Plane Linear Elastic Crack Tip Stress Fields – Mode I	
Homework #3 Due 2/16			
F 2/18	12	Case Study and Discussion - Rocket Motor Case (Chris Alban)	"Materials Selection Case Studies" handout Barsom & Rolfe "Fracture and Fatigue Control in Structures: Applications of Fracture Mechanics" Chapter 5
M 2/21	Wk 5 13	Stress Intensity Factors	Anderson: p. 53-66
W 2/23	14	Stress Intensity Factors	
Homework #4 Due 2/23			
F 2/25	15	Case Study and Discussion - F111 (Dan Niedermaier)	Buntin, "Application of Fracture Mechanics to the F-111 Airplane"
M 2/28	Wk 6 16	Plastic Zone Size and Shape	Anderson: p.78-90, 380-384
W 3/1	17	Fracture Toughness Testing	Anderson: p. 365-380
Project #1 Due 3/1			

F 3/3	18	Discussion (Bridget Welbes)	Annual Book of ASTM Standards, "Foreword" ASTM Standard E 399: "Standard Method for Plane Strain Fracture Toughness of Metallic Materials"
M 3/6	Wk 7 19	Use of LEFM in Design	Anderson, 459-468, 41-51, 69-72
W 3/8	20	Use of LEFM in Design	
Homework #5 Due 3/8: Analysis of fracture toughness test results			
F 3/10	21	Discussion on Rock Fracture Mechanics (Randi Williams)	Anderson, p. 354-357; Comprehensive Rock Engineering Principles, Practice, and Projects; 1993: "The Hydraulic Fracturing Method of Stress Measurement: Theory and Practice"
SPRING BREAK			
M 3/20	Wk 8 22	Energy Methods Relationship Between G and K_I	Anderson p. 41-46, 123-126
W 3/22	23	Compliance Method R-Curve	Anderson p. 46-51
Homework #6 Due 3/22:			
F 3/24	24	Case Study and Discussion - Crane Retrofit (Dave Reich)	Blake, "Practical Fracture Mechanics and Design," section on crane retrofit and materials control
M 3/27	Wk 9 25	NO CLASS	
W 3/29	26	HOUR EXAM I	(Covering material though lecture 21.)
F 3/31	27	Discussion (Chip Sauer)	Hutchinson, "Fundamentals of the Phenomenological Theory of Nonlinear Fracture Mechanics"
M 4/3	Wk 10 28	Plasticity Limitations on LEFM	Anderson p. 89-90

W 4/5	29	Beyond Linear Elasticity	Anderson p. 72-75
Homework #7 Due 4/10			
F 4/7	30	Discussion (Nicole Stark)	Williams, "Fracture Mechanics of Composites Failure"
M 4/10	Wk 11 31	Background for the J - Integral	Anderson: p. 186-193
W 4/12	32	Background for the J - Integral	
Project #2 Due 4/12			
F 4/14	33	Discussion on Rock Fracture Mechanics (Karl Gullerud)	Shah and Ouyang "Fracture Mechanics for Failure of Concrete" Gettu, Ouyang and Shah, "Fracture Mechancis of Concrete - A Review" (sections 6-6.2)
M 4/17	Wk 12 34	Elastic-Plastic Fracture Mechanics and the J – Integral	Anderson: p. 122-154
W 4/19	35	J – Integral	Anderson: p. 385-392
Homework #8 Due 4/19			
F 4/21	36	Discussion on J - Integral Testing (Tony Walls)	Shah, Swartz, and Ouyang, Chapter 10 of Fracture Mechanics of Concrete, "Fracture Mechanisms and Compressive Failure"
M 4/24	Wk 14 37	J as a Characterizing Parameter	
W 4/26	38	J_{IC} Criterion	
Homework #9 Due 4/26:			
F 4/28	39	Discussion of Fracture Toughness Determination Using K, J, and CTOD (Ben Leslie)	
M 5/1	Wk 15 40	NO CLASS	

W 5/3	41	Hour Exam II	
F 5/5	42	J_{IC} Testing	
M 5/8	Wk 16		
W 5/10			
2 hour evening lab on 3-point-bend experiment Homework #10 Due 5/10: Analysis of J-Integral and JIC Test Results			
5/19	Finals Week - Project #3 Due		

Note: Syllabus is subject to change.

FRACTURE MECHANICS - EGM 6570
Spring 2003

Instructor:
Dr. Cesar Levy
Office Hours: M-W 13:00 – 16:00 EAS 3462
Phone (305) 348 3643
E-mail: levyez@fiu.edu

Class Schedule:
T-R 16:10-17:25
Room: EAS 1116

TEXTBOOK:
Anderson, T.L., *Fracture Mechanics: Fundamentals and Applications*, 2nd Ed., CRC Press (1995).
Notes handed out in class

RECOMMENDED LITERATURE:
Broek, D., *Elementary Engineering Fracture Mechanics,* Kluwer Academic Publishers (1987).
Timoshenko, S.P., and Goodier, J.N., *Theory of Elasticity*, McGraw Hill (1970).
Hellan, K., *Introduction to Fracture Mechanics*, McGraw-Hill (1985).
Cherepanov, G.P. *Methods of brittle Fracture*, McGraw-Hill, (1979).

EXAMS AND GRADES:

2 exams	(25% each)
Writing Assignment	(25%)
Final Exam	(25%)

GRADING POLICY:

95-100	A	75-80	B-	55-60 D
90-95	A-	70-75	C+	55 & below F
85-90	B+	65-70	C	
80-85	B	60-65	C-	

COURSE CONTENTS:

1. Introduction to Fracture Mechanics, Conventional Design Criteria, Structural Failure in the Past
2. Theoretical Fracture Strength, Crack Modes, Fracture at Stresses Below Theoretical Fracture Strength, Griffith Contribution
3. Energy Principles, Elastic Crack Tip Study, Review of Theory of Elasticity, 2-D Elasticity,
4. Mode III solution, Definition of Tractions, Solution of Laplace Equation using Complex Variables
5. Cauchy-Riemann Equations and Mode III continued, near and far field solutions, energy of deformation
6. Energy of Deformation for Mode III continued, Energy of Deformation for a finite body using Superposition, Crack Extension Force, Stress Intensity Factor
7. Crack Extension Force, Stress Intensity Factor for Mode III (continued), Plane Stress, Plane Strain Problems, Mode I problem, Mode II problem,
8. Crack Extension Force, SIFs for Different Configurations, Compliance Change due to Crack, Constant SIF samples
9. LEFM, Griffith-Irwin Analysis, Crack Tip Plasticity, Plastic Zone Shapes, Stress Redistribution,
10. Fracture Toughness Testing (FTT), Relation Between Crack Extension Resistance Curves and Fracture Surfaces, Pop-in
11. Practical Aspects of FTT, Plate Thickness, Instrumentation for Fracture, Crack Opening Displacement
12. Sample Shapes, Introduction to the J Integral
13. J Integral Continued
14. J. Integral (Mode III), Eshelby Derivation of J Integral, Theoretical Basis for Measurement of J Integral
15. Experimental Determination of J Integral, J Intergral for Elastic-Plastic Materials, J Integral as Fracture Criterion
16. J Integral to Describe Crack Tip Singularities (linear elastic materials, power law hardening materials), Elastic Viscous Analogy, Nonlinear Viscous Materials, Plastic Fracture Mechanics -- Dugdale Mushkelishvili Model

FRACTURE MECHANICS - EGM 6570
Spring 2003

Instructor:
Dr. Cesar Levy
Office Hours: M-W 13:00 – 16:00 EAS 3462
Phone (305) 348 3643
E-mail: levyez@fiu.edu

Class Schedule:
T-R 16:10-17:25
Room: EAS 1116

TEXTBOOK:
Anderson, T.L., *Fracture Mechanics: Fundamentals and Applications*, 2nd Ed., CRC Press (1995).
Notes handed out in class

RECOMMENDED LITERATURE:
Broek, D., *Elementary Engineering Fracture Mechanics,* Kluwer Academic Publishers (1987).
Timoshenko, S.P., and Goodier, J.N., *Theory of Elasticity*, McGraw Hill (1970).
Hellan, K., *Introduction to Fracture Mechanics*, McGraw-Hill (1985).
Cherepanov, G.P. *Methods of brittle Fracture*, McGraw-Hill, (1979).

EXAMS AND GRADES:

2 exams	(25% each)
Writing Assignment	(25%)
Final Exam	(25%)

GRADING POLICY:

95-100	A	75-80	B-	55-60 D
90-95	A-	70-75	C+	55 & below F
85-90	B+	65-70	C	
80-85	B	60-65	C-	

COURSE CONTENTS:

1. Introduction to Fracture Mechanics, Conventional Design Criteria, Structural Failure in the Past
2. Theoretical Fracture Strength, Crack Modes, Fracture at Stresses Below Theoretical Fracture Strength, Griffith Contribution
3. Energy Principles, Elastic Crack Tip Study, Review of Theory of Elasticity, 2-D Elasticity,
4. Mode III solution, Definition of Tractions, Solution of Laplace Equation using Complex Variables
5. Cauchy-Riemann Equations and Mode III continued, near and far field solutions, energy of deformation
6. Energy of Deformation for Mode III continued, Energy of Deformation for a finite body using Superposition, Crack Extension Force, Stress Intensity Factor
7. Crack Extension Force, Stress Intensity Factor for Mode III (continued), Plane Stress, Plane Strain Problems, Mode I problem, Mode II problem,
8. Crack Extension Force, SIFs for Different Configurations, Compliance Change due to Crack, Constant SIF samples
9. LEFM, Griffith-Irwin Analysis, Crack Tip Plasticity, Plastic Zone Shapes, Stress Redistribution,
10. Fracture Toughness Testing (FTT), Relation Between Crack Extension Resistance Curves and Fracture Surfaces, Pop-in
11. Practical Aspects of FTT, Plate Thickness, Instrumentation for Fracture, Crack Opening Displacement
12. Sample Shapes, Introduction to the J Integral
13. J Integral Continued
14. J. Integral (Mode III), Eshelby Derivation of J Integral, Theoretical Basis for Measurement of J Integral
15. Experimental Determination of J Integral, J Intergral for Elastic-Plastic Materials, J Integral as Fracture Criterion
16. J Integral to Describe Crack Tip Singularities (linear elastic materials, power law hardening materials), Elastic Viscous Analogy, Nonlinear Viscous Materials, Plastic Fracture Mechanics -- Dugdale Mushkelishvili Model

Florida International University
Department of Mechanical Engineering

EGM 6570 FINAL EXAMINATION 22 April 2003

This examination will be a takehome exam. This exam allows you to use your book and notes only. This exam is due 25 April 2003 at 12 pm in my office EAS3462

Please sign the following:

I certify that I will neither receive nor give unpermitted aid on this examination. Violation of this may result in failure of the exam.

_____ _____

PRINT NAME SIGN NAME

This examination consists of **four problems with several parts to one of the problems. Do all problems.** Read each question carefully. Show all work!!!!!

Problem 1.

(a) Do Problem 4.1 in the back of your books. The problem is found on page 664

(b) Do problem 4.2 in the back of your books. The problem is found on page 664

Please read Chapter 4 before answering these questions.

Problem 2.

Do Problem 7.5 in the back of your books. The problem is found on page 668.

Please read Chapter 7 before answering this question.

Problem 3.

Do Problem 7.9 in the back of your books. The problem is found on page 670 and 671.

Please be careful as there is another problem 7.9 which starts on page 669. **DO NOT DO THAT ONE**

Problem 4.

Do Problem 10.1 in the back of your books. The problem is found on page 676 and 677 Discuss the sensitivities of the initial crack size and final crack size **DEPENDING ON THE PROBLEMS YOU ARE ASSIGNED**. As in class us a $\Delta a = 1$ mm to advance the crack in order to compute the number of cycles

Cases	Initial Crack Radius	Final Crack Radius
(a)	1 mm	10 mm
(b)	1 mm	10 mm
(c)	2 mm	20 mm
(d)	2 mm	20 mm

Cases (a,b) Cui
Cases (a,c) Srikanth
Cases (a,d,b) Srinath
Cases (b,c,d) Vamshi
Cases (a,c,d) Maddi

Cases (b,d) Li
Cases (c,d) Swapna
Trichi Do Problem 10.2 a on page 677 instead
Vedala Do Problem 10.2 b on page 677 instead

Florida International University
Department of Mechanical Engineering

EGM 6570 EXAMINATION 31 October 2011

This examination will be a takehome exam. This exam allows you to use your book and notes only. This exam is due 7 Nov 2011 at 4 pm in my office EAS3474

Please sign the following:

I certify that I will neither receive nor give unpermitted aid on this examination. Violation of this may result in failure of the exam.

_____ _____

PRINT NAME SIGN NAME

This examination consists of **four problems with several parts to one of the problems. Do all problems.** Read each question carefully. Show all work!!!!!

Problem 1. (RJS)

The Westergaard stress functions that solve the opening-mode problem of a crack of length, 2a, in an infinite body subjected to four equal point loads, P, on the crack faces, as shown in the figure are given by

$$Z(z) = \frac{2P}{\pi} \frac{z\sqrt{a^2 - b^2}}{(z^2 - b^2)\sqrt{z^2 - a^2}}$$

(a) Derive an exact expression for the Cartesian stress σ_{yy} valid everywhere in the body.
(b) From the results of part (a), derive the geometric stress intensity factors for this combination of geometry and loading

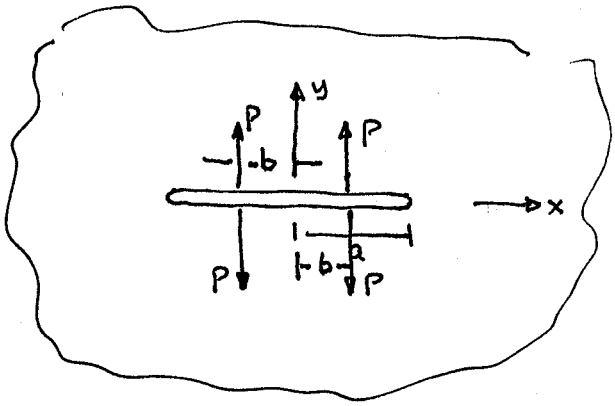

Problem 2: (RJS

A thin steel plate (σ_{ys} = 40 ksi), that is 6 inches wide contains a central crack 2.0 inches in length

(a) If the plane stress fracture toughness of the steel is 55 ksi$\sqrt{\text{in}}$, what is the maximum stress that can be supported by the plate (including the effects of local yielding at the crack tips)?
(b) What is the longest crack the plate can support without failure at an applied stress of 20 ksi?

Problem 3:

A 0.25 inch-thick wide aluminum (σ_{ys} = 40 ksi) tension panel has an edge crack 0.80 inch long. Based on fracture tests with a similar material for the same thickness, the fracture toughness has been measured as 45 ksi$\sqrt{in}$ for slowly applied loads.

(a) Compute the diameter of the plastic zone for both plane-stress and plane strain conditions.
(b) Based on your engineering judgement and the information available to you, which of the two plane conditions prevails? Why?
(c) What is the magnitude of the largest remotely applied steady state stress that the panel can support without failure?
(d) What would be the consequence of an impact load on your answer to part (c)?

Problem 4:

Based on prior experience, the 0.25 inch-thick steel bracket shown in the figure is prone to develop fatigue cracks in the area of the fillet as shown. After performing a series of experiments with simulated cracks of varying lengths, we find that the compliance is fitted to an equation of the form

$$\frac{v}{P} = \left(100 + 20\sin(\frac{\pi a}{4})\right) x10^{-6}\, in/lb$$

(a) Derive an expression for the geometric stress intensity factor for this bracket. Assume plane-stress conditions

(b) Visual inspection can detect cracks as short as 0.2 inch in the bracket. If the bracket is to be used for loads up to 2000 lb, what is the minimum fracture toughness K_{Ic} of the steel that must be specified for this application? A factor of safety against fracture of 2 is to be included in your analysis.

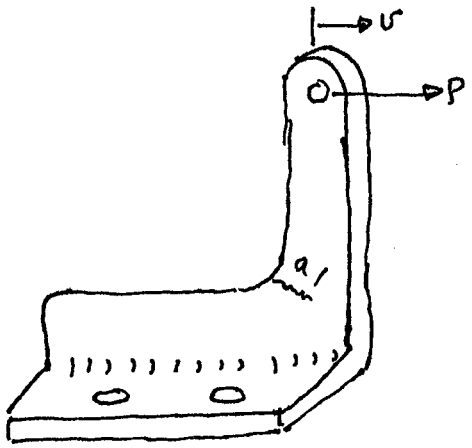

Florida International University
Department of Mechanical Engineering

EGM 6570 EXAMINATION 4 March 2003

This examination will be a takehome exam. This exam allows you to use your book and notes only. This exam is due 7 November 2003 at 1 pm in my office EAS3462

Please sign the following:

I certify that I will neither receive nor give unpermitted aid on this examination. Violation of this may result in failure of the exam.

_____ _____

PRINT NAME SIGN NAME

This examination consists of **four problems with several parts to one of the problems. Do all problems.** Read each question carefully. Show all work!!!!!

Problem 1.

The Westergaard stress functions that solve the opening-mode problem of a crack of length, 2a, in an infinite body subjected to four equal point loads, P, on the crack faces, as shown in the figure are given by

$$Z(z) = \frac{2P}{\pi} \frac{z\sqrt{a^2 - b^2}}{(z^2 - b^2)\sqrt{z^2 - a^2}}$$

(a) Derive an exact expression for the Cartesian stress σ_{yy} valid everywhere in the body.
(b) From the results of part (a), derive the geometric stress intensity factors for this combination of geometry and loading

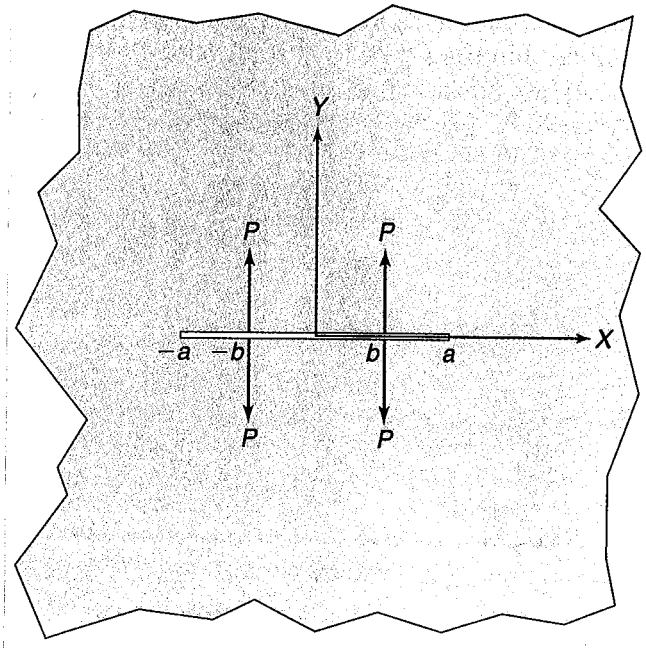

Problem 2:
A thin steel plate (σ_{ys} = 40 ksi), that is 6 inches wide contains a central crack 2.0 inches in length

(a) If the plane stress fracture toughness of the steel is 55 ksi$\sqrt{in}$, what is the maximum stress that can be supported by the plate (including the effects of local yielding at the crack tips)?
(b) What is the longest crack the plate can support without failure at an applied stress of 20 ksi?

Problem 3:

A 0.25 inch-thick wide aluminum (σ_{ys} = 40 ksi) tension panel has an edge crack 0.80 inch long. Based on fracture tests with a similar material for the same thickness, the fracture toughness has been measured as 45 ksi$\sqrt{in}$ for slowly applied loads.

(a) Compute the diameter of the plastic zone for both plane-stress and plane strain conditions.
(b) Based on your engineering judgement and the information available to you, which of the two plane conditions prevails? Why?
(c) What is the magnitude of the largest remotely applied steady state stress that the panel can support without failure?
(d) What would be the consequence of an impact load on your answer to part (c)?

Problem 4:

Based on prior experience, the 0.25 inch-thick steel bracket shown in the figure is prone to develop fatigue cracks in the area of the fillet as shown. After performing a series of experiments with simulated cracks of varying lengths, we find that the compliance is fitted to an equation of the form

$$\frac{v}{P} = \left(100 + 20\sin(\frac{\pi a}{4})\right) x10^{-6}\, in/lb$$

(a) Derive an expression for the geometric stress intensity factor for this bracket. Assume plane-stress conditions

(b) Visual inspection can detect cracks as short as 0.2 inch in the bracket. If the bracket is to be used for loads up to 2000 lb, what is the minimum fracture toughness K_{Ic} of the steel that must be specified for this application? A factor of safety against fracture of 2 is to be included in your analysis.

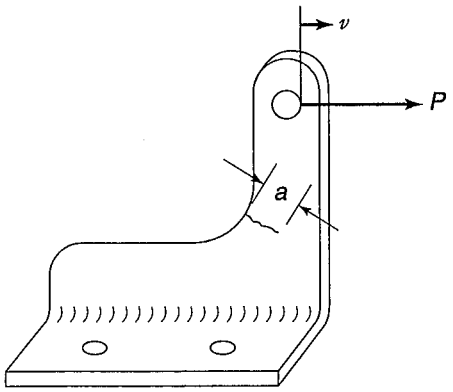

EXAMINATION #1

(1) Given,

$$Z(z) = \frac{2P}{\pi} \frac{z\sqrt{a^2-b^2}}{(z^2-b^2)\sqrt{z^2-a^2}}$$

Assuming $Y(z) = 0$

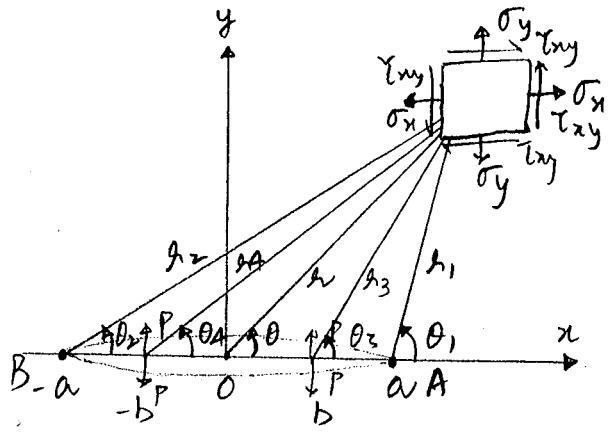

It can be observed that $Z(z)$ has singularities at $z = \pm a$ & $z = \pm b$,

we will find it convenient to introduce additional coordinate centered at each singularity.

Say, $z - a = (x-a) + iy = r_1 e^{i\theta_1}$

$z + a = r_2 e^{i\theta_2}$

$z - b = r_3 e^{i\theta_3}$

$z + b = r_4 e^{i\theta_4}$

$$\therefore Z(z) = \frac{2P\sqrt{a^2-b^2}}{\pi} \cdot \frac{r e^{i\theta}}{r_3 r_4 \cdot e^{i(\theta_3+\theta_4)}} \cdot \sqrt{r_1 r_2}\, e^{i\left(\frac{\theta_1+\theta_2}{2}\right)}$$

$$\therefore Z(z) = \frac{2P}{\pi}\sqrt{a^2-b^2} \cdot \frac{r}{\sqrt{r_1 r_2 \cdot r_3 r_4}} \cdot e^{i\left(\theta - \frac{\theta_1}{2} - \frac{\theta_2}{2} - \theta_3 - \theta_4\right)} \quad \ldots\ldots (1)$$

Also

$$Z'(z) = \frac{2P}{\pi}\sqrt{a^2-b^2}\left[\frac{(z^2-b^2)\cdot\sqrt{z^2-a^2} - z\left[\sqrt{z^2-a^2}\cdot 2z + (z^2-b^2)\times 1 \times \frac{2z}{2\sqrt{z^2-a^2}}\right]}{(z^2-b^2)^2\cdot(z^2-a^2)}\right]$$

$$= \frac{2P\sqrt{a^2-b^2}}{\pi}\left[\frac{z^4 - z^2a^2 - z^2b^2 + a^2b^2 - 2z^4 + z^2a^2 - z^4 + z^2b^2}{(z^2-b^2)^2(z^2-a^2)^{3/2}}\right]$$

(2) Given $\sigma_{ys} = 40$ ksi ;

$2W = 6$ in ;

$2a = 2$ in [central crack]

(a) $K_{IC} = 55$ ksi $\sqrt{in}$

To include local yielding at crack tips, for plane stress condition we have, $r_y = \frac{1}{2\pi}\left(\frac{K_I}{\sigma_{ys}}\right)^2$ ..... (2.64)

$= \frac{1}{2\pi}\left(\frac{55}{40}\right)^2 = 0.3009$ in

From 2.67, $a_{eff} = a + r_y = 1.3009$ in ✓

Also From table 2.4, for CCT,

$K_I = \frac{P}{B\sqrt{W}} f(a/W)$ where $f(a/W) = \sqrt{\frac{\pi a}{4W}\sec\left(\frac{\pi a}{2W}\right)}\left[1 - 0.025\left(\frac{a}{W}\right)^2 + 0.06\left(\frac{a}{W}\right)^4\right]$

$\Rightarrow K_I = \frac{P}{B(2W)} \cdot 2\sqrt{W}\, f(a/W) = 0.6604$ } Here $a = a_{eff}$

$\Rightarrow \sigma_{max} = \frac{K_I}{2\sqrt{W}\cdot f(a/W)} = \frac{55}{2\sqrt{3}\times 0.6604} = 24.041$ Ksi ✓

(b) When $\sigma = 20$ ksi

$f(a/W) = \frac{55}{20\cdot 2\sqrt{3}} = 0.7939$

i.e. $0.7939 = \sqrt{\frac{\pi a}{4W}\sec\left(\frac{\pi a}{2W}\right)}\left[1 - 0.025(a/W)^2 + 0.06(a/W)^4\right]$ — neglecting = 0 — why? must check to see that this is OK after you found soln.

solving for a, we have $a = 2.059$ in

$\frac{\pi a}{2W} = \cos^{-1}\left(\frac{\pi a}{4W\times 0.7939}\right)$ solved using EXCEL Trial & error.

Here $a = a_{eff} = 2.059$ in

$\therefore a = a_{eff} - r_y = 1.758$ in

OR

(3) Given, $t = 0.25$ in

$\sigma_{ys}(Al) = 40$ ksi

$a = 0.80$ in

For slowly applied loads, $K_{Ic} = 45$ ksi $\sqrt{in}$

(a) r_y for plane stress condition,

$$r_y = \frac{1}{2\pi}\left(\frac{K_I}{\sigma_{ys}}\right)^2 \quad \text{..... (2.64)}$$

$$= \frac{1}{2\pi}\left(\frac{45}{40}\right)^2 = 0.201 \text{ in}$$

r_p, Second order estimate $= 0.402$ in ✓

For plane strain condition,

$$r_y = \frac{1}{6\pi}\left(\frac{K_I}{\sigma_{ys}}\right)^2 \quad \text{- - - - (2.68)}$$ ✓

$$= 0.067 \text{ in}$$

(b) Since the plastic zone under plane strain is small compared to the thickness, we conclude that plane strain condition prevails. X use $B > 2.5\left(\frac{K_I}{\sigma_{yp}}\right)^2$ to see if this is true

(c) Solving again as solved in Problem 12,

$$a_{eff} = a + r_y = 0.8 + 0.067 = 0.867 \text{ in}$$ X method OK results not

From eqn. 2.42, for a semi-infinite plate with edge crack,

$$K_I = 1.12\,\sigma\sqrt{\pi a}$$

$$\Rightarrow \sigma_f = \frac{K_{Ic}}{1.12\sqrt{\pi a}} = \frac{45}{1.12\sqrt{\pi \times (0.867)}} = 24.35 \text{ ksi}$$ } Here we take $a = a_{eff}$.

$\therefore \sigma_f = 24.35$ ksi X

(2) Given $\sigma_{ys} = 40$ ksi ;

$2W = 6$ in ;

$2a = 2$ in [central crack]

(a) $K_{Ic} = 55$ ksi $\sqrt{in}$

To include local yielding at crack tips, for plane stress condition we have, $r_y = \frac{1}{2\pi}\left(\frac{K_I}{\sigma_{ys}}\right)^2$ ..... (2.64)

$= \frac{1}{2\pi}\left(\frac{55}{40}\right)^2 = 0.3009$ in

From 2.67, $a_{eff} = a + r_y = 1.3009$ in ✓

Also

From table 2.4, for CCT,

$K_I = \frac{P}{B\sqrt{W}}\, f(a/W)$ where $f(a/W) = \sqrt{\frac{\pi a}{4W}\sec\left(\frac{\pi a}{2W}\right)}\left[1 - 0.025\left(\frac{a}{W}\right)^2 + 0.06\left(\frac{a}{W}\right)^4\right]$

$\Rightarrow K_I = \frac{P}{B(2W)} \cdot 2\sqrt{W}\, f(a/W) = 0.6604$ } Here $a = a_{eff}$

$\Rightarrow \sigma_{max} = \frac{K_I}{2\sqrt{W}\cdot f(a/W)} = \frac{55}{2\sqrt{3}\times 0.6604} = 24.041$ Ksi ✓

(b) When $\sigma = 20$ ksi

$f(a/W) = \frac{55}{20\cdot 2\sqrt{3}} = 0.7939$

i.e. $0.7939 = \sqrt{\frac{\pi a}{4W}\sec\left(\frac{\pi a}{2W}\right)}\left[1 - 0.025(a/W)^2 + 0.06(a/W)^4\right]$ — neglecting = 0 — why? must check to see that this is OK after you found solution

solving for a, we have $a = 2.059$ in

$\frac{\pi a}{2W} = \cos^{-1}\left(\frac{\pi a}{4W\times 0.7939}\right)$ solved using EXCEL Trial & error.

Here $a = a_{eff} = 2.059$ in

$\therefore a = a_{eff} - r_y = 1.758$ in

OR

(d) Impact loading impart high displacement rates. As a result, a material with sufficient fracture resistance to static loading conditions may prove unsatisfactory in the event of dynamic or impact loading. ie., may fail well under its nominal resistance value. ✓

(4) Given,

$B = 0.25$ in

$$C = \frac{v}{P} = \left[100 + 20 \sin\left(\frac{\pi a}{4}\right)\right] \times 10^{-6} \text{ in/lb}$$

V & P are in same direction so C is compliance

Dimensionless compliance, $\phi(a/w)$ can be found from the formula $\phi(a/w) = EB \cdot (v/P) = EB\left[100 + 20 \sin\left(\frac{\pi a}{4}\right)\right] \times 10^{-6}$

Since the given force, P is not $\perp^{lr}$ to the crack, we transform the system to a force, moment form where in the P is $\perp^{lr}$ to the crack length with $M = Pa$., as shown.

$\therefore$ We can find K_I due to tension as below.

$$G = \frac{P^2}{2} \frac{\partial C}{\partial A} \quad \& \quad K_I^2 = EG$$

$$= \frac{P^2}{2} \frac{\partial C/\partial a}{\partial A/\partial a}$$

$$= \frac{P^2}{2} \cdot \frac{20 \cos\left(\frac{\pi a}{4}\right) \times 10^{-6} \times \frac{\pi}{4}}{0.25}$$

$A = B \cdot a$

$\frac{\partial A}{\partial a} = B = 0.25$

$$G = 10\pi \times 10^{-6} P^2 \cos\left(\frac{\pi a}{4}\right)$$

$$\therefore K_I = \sqrt{EG} = 5.61 \times 10^{-3} P \sqrt{E \cos\left(\frac{\pi a}{4}\right)}$$

7.6 A fracture toughness test is performed on compact specimen fabricated from a **5**mm thick sheet aluminum alloy. The specimen width (***W***)=**50.0** mm and ***B***=**5** mm (the sheet thickness). The initial crack length is **26.0** mm. Young's modulus=**70,000** MPa. Compute the *K-R* curve from the load-displacement data tabulated below. Assume that all nonlinearity in the $P-\Delta$ curve us due to crack growth. (See Chapter 12 for the appropriate compliance and stress intensity relationships)

Load, KN	Load line Displacement, mm
0	0
0.5433	0.0635
1.087	0.1270
1.630	0.1906
2.161	0.2552
2.361	0.2817
2.541	0.3096
2.699	0.3392

Load, KN	Load line Displacement, mm
2.851	0.3698
2.913	0.3860
2.903	0.3971
2.850	0.4113
2.749	0.4191
2.652	0.4274
2.553	0.4355
2.457	0.4443

1 KN = 224.8 lb 25.4 mm = 1 in 1 MPa = 0.145 ksi

$$f\left(\frac{a}{W}\right)=\frac{K_I B\sqrt{W}}{P} \quad \Rightarrow \quad K_I=\frac{f\left(\frac{a}{W}\right)\cdot P}{B\cdot\sqrt{W}}$$

$$f\left(\frac{a}{W}\right)=\frac{2+\frac{a}{W}}{\left(1-\frac{a}{W}\right)^{3/2}}\left[0.866+4.64\left(\frac{a}{W}\right)-13.32\left(\frac{a}{W}\right)^2+14.72\left(\frac{a}{W}\right)^3-5.60\left(\frac{a}{W}\right)^4\right]$$

$$Z_{LL}=\frac{BE\Delta}{P}$$

$$U_{LL}=\frac{1}{\sqrt{Z_{LL}}+1}$$

$$\frac{a}{W}=1.00196-4.06319\,U_{LL}+11.242\,U_{LL}^2-106.043\,U_{LL}^3+464.335\,U_{LL}^4-650.677\,U_{LL}^5$$

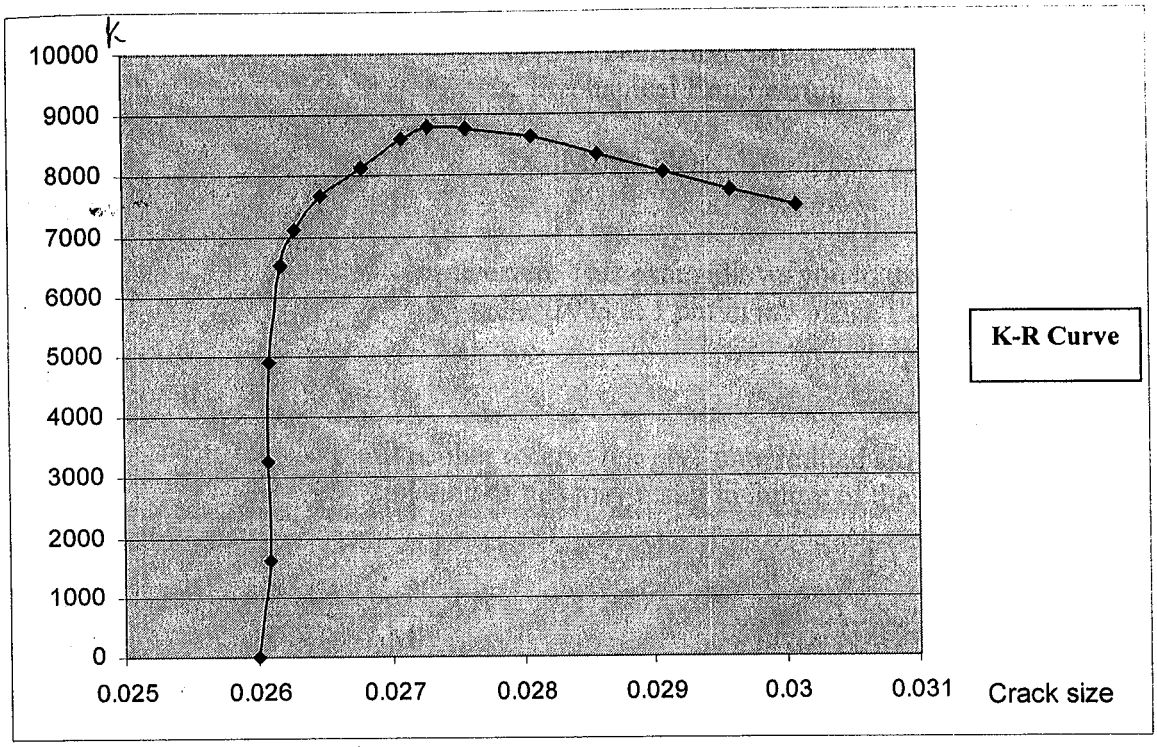
K
10000
9000
8000
7000
6000
5000
4000
3000
2000
1000
0
0.025
0.026
0.027
0.028
0.029
0.03
0.031
Crack size
K-R Curve

EXAMINATION #1

(1) Given,

$$Z(z) = \frac{2P}{\pi} \frac{z\sqrt{a^2-b^2}}{(z^2-b^2)\sqrt{z^2-a^2}}$$

Assuming $Y(z) = 0$

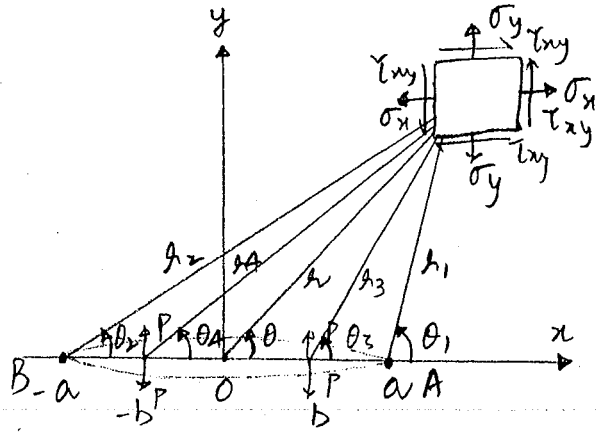

It can be observed that $Z(z)$ has singularities at $z = \pm a$ & $z = \pm b$,

we will find it convenient to introduce additional coordinate centered at each singularity.

Say, $z - a = (x-a) + iy = r_1 e^{i\theta_1}$

$z + a = r_2 e^{i\theta_2}$

$z - b = r_3 e^{i\theta_3}$

$z + b = r_4 e^{i\theta_4}$

$$\therefore Z(z) = \frac{2P\sqrt{a^2-b^2}}{\pi} \cdot \frac{r e^{i\theta}}{r_3 r_4 \cdot e^{i(\theta_3+\theta_4)}} \cdot \sqrt{r_1 r_2}\, e^{i\left(\frac{\theta_1+\theta_2}{2}\right)}$$

$$\therefore Z(z) = \frac{2P}{\pi}\sqrt{a^2-b^2} \cdot \frac{r}{\sqrt{r_1 r_2}\cdot r_3 r_4} \cdot e^{i\left(\theta - \frac{\theta_1}{2} - \frac{\theta_2}{2} - \theta_3 - \theta_4\right)} \quad \ldots\ldots (1)$$

Also

$$Z'(z) = \frac{2P}{\pi}\sqrt{a^2-b^2}\left[\frac{(z^2-b^2)\cdot\sqrt{z^2-a^2} - z\left[\sqrt{z^2-a^2}\cdot 2z + (z^2-b^2)\times 1\right]}{(z^2-b^2)^2\cdot(z^2-a^2)}\right]$$

$$= \frac{2P\sqrt{a^2-b^2}}{\pi}\left[\frac{z^4 - z^2a^2 - z^2b^2 + a^2b^2 - 2z^4 + z^2a^2 - z^4 + z^2b^2}{(z^2-b^2)^2(z^2-a^2)^{3/2}}\right]$$

$$\therefore Z'(z) = \frac{2P\sqrt{a^2-b^2}}{\pi}\left[\frac{-2z^4 + z^2a^2 + a^2b^2}{(z^2-b^2)^2(z^2-a^2)^{3/2}}\right]$$

$$\Rightarrow Z'(z) = \frac{2P\sqrt{a^2-b^2}}{\pi}\left[\frac{-2r^4 e^{i4\theta} + r^2a^2 e^{i2\theta} + a^2b^2}{r_3^2 r_4^2 e^{i(2\theta_3+2\theta_4)} \times (r_1 r_2)^{3/2} \cdot e^{i\frac{3}{2}(\theta_1+\theta_2)}}\right]$$

$$= \frac{2P\sqrt{a^2-b^2}}{\pi}\left[\frac{-2r^4 e^{i(4\theta-q)}}{P} + \frac{r^2a^2}{P}\cdot e^{i(2\theta-q)} + \frac{a^2b^2 e^{-iq}}{P}\right]$$

where
$P = (r_1 r_2)^{3/2} r_3^2 r_4^2$
$q = -\frac{3}{2}(\theta_1+\theta_2) - 2(\theta_3+\theta_4)$

(a) $\sigma_{yy} = Re\,Z + y(Im\,Z' + \underbrace{Re\,Y'}_{=0})$

$$\Rightarrow \sigma_{yy} = \frac{2P\sqrt{a^2-b^2}}{\pi} \times \frac{r}{\sqrt{r_1 r_2 \cdot r_3 r_4}} \cos\left(\theta - \frac{\theta_1}{2} - \frac{\theta_2}{2} - \theta_3 - \theta_4\right)$$

$$+ \frac{r_1 \sin\theta_1}{(r_1 r_2)^{3/2} r_3^2 r_4^2} \cdot \frac{2P\sqrt{a^2-b^2}}{\pi}\left[-2r^4 \sin\left(4\theta - \frac{3\theta_1}{2} - \frac{3\theta_2}{2} - 2\theta_3 - 2\theta_4\right) + r^2a^2 \sin\left(2\theta - \frac{3\theta_1}{2} - \frac{3\theta_2}{2} - 2\theta_3 - 2\theta_4\right)\right]$$ ✓

(b) Stress intensity factor, $K = \lim_{\delta^+ \to 0} Re\,Z|_{y=0} \cdot \sqrt{2\pi\delta}$

Here $Re\,Z|_{y=0}$ is simply $Z(x) = \frac{2P}{\pi}\frac{x\sqrt{a^2-b^2}}{(x^2-b^2)\sqrt{x^2-a^2}}$

$\therefore$ At right crack tip, $K_A = \lim_{x \to a} \frac{2P}{\pi}\frac{x\sqrt{a^2-b^2}}{(x^2-b^2)\sqrt{x^2-a^2}} \cdot \sqrt{2\pi(x-a)}$

$$= 2P\sqrt{\frac{a}{\pi(a^2-b^2)}}$$ ✓

Similarly

At Left Crack tip, $K_B = \lim_{x \to -a} \frac{2P}{\pi}\cdot\frac{x\sqrt{a^2-b^2}}{(x^2-b^2)\sqrt{(a-x)(x+a)}} \cdot \sqrt{2\pi(x+a)}$

Problem 2 $\sigma_{ys} = 40$ksi $W = 6$ $2a = 2$inches $a = 1$in $K_{I_c} = 55$ ksi$\sqrt{\text{in}}$

(a) since plate is thin $\Rightarrow$ plane stress $\Rightarrow$ $r_y = \frac{1}{2\pi}\left(\frac{K_{Ic}}{\sigma_{ys}}\right)^2 = .3009$ in

$a_{eff} = a + r_y = 1.3009$ in

Now for center cracked panel, with $a = a_{eff}$

$$K_{I_c} = \sigma_{max}\sqrt{\pi a}\left[\sec\left(\frac{\pi a}{2W}\right)^{1/2}\right]\left[1 - .025\left(\frac{a}{W}\right)^2 + 0.06\left(\frac{a}{W}\right)^4\right]$$

solve $55 = \sigma_{max} \cdot 2.9726$

$\sigma_{max} = 18.50$ ksi

(b) again to find the longest crack solve iteratively

$$K_{I_c} = 20\text{ksi}\sqrt{\pi a}\left[\sec\left(\frac{\pi a}{2W}\right)^{1/2}\right]\left[1 - .025\left(\frac{a}{W}\right)^2 + .06\left(\frac{a}{W}\right)^4\right]$$

$\therefore$ $a_{eff} = 1.196 = a + r_y$ $\therefore$ $a = .895$ and $\underline{2a = 1.7902\text{ in}}$

Problem 3

(a) plane stress $r_y = \frac{1}{2\pi}\left(\frac{K_I}{\sigma_{ys}}\right)^2 = .2014$ in

plane strain $r_y = \frac{1}{6\pi}\left(\frac{K_I}{\sigma_{ys}}\right)^2 = .0671$ in

(b) for plane strain

$B \geq 2.5\left(\frac{K_I}{\sigma_{ys}}\right)^2 = 3.164$ in but since $B \ll 3.164$ in this case is in plane stress

(c) Since this is an edge crack & W is not given $K_{Ic} = \sigma\sqrt{\pi a} \cdot 1.12$

If you account for plastic zone $a_{eff} = .8 + .2014 = 1.014$ in & $K_{I_c} = 45$ ksi$\sqrt{\text{in}}$

$$\therefore \quad \sigma_{max} = \frac{K_{Ic}}{1.12\sqrt{\pi a_{eff}}} = 22.51\text{ ksi}$$

(d) if impact load $\sigma > \sigma_{max}$ and crack would grow

(d) Impact loading impart high displacement rates. As a result, a material with sufficient fracture resistance to static loading conditions may prove unsatisfactory in the event of dynamic or impact loading. ie., may fail well under its nominal resistance value. ✓

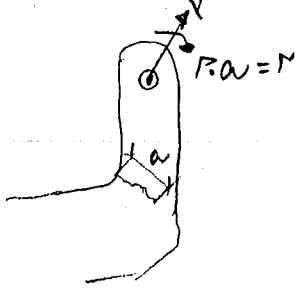

(4) Given,

$B = 0.25$ in

$$C = \frac{v}{P} = \left[100 + 20 \sin\left(\frac{\pi a}{4}\right)\right] \times 10^{-6} \text{ in/lb}$$

V & P are in same direction so C is compliance

Dimensionless compliance, $f(a/w)$ can be found from the formula $f(a/w) = EB \cdot (v/P) = EB\left[100 + 20 \sin\left(\frac{\pi a}{4}\right)\right] \times 10^{-6}$

[redacted]

∴ we can find K_I due to tension as below.

$$G = \frac{P^2}{2} \frac{\partial C}{\partial A} \quad \& \quad K_I^2 = EG$$

$$= \frac{P^2}{2} \frac{\partial C/\partial a}{\partial A/\partial a}$$

$$= \frac{P^2}{2} \cdot \frac{20 \cos\left(\frac{\pi a}{4}\right) \times 10^{-6} \times \frac{\pi}{4}}{0.25}$$

$A = B \cdot a$

$\frac{\partial A}{\partial a} = B = 0.25$

$$G = 10\pi \times 10^{-6} P^2 \cos\left(\frac{\pi a}{4}\right)$$

$$\therefore K_I = \sqrt{EG} = 5.61 \times 10^{-3} P \sqrt{E \cos\left(\frac{\pi a}{4}\right)}$$

for part (b) since this is an edge crack. K_{I_c} must be calculated using $E_{steel} = 29.7 \times 10^6$ psi

$a = 0.2$ in and $P = 2000$ lb. Also $FS \cdot K_{I_c}$ actual = K_{I_c} theoretical

$\therefore$ $FS \cdot P_{actual} = P_{theoretical}$ $\therefore$ $P \leq 1000$ lb

$$K_{I_c} = 5.61 \times 10^{-3} (1000) \sqrt{E \cos\left(\frac{\pi a}{4}\right)} = 30384.43 \text{ psi}\sqrt{\text{in}} = 30.38 \text{ ksi}\sqrt{\text{in}}$$

I. ASTM model for K_{Ic} testing

A. designed to produce valid K_{Ic} results - How?

1. must meet $c_o \geq 2.5 \left(K_{Ic}/\sigma_y\right)^2$
2. " " $B \geq 2.5 \left(K_{Ic}/\sigma_y\right)^2$; $W/B \cong 2$
3. starting crack length must be 0.45 - 0.55 W (width of specimen)
4. crack must be sharp and must be introduced via a fatigue crack starting from a V-notch
5. The fatigue crack must be introduced by low type cycling
6. A displacement gage will be used to accurately measure the relative displacement of two precisely located gages positions
7. Temperature and load rate requirements

B. Why these requirements -

1. $c_o \geq 2.5 \left(K_{Ic}/\sigma_y\right)^2$. this is a requirement that is necessary and sufficient in order for LEFM to hold

Proof:

Consider a plate loaded in tension

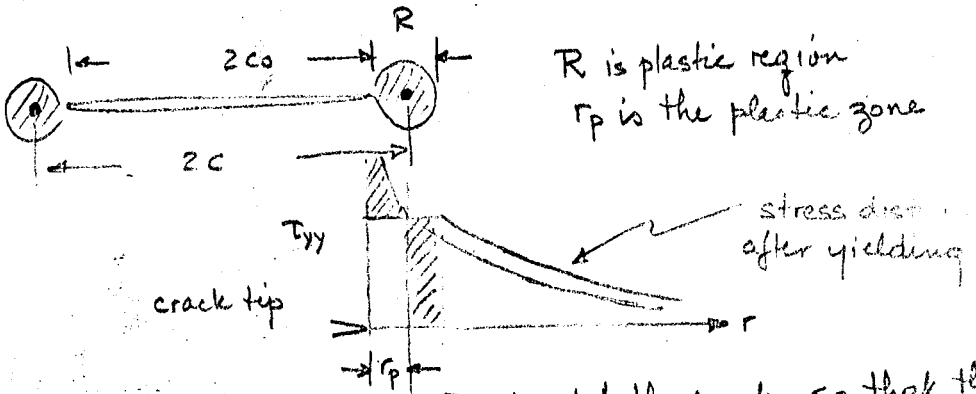

- We assume that the stresses are redistributed ahead of the crack so that the load bearing capacity in front of the crack is unchanged when yielding occurs. We assume that the shaded areas under the graph are the same.
- Thus $2c = 2c_o + 2r_p = 2c_o + R$ is the effective length of the crack
- In plane strain mode I $R = \frac{1}{6\pi}\left(K_I/\sigma_y\right)^2$

and $c = c_o + \frac{1}{12\pi}\left(K_I/\sigma_y\right)^2$

then $K_I = \sigma\sqrt{\pi c} = \sigma\sqrt{\pi c_o + \frac{1}{12}\left(K_I/\sigma_y\right)^2}$

if the stress σ ↑ K_I ↑ also K_I ↑ due to the plastic zone correction.

Thus $$K_I = \sigma\sqrt{\pi c_0}\left\{1 - \frac{1}{12}\left(\sigma/\sigma_y\right)^2\right\}^{-1/2} \qquad (1)$$

- In a test as $\sigma \to \sigma_y$, $K_I \to K_{Ic}$

- If σ reaches σ_y before $K_I = K_{Ic}$ we get yielding and by our elastic-plastic model r_p (and R) $\to \infty$. Hence we violate the LEFM assumption of <u>small scale yielding</u>

- We want $K_I = K_{Ic}$ before $\sigma = \sigma_y$. Thus let $K_I = K_{Ic}$ in (1) and solve for the crack length $2c_0$

$$2c_0 = \frac{2}{\pi}\left(\frac{K_{Ic}}{\sigma_y}\right)^2\left\{\left(\sigma_y/\sigma\right)^2 - \frac{1}{12}\right\} \qquad K_I = K_{Ic}$$

This will cause <u>unstable</u> crack growth

- The crack length that produces yielding is when $\sigma_y = \sigma$

$$\text{or} \quad 2c_0 = \frac{11}{12}\cdot\frac{2}{\pi}\left(K_{Ic}/\sigma_y\right)^2 \sim \frac{1}{2}\left(\frac{K_{Ic}}{\sigma_y}\right)^2$$

if $\sigma > \sigma_y$ then $2c_0 < \frac{1}{2}\left(K_{Ic}/\sigma_y\right)^2$ unacceptable

$\sigma < \sigma_y$ then $2c_0 > \frac{1}{2}\left(K_{Ic}/\sigma_y\right)^2$ or $c_0 > \frac{1}{4}\left(K_{Ic}/\sigma_y\right)^2$

- Because we want to make adequate measurements of K_{Ic}

we want $c_0 >> \frac{1}{4}\left(K_{Ic}/\sigma_y\right)^2$

Srawley and Brown suggested that $c_0 \geq 2.5\left(K_{Ic}/\sigma_y\right)^2$ and this is accepted as the <u>standard</u>.

2. $B \geq 2.5 \left(K_{Ic}/\sigma_y\right)^2$: This requirement arises from the consideration that we want only MODE I type fracture

Proof:

- As has been shown to you in class in order for cracks to propagate, for perfectly brittle materials, the crack extension force $G_I = 2\gamma_s$, where γ_s is the surface energy. However for materials that deform plastically, then crack extension will only occur when $G_I = 2\gamma_s + p$, where p is the plastic work of crack extension. p is not a constant and depends on the size of the plastic zone, σ_y, the work hardening rate, etc AND they all in turn depend on the crack length.
- If we define $R \equiv$ crack extension resistance $= 2\gamma_s + p$, then for unstable growth we must have that

$$G_I \geq R$$

and also $$\partial G_I/\partial c \geq \frac{\partial R}{\partial c}$$

Thus if we remember that $G_I = \frac{\sigma^2 \pi c}{2\mu}(1-\nu)$ and look at a typical G_I versus c curve,

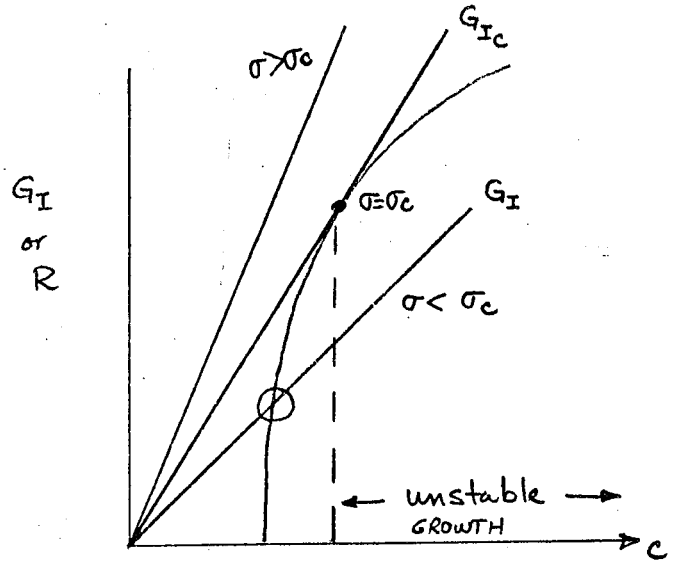

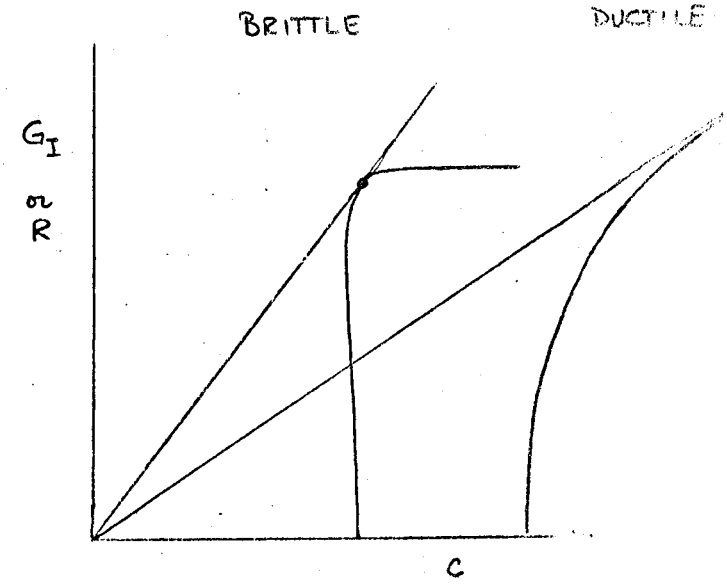

Note that the brittle material shows little plastic deformation and has a well defined $G_I = R$ point of intersection and occures below the

What has been found is that as the plate is made thinner the R curve will vary and will no longer have a distinct intersection point. The reason for this is the growth of "shear lips" from the free surface and the thinness of the plate (plane stress conditions).

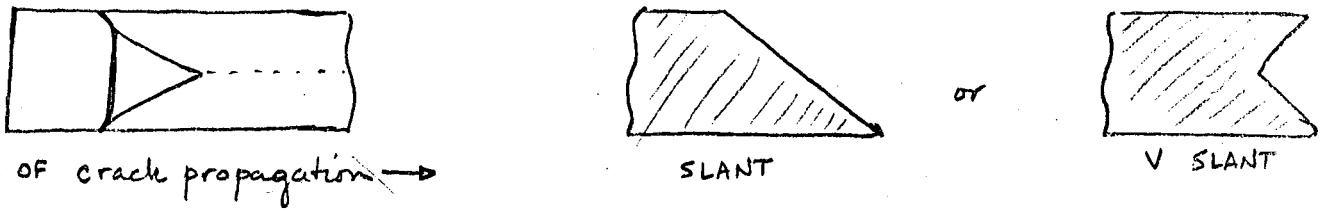

The growth of the shear lips is due to the plastic zone being constrained in the thickness direction. So it will spread in front of the crack tip. The mechanism that will cause crack extension will be due to failure in shear (mode III); hence we see the slant formation.

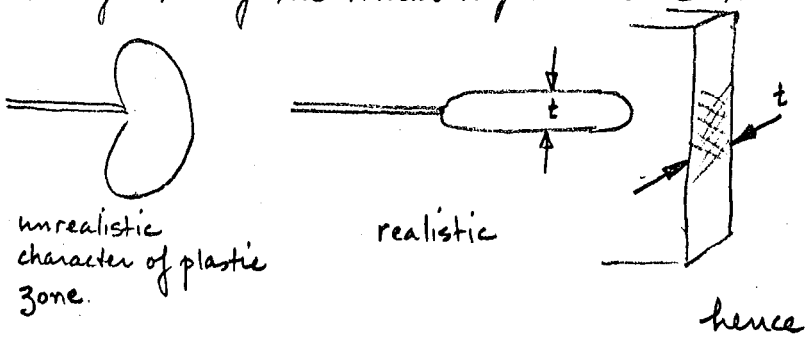

As the plate width is increased, the formation of the shear lips is reduced due to the plane strain effect and the cross-section will look like this

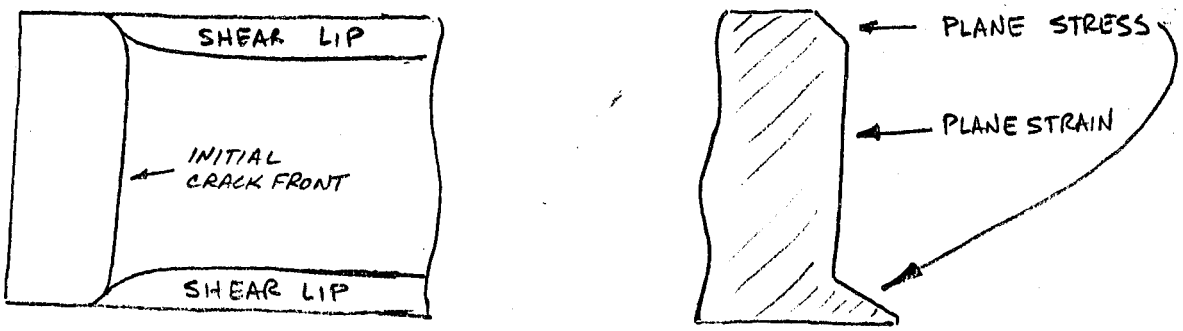

Many have proposed models to describe what occurs here. One such model is that of Krafft, Sullivan and Boyle (1961) modified by Bluhm

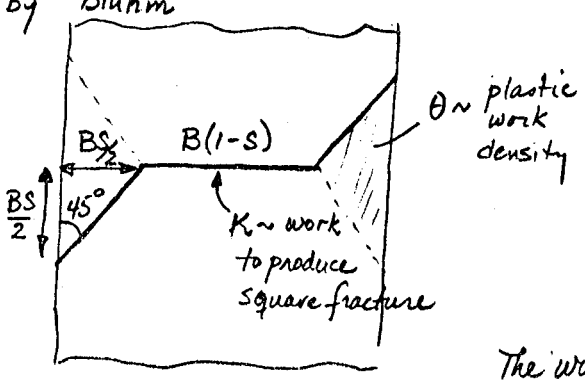

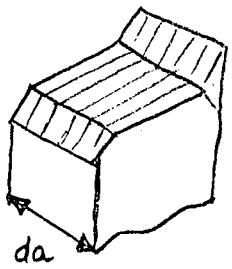

1. square fracture $\neq f(C_0)$
2. shear lips are assumed to occur at 45°
3. flat fracture is a surface phenomenon
4. Shear lip is volumetric

The work done to create the crack surface da is:

Now $G_I = \frac{1}{B}\frac{dW}{da} = \kappa(1-S) + \frac{BS^2\theta}{2}$. Note that S is picked so that BS = constant as crack length ↑

Thus as $B \to \infty$ $S \to 0$ and $G_I \to \kappa$.

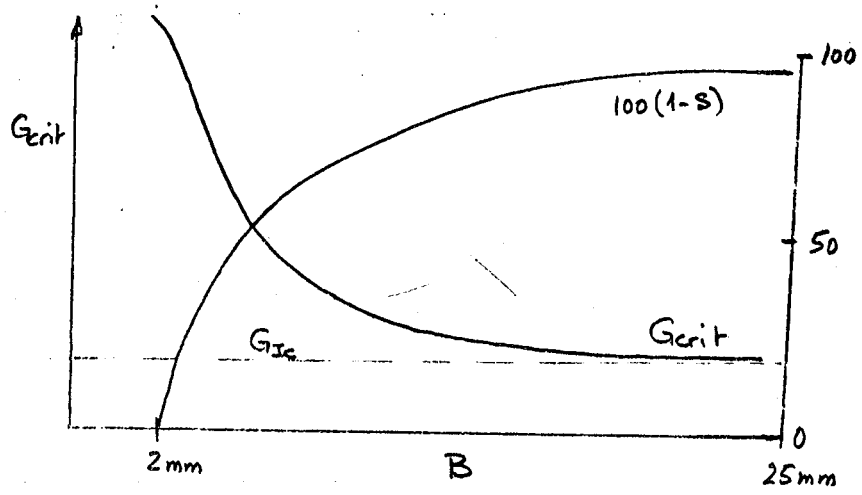

From data for Aluminum 7075-T6

$\kappa \sim 200$ kJ/m²

$\theta \sim 20$ kJ/m²

Look at the plastic zone and superpose the model of Krafft:

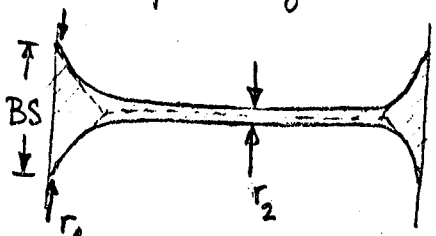

$r_{p/B} \ll 1$ or $\frac{r_p}{B} < S \ll 1$

$BS \gg r_{\text{plane stress}} \sim r_p = \frac{1}{2\pi}\left(\frac{K_{Ic}}{\sigma_y}\right)^2$ (*)

since $r_1 > r_2$ (plane strain). If (*) is true then plain strain conditions will extend over most of the cross-section and we will have essentially mode I fracture.

hence $B \gtrsim \left(\frac{K_{Ic}}{\sigma_y}\right)^2$. To determine the real equation, tests were done on many types of metals and here are some of the results.

Example: Maraging Steel $\sigma_y = 259$ KSi

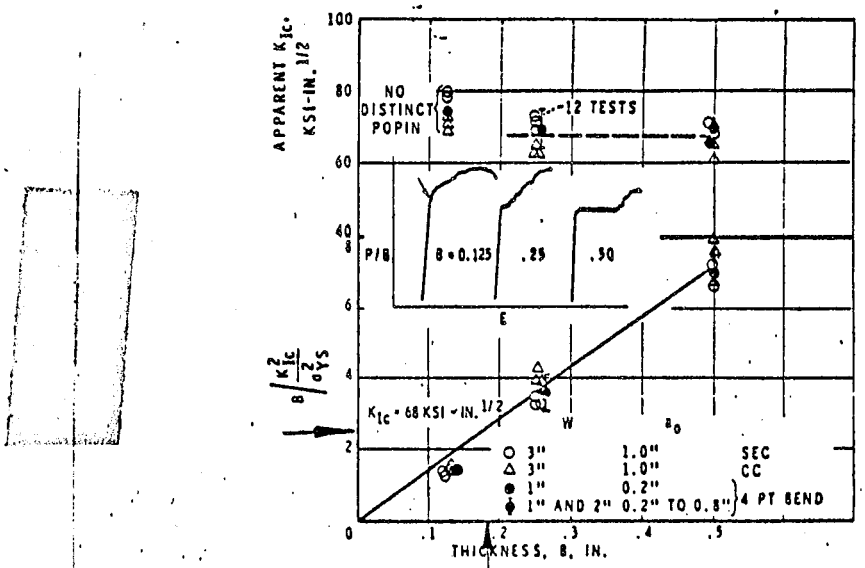

FIG. 14—*Effect of thickness on popin behavior and apparent K_{Ic} for 259 ksi*

conclusion:

$B \geq 2.5\left(\frac{K_{Ic}}{\sigma_y}\right)^2$

Specimen Size Requirements

We have argued that to limit yielding we must make large samples with long cracks. Thus $K_I \to K_{Ic}$ before $\sigma \to \sigma_y$. From our analysis we expect

$$C_0 \geq 2.5 \left(\frac{K_{Ic}}{\sigma_y} \right)^2$$

This needs to be checked. Also, How thick must sample be for plane strain conditions?

Consider 7075-T6 (MS&E 202C experiment).

$\sigma_y = 75$ ksi

$K_{Ic} = 26$ ksi $\sqrt{in}$

$2.5 \left(\frac{K_{Ic}}{\sigma_y} \right)^2 =$ 0.3 in

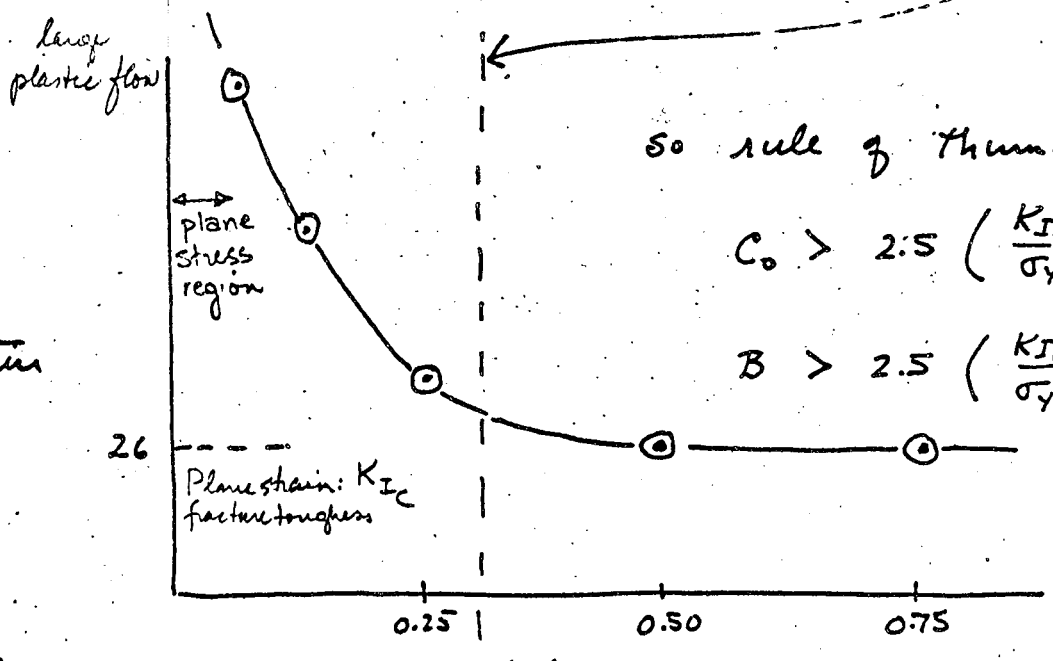

So rule of thumb:

$$C_0 > 2.5 \left(\frac{K_{Ic}}{\sigma_y} \right)^2$$

$$B > 2.5 \left(\frac{K_{Ic}}{\sigma_y} \right)^2$$

Usually more difficult to achieve due to how the specimen is machine

Specimen Size Requirements

we have already discussed the fact that there is a critical thickness to achieve plane strain conditions and to measure K_{I_c}. Also, there is a critical crack length. Generally speaking, there are no reliable techniques for predicting the critical crack length or critical thickness. One simply measures K_c to determine if it is independent of crack length or thickness.

Crack Length Effects

Example: Maraging Steel. $\sigma_y = 242$ KSi

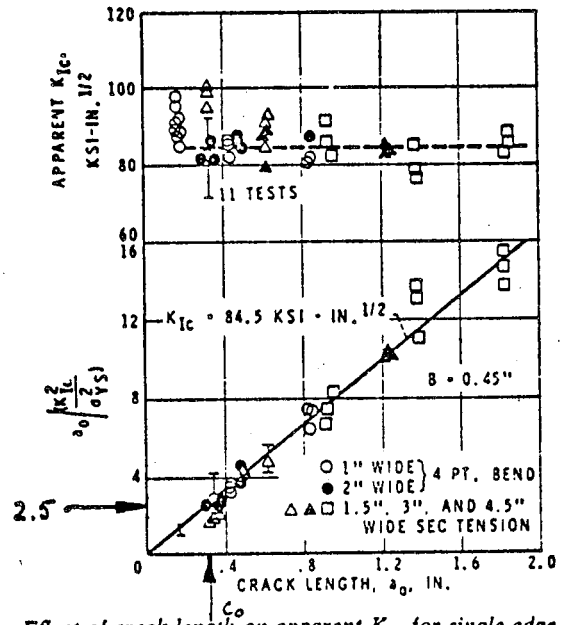

FIG. 10—*Effect of crack length on apparent K_{Ic} for single-edge-cracked tension and bend tests on 242 yield strength maraging steel.*

כלפת מריג'נג 242

Conclusion:

$$\frac{c_o}{\left(K_{Ic}^2/\sigma_y^2\right)} \geq 2.5 \qquad \text{hence} \qquad c_o \geq 2.5\left(\frac{K_{Ic}}{\sigma_y}\right)^2$$

Example: Maraging Steel $\sigma_y = 259$ ksi

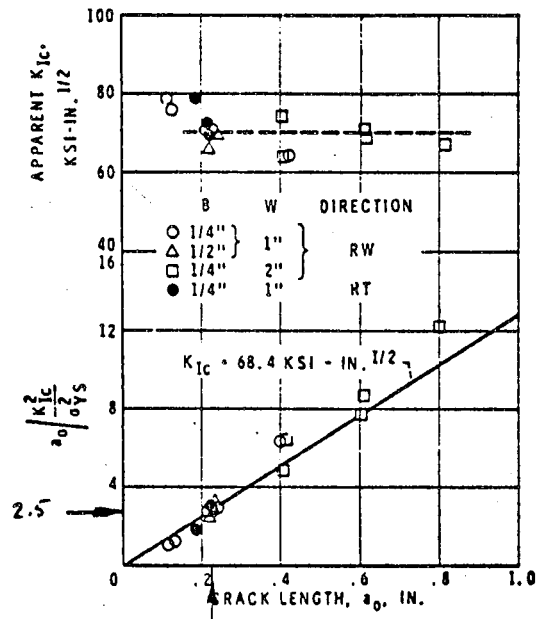

min C_o = arrow

FIG. 11—*Effect of crack length on apparent K_{Ic} for 4-point bend tests on 259 ksi yield strength maraging steel.*

conclusion $C_o \geq 2.5 \left(\frac{K_{Ic}}{\sigma_y}\right)^2$

Plate Thickness Effects

Example: Marasing Steel $\sigma_y = 242$ ksi

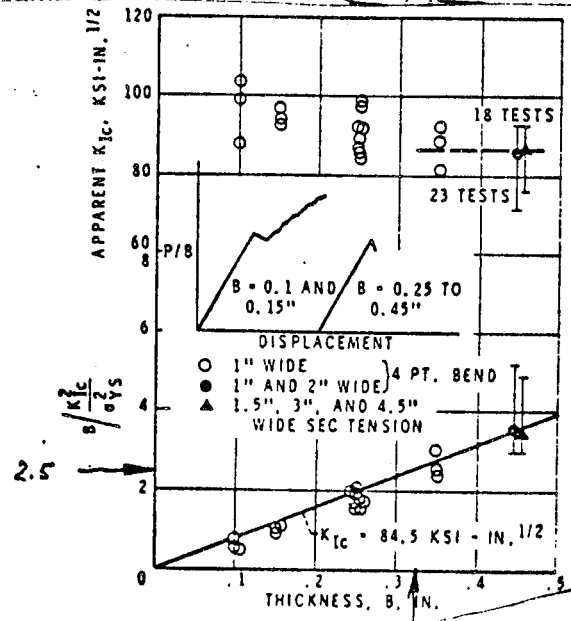

min B

conclusion:

$B \geq 2.5 \left(\frac{K_{Ic}}{\sigma_y}\right)^2$

FIG. 13—*Effect of thickness on apparent K_{Ic} for 242 ksi yield strength maraging steel tested using bend and single-edge-crack tension specimens.*

2b. The ratio of W/B is picked to be $\cong 2$ so that the stress state ahead of the crack tip is not affected by the free surfaces of the specimen.

Proof: Before we answer this question we must answer the questions

1) how long should the initial crack length be?
2) what is the effect of the width, W, of the specimen?

1) To determine the length of the crack we look at the stress $\hat{\sigma} = \frac{K_I}{\sqrt{2\pi r}} + \ldots$ where $\hat{\sigma}$ is the 1 term expansion for the opening stress that cause the crack to propagate, r is the distance ahead of the crack tip in the direction of propagation, and $K_I = \sigma\sqrt{\pi c_0}$ (σ being the far field stress). For different test pieces, if we plot $(\hat{\sigma} - \sigma_1)/\sigma_1$ where σ_1 is the actual stress, then we find that

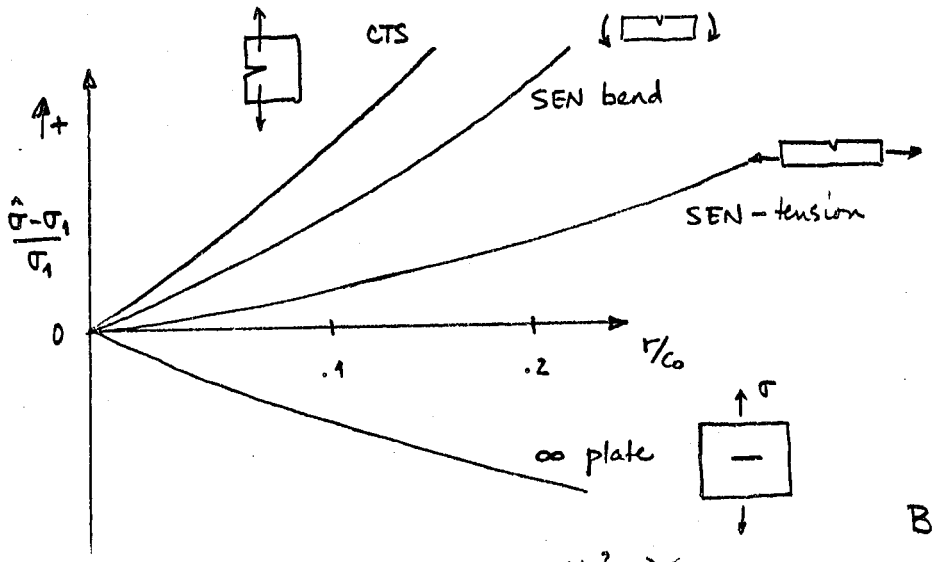

at $r/c_0 = .02$: Wilson found (1966)

CTS: 7% error
SEN-B: 6% error
SEN-T: 2% error
∞ PL: −1.5% error

why .02 ? This is a value judgment and we want to describe what happens in front of the crack by one parameter and accurately. Basically this implies that

$$r_p \text{ (plane strain)} = \tfrac{1}{3}\left(\frac{K_{Ic}^2}{2\pi\sigma_y^2}\right) \leq 0.02 c_0$$

thus $c_0 \geq 50\, r_p$

2) To determine how wide the specimen must be, we must look at $(W - c_0)$ and insure that $(W - c_0)$ is not too small, compared to the radius of the plastic zone at fracture. If $(W - c_0)$ is too small then the free surfaces (at A) affects your results.

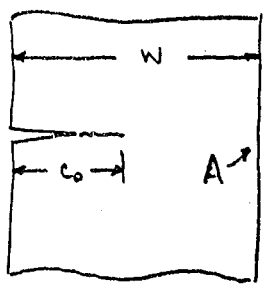

Smith (1965) looked at the solution of an infinite set of parallel cracks, each of length $2c_0$ and the distance between their centers being $2W$ and looked at what happens when each tip spreads plastically.

He found that

$$2r_p = c_0\left\{\frac{2W}{\pi c_0}\sin^{-1}\left[\sin\left(\frac{\pi c_0}{2W}\right)\sec\left(\frac{\pi\sigma}{2\sigma_y}\right)\right] - 1\right\}$$

and that the distance W does indeed play an important role. For the specimen whose $W/c_o = 2$, an error of 25% in the size of the plastic zone can be found but an error in the value of K_I is less than 1%. Hence the standard has been to take $\underline{(W - c_o) = c_o}$ (or $W/c_o = 2$).

Previously we had shown that $B \geq 2.5 \left(\frac{K_{Ic}}{\sigma_y}\right)^2 = 5\pi r_p$ since $r_p = \frac{1}{2\pi}\left(\frac{K_{Ic}}{\sigma_y}\right)^2$ in plane stress. Now r_p in plane strain $= \frac{1}{3} r_p$ (plane stress)

thus $B \geq 15\pi r_p$ (plane strain) $\cong 47 r_p$

Note that since $B \cong c_o$, then $W/c_o \cong W/B \cong 2$; hence the standard

$\underline{\underline{W/B \cong 2}}$. (This also implies that $c_o \geq 2.5 \left(\frac{K_{Ic}}{\sigma_y}\right)^2$).

Thus $c_o \cong B = W/2$. (Really $.45W \leq c_o \leq .55W$ by experimental experience)

Note that we have also shown point number 3 in the above proof.

There are several models used for testing

1. The Center Cracked Plate
2. The Double Edge Cracked Plate
3. The Single Edge Cracked Plate (Tension SEN)

* 4. The Single Edge Cracked Bend Specimen (3 point loaded)

* 5. The Compact Tension Test Specimen (CTT)

* 6. The C-shaped Specimen (used to represent K_{Ic} testing of cylinders and thick bars).

* represents the <u>recommended</u> test specimens

If the dimensions of the standard test specimens lead to impractical dimensions, alternative sizes are allowed. For bend specimens, the thickness $.25W \leq B \leq W$; The CTT may have dimensions $.25W \leq B \leq 0.5W$ (also true for the C shaped specimen.

On the next few pages are given the specimen and its dimensions Note the ASTM E-399 - it is the "תורה" for K_{Ic} testing.

Sample Shapes

PREFERRED RANGE OF THICKNESS W/2 TO W/4

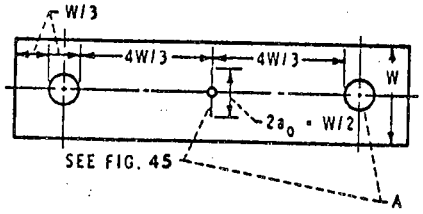

CENTER CRACKED PLATE

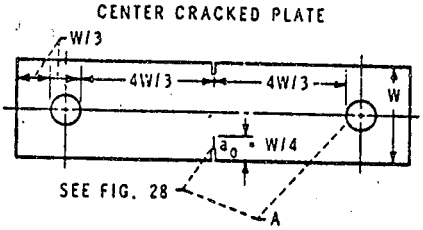

DOUBLE EDGE CRACKED PLATE

FIG. 42—*Proportions for center- and double-edge-cracked plate specimens. A-surfaces must be symmetric to specimen centerline within W/1000.*

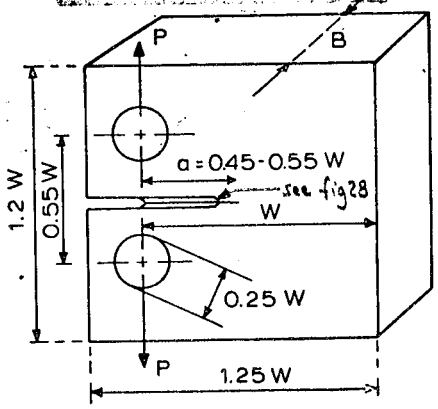

compact tension test - CTT

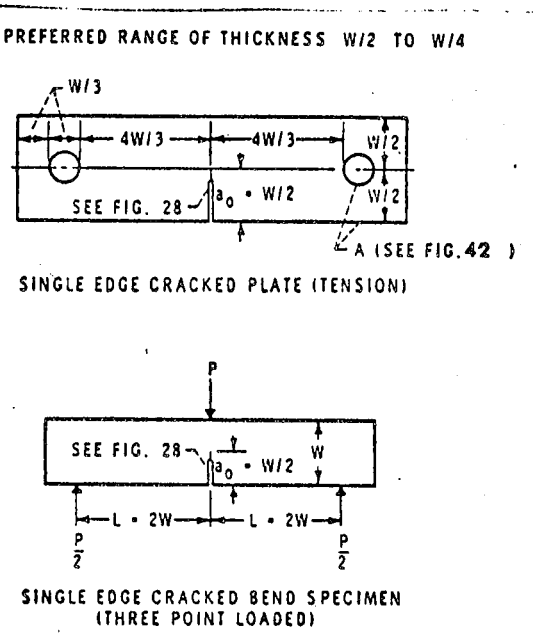

FIG. 43—*Proportions for single-edge-cracked tension and bend specimens.*

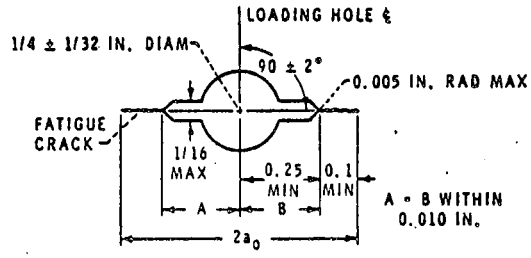

FIG. 45—*Fatigue crack starter for center-cracked plate specimens.*

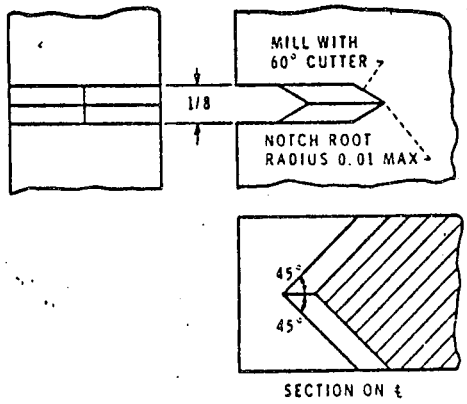

FIG. 28—*Chevron notch for edge-crack plate specimens.*

4&5. Crack must be sharp and must be introduced via a fatigue crack starting from a V-notch and the fatigue crack must be introduced by low type cycling (low K_{max}).

Proof: it has been found through testing of high strength steel and other materials that K_{crit} was an increasing function of root radius of the crack, if the radius was above some "cut off" radius.

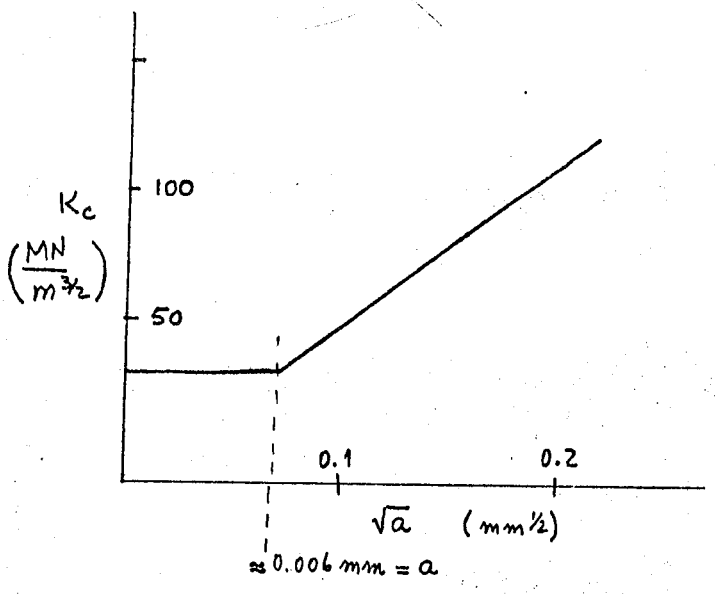

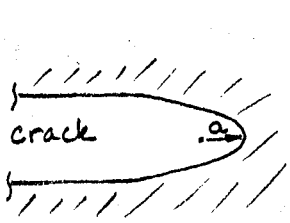

Thus in order to obtain a constant level of K_c, one must introduce sharp cracks by means of fatigue. However one must be careful about how one introduces the crack.

If the crack is introduced as a notch in a thick member, then the fatigue crack will propagate from a corner and will result in an irreproducible curved crack-front and this is not suitable for a standard test. We then have to modify the introduced crack so that the fatigue crack propagates in a relatively straight crack front. What is done is to introduce a Chevron Notch, or a straight-through notch or a slot ending in a drilled hole.

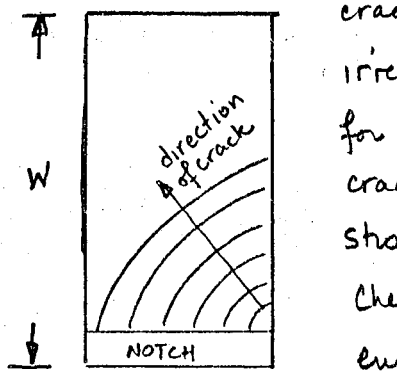

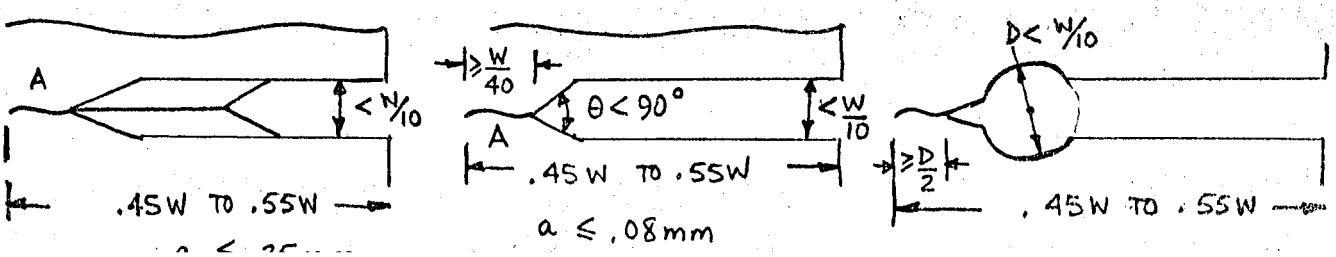

we will concentrate on the chevron notch, but the following hold for the other two models.

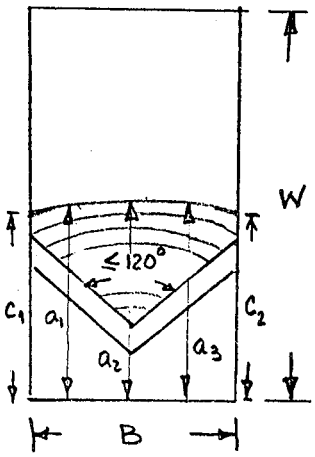

- The crack length is defined to be $a = \frac{1}{3}(a_1 + a_2 + a_3)$ where a_1, a_3 are equally spaced between the surface and the center and a_2 is at the center.
- If a_1, a_2, a_3 are $> a(1.10)$, test is invalid
- If c_1, c_2 are $> a(1.10)$, —— " ——
- If either c_1 and c_2 do not appear on the surface of the specimen, test is invalid.
- For the straight through notch
  - c_1, c_2 must be $< (1.15)a$ for a valid test
  - a_1, a_2, a_3 " " $< (1.10)a$ —— " ——
  - and the fatigue crack must be $\geq W/40$ for a valid test.

נ.ב.: אתה יכול לבדוק את הפרמטרים האלה מיד אחרי שעשית את הניסיון.

By using a chevron notch you have the additional advantage that the fatigue crack starts almost immediately upon cycling. You need between 10^4–10^6 cycles.

In order to ensure that a sharp notch will form there are several rules that you have to observe, the most important is that the maximum stress intensity during cycling of the last 2.5% of fatigue must not exceed $0.6K_Q (= K_{Ic})$. The reason for this is that K_{Ic} grows with the maximum stress intensity during fatigue.

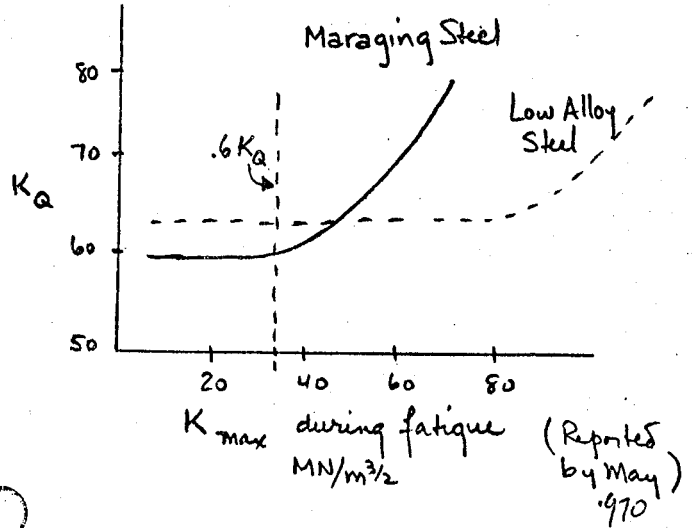

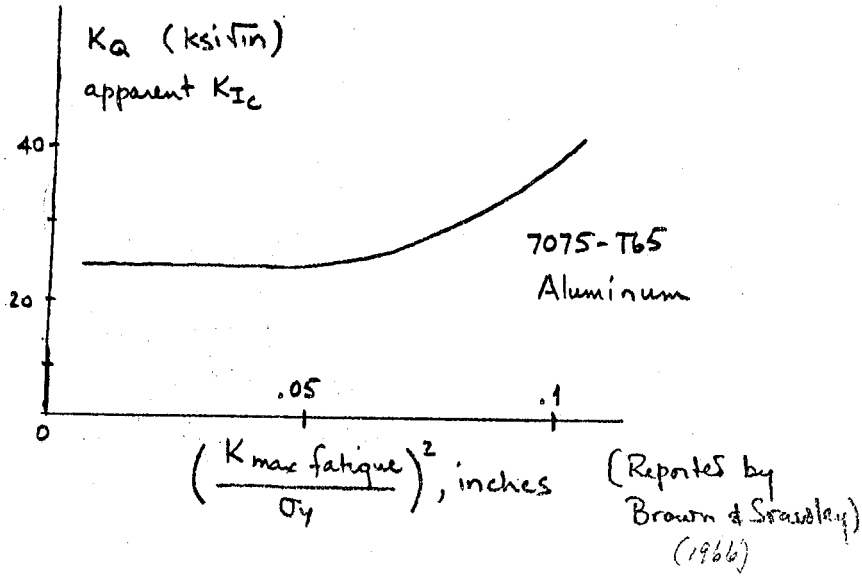

Finally the plane of the crack should not twist or tilt by more than ±10°. If it does, that implies mixed mode fracture and the test is invalid.

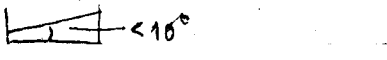

6. A displacement gage must measure accurately of the displacement across the "mouth" of the crack in order to satisfy the condition $P_{max}/P_Q < 1.1$ (where P_{max} = load at failure and P_Q is the 'pop-in' load).

Below is the design of the strain gage recommended by J.E. Srawley to measure the crack opening displacement. The strain gages (T_1, T_2, C_1, C_2) are connected by means of a wheatstone bridge, so that the displacement versus load can be recorded automatically. The gages T_1, T_2 will be in tension ; C_1 and C_2 will be in compression. When the test is complete, you will be able to compute the crack length from the relative displacement of the two crack faces.

Instrumentation

measurement of crack face displacements.

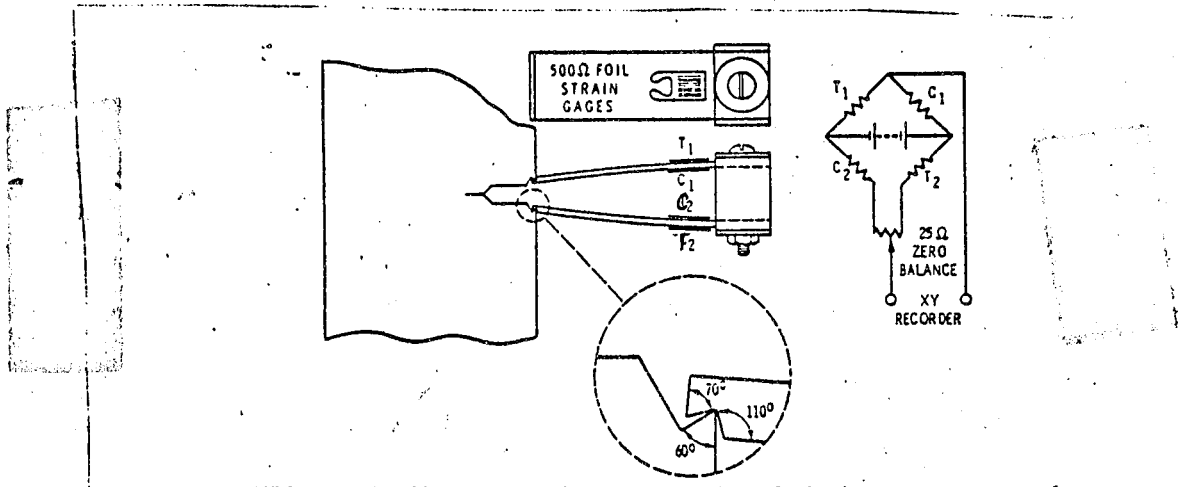

FIG. 19—*Double cantilever beam gage and method of mounting on crack-notched specimen for displacement measurement (designed by J. E. Srawley).*

This graph will then allow you to obtain the load versus crack length, and finally after using the relationship

$$K = \sigma \sqrt{\pi C_o}\, f_1(C_o/W) = \sigma \sqrt{W}\, f(C_o/W)$$

you will be able to obtain the value of K_Q.

Let's look at how this is done. First, the strain gages will record graphs that look like those on the following page

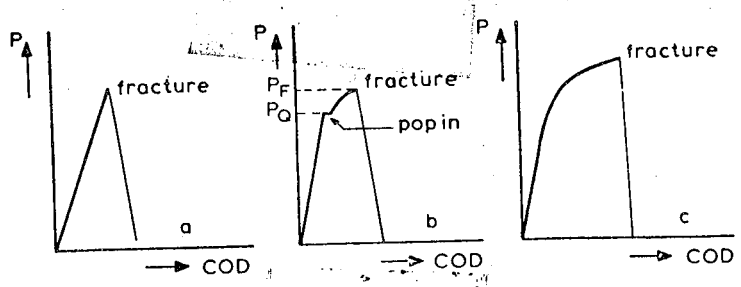

Figure 7.9. Test records

The first is the ideal case; here there is no plasticity. COD stands for crack opening displacement. Here total fracture occurs upon reaching K_{I_c}. In many cases rapid crack extension occurs at a load P_Q; either the load remains constant or there is a small drop in load, but the crack is arrested and the load can be further increased to P_F (or P_{max}) where total fracture occurs. The displacement due to the increase in P above P_Q is due to nonlinear elastic effects and small plasticity. To determine K_Q, the value of P_Q must be used. Here if $P_F/P_Q > 1.1$ the test is invalid. Another reason for crack arrest after pop in can be due to the growth of the shear lips.

In the third case, the crack grows to P_F via nonlinearity and plasticity. Here we define P_Q as follows:

- Draw the line tangent to the original record - find the slope of the line
- Next, take 98% of the slope and draw that straight line
- where that line crosses the original record we define P_Q
- However, if there is a load which is larger than the value found by the intersection of the 98% slope and the original record, then this larger load is defined to be P_Q.

The inequality $P_{max}/P_Q > 1.1$ replaces a more complicated method of finding where plasticity began on the P- COD record. (For those interested see Brock Pgs 178-180 or Knott Pgs 138-144). The disadvantage of the old method was the fact that the region of plasticity was very difficult to measure with any accuracy on the P- COD record, and the method could be more restrictive with respect to some cases of fracture. Even though $P_{max}/P_Q > 1.1$ is a subjective restriction, it is easier to measure.

It is possible to compute the crack length from the measured displacements across the crack faces.

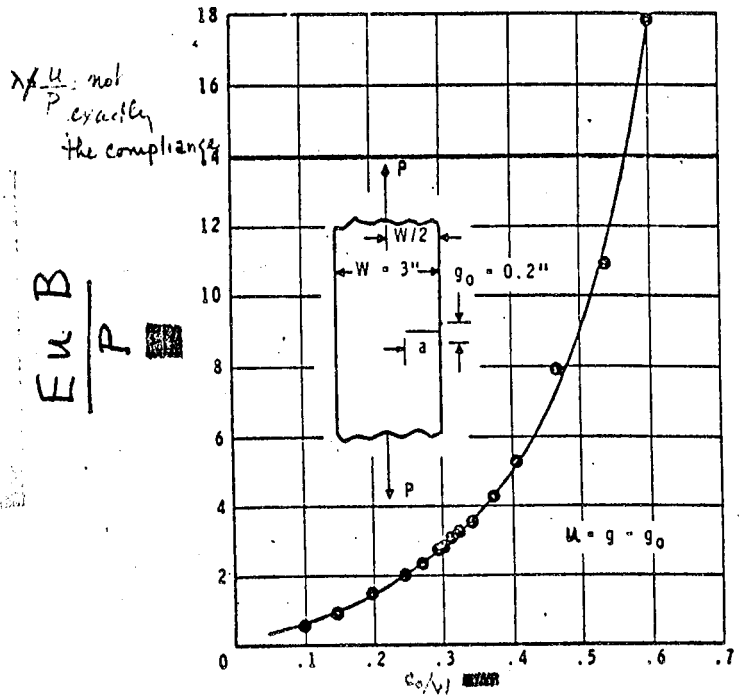

FIG. 22—*Calibration curve for converting displacement measurements to crack length single-edge-crack tension specimens.*

Once you have measured the load P_Q, use a graph like this to give you the crack length. (Note that you will probably have to calibrate your test set-up first before doing any tests that can be used for official data). Next use your crack length to width ratio (c_0/W) in the proper formula for the test you are doing to find $f(c_0/W)$. Srawley defines K_Q as follows:

For the SEN Bend specimen

$$K_Q = P_Q S/BW^{3/2} \cdot f(c_0/W) \quad \text{where} \quad P_Q S/BW^{3/2} = \sigma\sqrt{W}$$

$$f(\zeta = c_0/W) = 3\zeta^{1/2}\left[1.99 - \zeta(1-\zeta)(2.15 - 3.93\zeta + 2.7\zeta^2)\right] / \left[2(1+2\zeta)(1-\zeta)^{3/2}\right]$$

For the CTT

$$K_Q = P_Q/BW^{1/2} \cdot f(c_0/W) \quad \text{where} \quad P_Q/BW^{1/2} = \sigma\sqrt{W}$$

$$f(\zeta = c_0/W) = (2+\zeta)\left[0.886 + 4.64\zeta - 13.32\zeta^2 + 14.72\zeta^3 - 5.6\zeta^4\right] / (1-\zeta)^{3/2}$$

For the C-Shaped specimen, see the ASTM E-399 Standard.

7. Temperature and Loading Requirements for fatigue loading

a. If fatigue fracture is conducted at temperature T_1 and the actual test is done at temperature T_2 then $K_{max} \leq .6 \left(\sigma_{Y_1}/\sigma_{Y_2}\right) K_Q$

Proof:

From tests performed on low alloy steel by Wessel (1969), it was found that the variation in σ_y versus temperature and Fracture Toughness versus temperature looked like this for the CTT specimen:

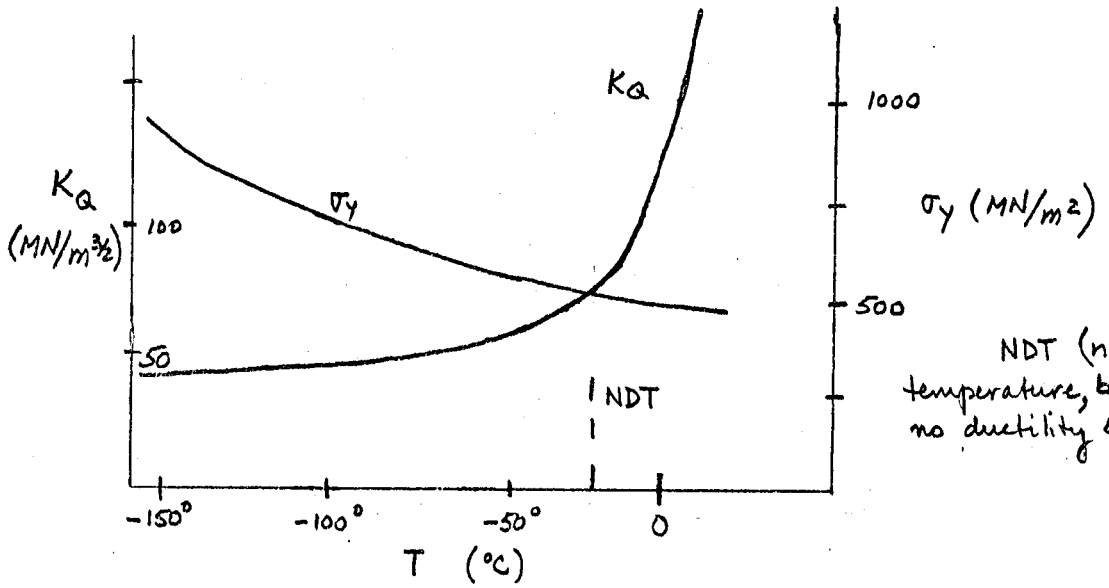

NDT (nil ductility temperature) - temperature, before which it is assumed, no ductility exists in the material.

As the temperature drops the material becomes more brittle, the stress needed to cause yielding and plasticity increases, but the value of K_{I_c} (or K_Q) decreases. As the temperature increases the material tends to become more "plastic"; hence the value of σ_y must decrease. As the material yields more readily, the amount of energy needed to cause brittle fracture increases, and this causes K_{I_c} to increase also.

if for the same thickness $B \geq 2.5 \left(\frac{K_{Ic}}{\sigma_y}\right)^2 \Rightarrow \left(\frac{K_{Ic}}{\sigma_y}\right)^2_{T_1} = \left(\frac{K_{Ic}}{\sigma_y}\right)^2_{T_2}$.

Thus $(K_{I_c})_{T_1} = \left(\frac{\sigma_{Y T_1}}{\sigma_{Y T_2}}\right)(K_{I_c})_{T_2}$. If we test the material at T_2, then $(K_{I_c})_{T_2} \equiv K_Q$. If we fatigued the material at T_1, then $K_{max} \leq .6 (K_{I_c})_{T_1}$. Hence $K_{max} \leq .6 \left(\frac{\sigma_{Y T_1}}{\sigma_{Y T_2}}\right) K_Q$.

- From this we can also see the following:

a plate with small thickness will show plane stress behavior and high toughness at room temperature. However at low temperatures, the material has a higher yield stress and thus causes the plastic zone $\left(r_p \sim \left(\frac{K_{Ic}}{\sigma_y}\right)^2\right)$ to be smaller. The material may then fracture either in plain strain or in plane strain / plane stress, due to the dependence of σ_y on Temperature.

- The trend shown by low alloy steel also can be found for other materials and is correct in general. There may exist materials for which this is not true.

b. According to ASTM 399 the fatigue crack is loaded cyclically with a ratio of minimum to maximum stress between -1 and $+0.1$ (ie S_{min}/S_{max}). As has been shown (or will be shown to you), Paris, Gomez and Anderson (1961) showed that

$$\frac{dc}{dN} = f(K_{max}, R)$$ where c is the crack length; N is the cycles

K_{max} is max K during cycle, $R = S_{min}/S_{max}$

- Schijve found that when $R < 0$, $\frac{dc}{dN} = f(K_{max})$ only (based on the data for 7075-T6 Aluminum Alloy) and $\frac{dc}{dN}$ increases as K_{max} increases.
- This is a reason that you are required to keep $K_{max} \leq .6\, K_Q$ for the last 2½ % of crack growth.
- The thickness also plays an important part here also. As the crack begins to propagate from the notch, it always starts as a tensile mode crack ⊥ to the sheet surface. As the crack grows the plastic zone increases and plane stress develops. This in turn causes the shear lips to grow. As the crack continues to grow in plane stress, the crack would transition to a shear mode fracture forming either the slant or V slant shapes discussed earlier. The shear lips would then tend to slow down crack growth because their radius of plasticity is larger (hence we have a type of ductile crack growth in the material) and it would take the crack more cycles to grow.
- In plain strain, the shear lips are confined to the surface and the radius of plasticity over a majority of the crack surface is smaller. Therefore the fracture is more brittle and thus requires a lower number of cycles to grow the crack. This is why you only need 10^4 to 10^6 cycles. For example in 2024-T3 Aluminum an initial crack of 3 mm grows to 10 mm in about 10^4 cycles for a thickness of 4 mm, whereas it takes

As R increases above zero, as expected, the K_{max} values obtained for the same crack growth rate increases. This is due to the fact that the amplitudes of the stresses and the mean stresses experienced by the crack are higher and K_{max} is higher $\left\{ \frac{dc}{dN} \sim f([1-R]K_{max}) \right.$; if $\frac{dc}{dN}$ is constant and R increases $\left. 1-R$ decreases and causes K_{max} to increase $\right\}$.

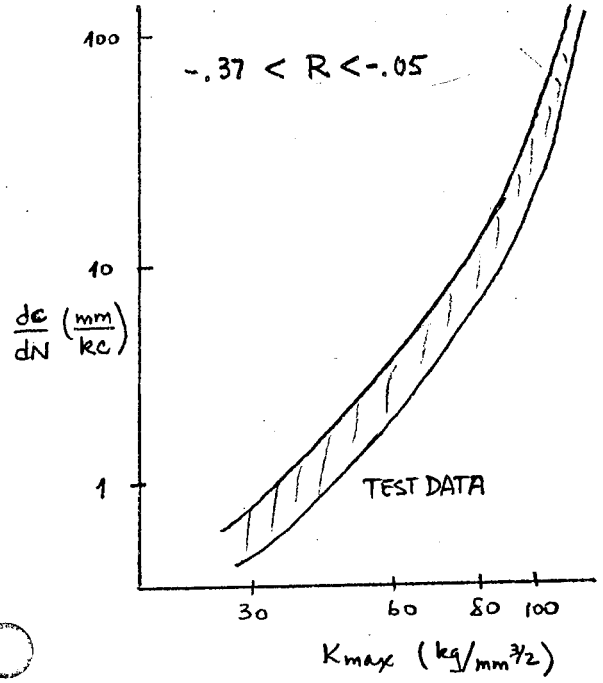

Schijve - data for 7075-T6 Aluminum

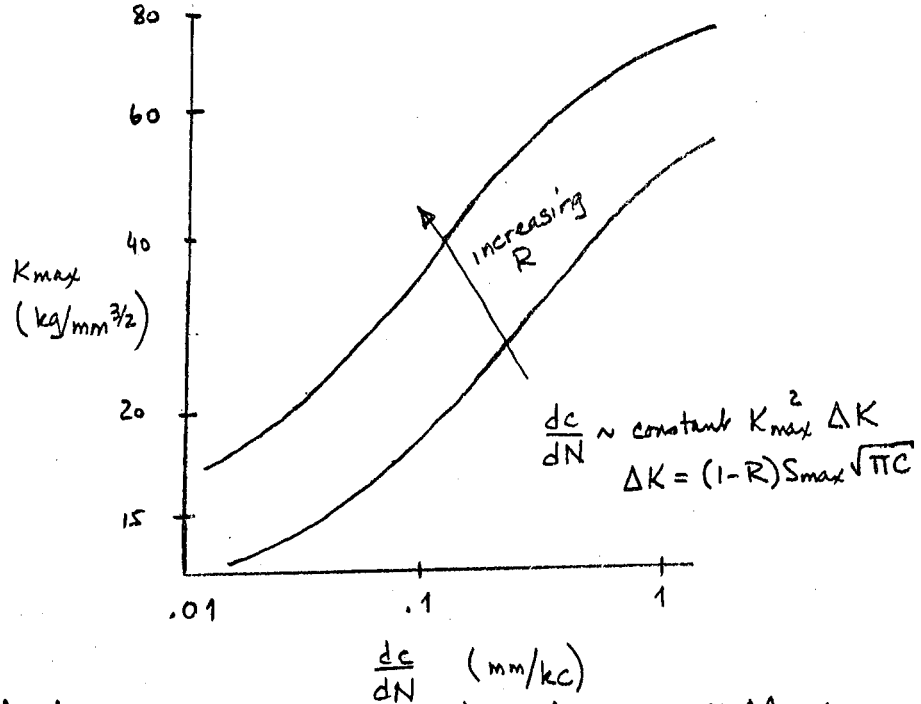

Brock & Schijve data for 2024-T3 Aluminum

c. Humidity - According to the work of Meyn, Bradshaw and others, it was found that humidity also affects the rate of crack growth. For aluminum alloys it was found that growth rates were lower in dry environments than in normal wet environments. Achter found the opposite to be true for other materials. This effect can be explained by the corrosive action of the environment and is time-dependent, just as fatigue crack growth is time dependent. This is probably the reason you are required to report the relative humidity for the test.

d. Load rate for the test

The ASTM requires that moderate increase in the load is to be used when the fracture toughness is carried out. The reason for this is that K_{Ic} can be affected by the load rate. Results of Radon and Turner on semi-heat treated steels, and the University of Illinois tests on Mild Steel, as reported by Krafft and Turin show that for low load rates K_{Ic} is a decreasing function

of load rate; however this turns out not to be the case for the high strength Titanium alloy (6Al-4V). For this alloy, K_{I_c} is an increasing function of load rate. What is true for both cases is that for high load rates K_{I_c} increases with load rate ~~for both~~. This is basically an adiabatic affect (i.e. no heat dissipation).

- For high load rates, the deformation ahead of the crack occurs so quickly that the heat generated cannot be dissipated to the rest of the specimen. Thus the temperature ahead of the crack increases substantially, also increasing the plasticity (hence the ductility) ahead of the crack. As shown before, this implies that for the plain strain radius to ~~remain the same~~ increase $\left(r_p \sim \left(\frac{K_{Ic}}{\sigma_y}\right)^2\right)$, that implies that K_{Ic} must also increase. Thus in order to minimize this effect, the load rate must be low to moderate, as is required in the test. The report by Krafft and Irwin on Crack-Velocity Considerations given in ASTM STP 381 goes into more details of this effect.

In summary, we have discussed

- The thickness requirements for a good K_{I_c} test;
- How thickness is related to the width of the specimen;
- How crack length is related to the width;
- How the initial crack is to be introduced into the specimen;
- How temperature and load rate affect the value of K_{I_c}
- What must be measured and how this is an indication of a valid test.